University of Denver
Digital Commons @ DU

Electronic Theses and Dissertations | Graduate Studies

1-1-2012

Structural Polymorphism in Tau Filaments: An Implication for Neurodegenerative Diseases

Ayisha Siddiqua
University of Denver

Follow this and additional works at: https://digitalcommons.du.edu/etd

 Part of the Biochemistry, Biophysics, and Structural Biology Commons, and the Chemistry Commons

Recommended Citation

Siddiqua, Ayisha, "Structural Polymorphism in Tau Filaments: An Implication for Neurodegenerative Diseases" (2012). *Electronic Theses and Dissertations*. 926.
https://digitalcommons.du.edu/etd/926

This Dissertation is brought to you for free and open access by the Graduate Studies at Digital Commons @ DU. It has been accepted for inclusion in Electronic Theses and Dissertations by an authorized administrator of Digital Commons @ DU. For more information, please contact jennifer.cox@du.edu,dig-commons@du.edu.

STRUCTURAL POLYMORPHISM IN TAU FILAMENTS: AN IMPLICATION FOR NEURODEGENERATIVE DISEASES

_____

A Dissertation

Presented to

The Faculty of Natural Sciences and Mathematics

University of Denver

_____

In Partial Fulfillment

of the Requirements for the Degree

Doctor of Philosophy

_____

by

Ayisha Siddiqua

March 2012

Advisor: Dr. Martin Margittai

Author: Ayisha Siddiqua
Title: STRUCTURAL POLYMORPHISM IN TAU FILAMENTS: AN IMPLICATION FOR NEURODEGENERATIVE DISEASES
Advisor: Dr. Martin Margittai
Degree Date: March 2012

Abstract

Tau filaments are the pathological hallmark of >20 neurodegenerative diseases including Alzheimer's disease, Pick's disease, and progressive supranuclear palsy. In the adult human brain, six isoforms of tau are expressed that differ by presence or absence of the second of the four semiconserved repeats. As a consequence, half of the tau isoforms have three repeats (3R tau), whereas the other half has four repeats (4R tau).

Site-directed spin labeling of recombinant tau in conjunction with electron paramagnetic resonance spectroscopy was used to obtain structural insights into tau filaments. The studies showed that the filaments of 4R tau and 3R tau share a highly ordered core structure in the third repeat with parallel, in-register arrangement of β-strands. This structure in 3R and 4R is conserved regardless of whether full-length isoforms (htau40 and htau23) or truncated constructs (K18 and K19) are used. When mixed, 3R tau and 4R tau coassembled into heterogeneous filaments. Hence, these findings indicate that there are at least three compositionally distinct types of filaments: homogeneous 3R tau, homogeneous 4R tau, and heterogeneous 3R/4R tau.

In vitro experiments show that the seeded filament growth, a prerequisite for tau spreading in tissue culture and brain, is crucially dependent on the isoform composition of individual seeds. Seeds of 3R tau and 3R/4R tau recruit both types of isoforms whereas seeds of 4R tau can recruit 4R tau, but not 3R tau, establishing an asymmetric barrier.

Conformational templating of 4R tau onto 3R tau seeds eliminates this barrier, giving rise to a new type of tau filament.

Conformational studies at the molecular level of tau filaments were done using Double electron-electron resonance spectroscopy, which allows the determination of distances between pairs of spin labels. These studies revealed structural differences between filaments of 3R tau and 4R tau. Furthermore, they indicated that 4R tau assumed the conformation of 3R tau when templated on 3R tau seeds. Our measurements have also provided insights into the heterogeneity of tau filament structure.

Conformational differences due to variation in filament composition and seeding properties of tau filaments have shown that they are structurally polymorphic in nature. This structural polymorphism of tau filaments has widespread implications in understanding and treatment of neurodegenerative diseases.

Acknowledgements

I would like to thank my thesis supervisor and mentor Dr. Martin Margittai for all guidance, help, support and encouragement during my doctoral programme. He challenged me and stimulated my intellectual curiosities which have helped me to enrich this thesis.

I thank the members of my research progress committee, Dr. Sandra Eaton and Dr. Keith Miller and other members of Dr. Margittai group current and former Paul Dinkel, Huy Huynh and Monil Shah.

I would also like to thank members of the Eaton group, Dr. Gareth Eaton, Dr. Mike Swanson and Virginia Meyer. I want to acknowledge the department for providing me the financial support to do my PhD and also acknowledge the funding agency CurePSP for funding this project.

I thank other graduate students for making my study in the school, an enjoyable and memorable one in my life. Finally, I would like to thank my parents and my husband for being very supportive through my PhD program.

Table of Contents

List of Figures

List of Tables

ABBREVIATIONS

aa	Amino acid
AD	Alzheimer's disease
APS	Ammonium persulfate
CBD	Corticobasal degeneration
CD	Circular dichroism
CW	Continuous wave
DEER	Double electron-electron resonance
DTT	Dithiothreitol
EB	Elution buffer
EDTA	Ethylenediamine tetraacetic acid
EPR	Electron paramagnetic resonance
FRET	Fluorescence resonance energy transfer
FTIR	Fourier transform infrared spectroscopy
GndHCl	Guanidine hydrochloride
HEPES	(4-(2-hydroxyethyl)-1-piperazineethanesulfonic acid, sodium salt)
htau40	Human tau40
htau23	Human tau23
IAPP	Islet amyloid polypeptide
IPTG	Isopropyl-beta-D-thiogalactopyranoside
LB	Luria-Bertani
MAPT	Microtubule associated protein tau

MBTR	Microtubule binding tau repeats
MTSL	[1-oxyl-2,2,5,5-tetramethyl-Δ^3 – pyrroline-3-methyl]methanethio-sulfonate
NaCl	Sodium chloride
NFTs	Neurofibrillary tangles
PAGE	Polyacrylamide gel electrophoresis
PCR	Polymerase chain reaction
PELDOR	Pulse electron-electron double resonance
PHF	Paired helical filament
PIPES	Piperazine-N, N'-bis(2-ethanesulfonic acid)
SDS	Sodium dodecyl sulphate
SDSL	Site directed spin labeling
TEMED	N,N,N'N' – Tetra-methylethylenediamine
ThT	Thioflavin T

Chapter One: Introduction

1.1 Tau protein

Tau protein was first isolated in 1975 from porcine brain and given the name tau (τ) as it was found to induce tubule formation (Weingarten et al, 1975). Tau, a 55-62 kD protein (Olmsted, 1986) is incorporated into growing microtubules as an integral structural component and required for both initiation and elongation (Witman et al., 1976) . Microtubules are a major component of the cytoskeletal system in eukaryotes (Olmsted & Borisy, 1973) and studies have shown that in the absence of tau, purified tubulin, a 6S dimer does not form microtubules (Olmsted & Borisy, 1973). Microtubules are part of mitotic and meiotic component in cells and also major component of nerve axons (Schmitt, 1968). Tau proteins apart from being an integral component of microtubules in nerve axons, support the outgrowth of axons, modulate the transport of vesicles and organelles along microtubules, serve as an anchor for enzymes and regulate the dynamics of microtubules (Cassimeris & Spittle, 2001; Drubin & Kirschner, 1986; Garcia & Cleveland, 2001; Weingarten et al., 1975).

Tau protein, also referred to as microtubule associated protein (MAPT), has an unusual character compared to most other proteins. It is heat resistant and acid treatment doesn't result in it losing its function and also it has a low content of secondary structures (Cleveland et al., 1977). These properties may be due to a high fraction of basic and

hydrophilic amino acid residues which resist the compact folding of most proteins. The primary sequence of tau has a low hydrophobic content (mean hydrophobicity = 0.404) and a net charge of +2 (Jeganathan et al., 2008). Biophysical studies have revealed that tau is a prototypical “natively unfolded” protein (Schweers et al., 1994) . In the human proteome these type of proteins have been classified as ‘‘natively unfolded’’ or ‘‘intrinsically unstructured proteins’’ [IUPs] (Dunker et al., 2008).

In the adult human brain, six isoforms of microtubule associated protein tau (MAPT) are expressed. The MAPT gene consists of 16 exons and alternative mRNA splicing gives rise to six tau isoforms (352-441 amino acids) (Goedert et al., 1988; Goedert et al., 1989). The tau isoforms are classified based on the presence or absence of 29- or 58 amino acid insert in the N terminus and inclusion or exclusion of a 31-amino acid repeat segment in the C terminus. Among the six isoforms, three isoforms have four repeats (4R) and the other 3 isoforms have three repeats (3R) **(Figure 1.1 A)**. In adult brain, transcripts coding for 4R and 3R are expressed and in fetus only the smallest isoform (htau 23) is expressed (Goedert et al., 1989; Goedert et al., 1989). The 3R and the 4R regions are characterized by a Pro-Gly-Gly-Gly motif present in each repeat (Goedert et al., 1988; Goedert et al., 1989). The amino acid sequence and the corresponding DNA sequence of the full length tau isoform 4R htau40 are given in **Figure 1.2**. The repeats carry out the major known biological function of tau: the binding to and stabilization of microtubules (Butner & Kirschner, 1991; Goode & Feinstein, 1994). In disease conditions these tau monomers can aggregate to form filaments. These

filaments belong to the major class of amyloid fibrils which are seen in various diseases **(Figure 1.3)**.

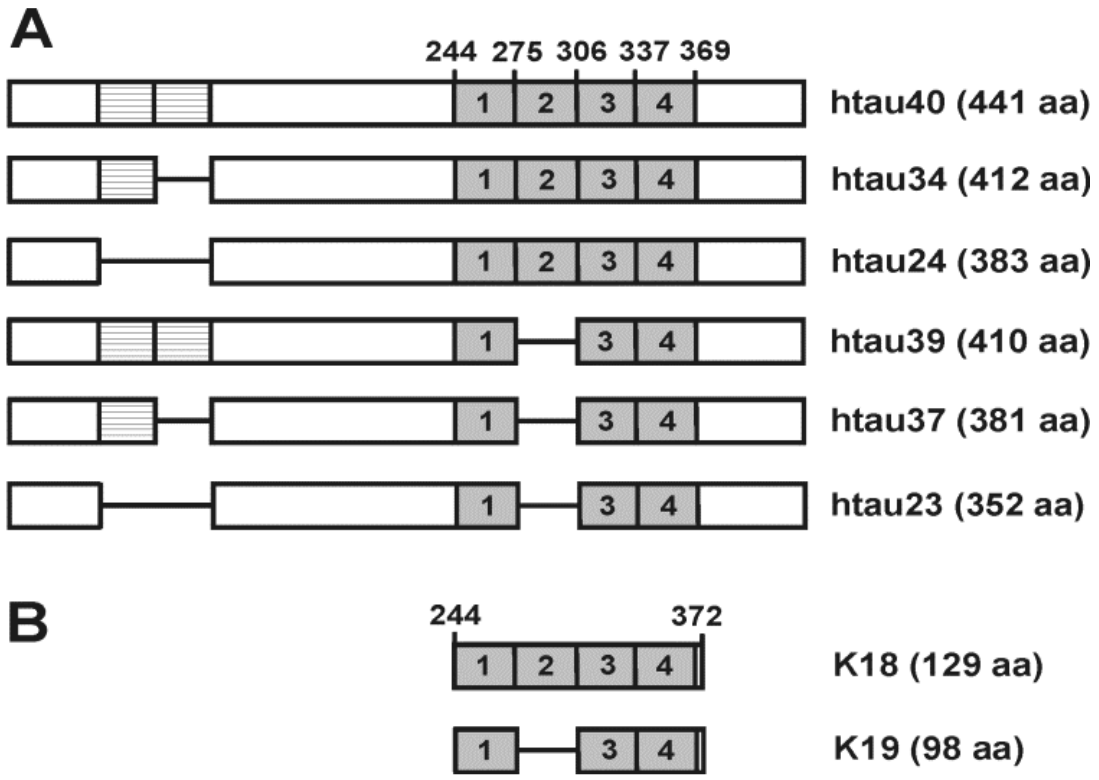

Figure 1.1: Bar diagrams of tau isoforms and constructs: (A) Tau isoforms are defined by the presence or absence of two inserts in the N-terminal half (striped) and the inclusion or exclusion of the second microtubule binding repeat in the C-terminal half (marked as 2). Isoform sizes range from 352 amino acids (aa) to 441 amino acids and are provided on the right. (B) The truncated constructs K18 and K19 contain the repeats (four for K18 and three for K19) plus three additional residues at the C termini (Siddiqua & Margittai, 2010).

```
   1 - ATGGCTGAGCCCCGCCAGGAGTTCGAAGTGATGGAAGATCACGCTGGGACGTACGGGTTG - 60
     - M  A  E  P  R  Q  E  F  E  V  M  E  D  H  A  G  T  Y  G  L
  61 - GGGGACAGGAAAGATCAGGGGGGCTACACCATGCACCAAGACCAAGAGGGTGACACGGAC - 120
     - G  D  R  K  D  Q  G  G  Y  T  M  H  Q  D  Q  E  G  D  T  D
 121 - GCTGGCCTGAAAGAATCTCCCCTGCAGACCCCCACTGAGGACGGATCTGAGGAACCGGGC - 180
     - A  G  L  K  E  S  P  L  Q  T  P  T  E  D  G  S  E  E  P  G
 181 - TCTGAAACCTCTGATGCTAAGAGCACTCCAACAGCGGAAGATGTGACAGCACCCTTAGTG - 240
     - S  E  T  S  D  A  K  S  T  P  T  A  E  D  V  T  A  P  L  V
 241 - GATGAGGGAGCTCCCGGCAAGCAGGCTGCCGCGCAGCCCCACACGGAGATCCCAGAAGGA - 300
     - D  E  G  A  P  G  K  Q  A  A  A  Q  P  H  T  E  I  P  E  G
 301 - ACCACAGCTGAAGAAGCAGGCATTGGAGACACCCCCAGCCTGGAAGACGAAGCTGCTGGT - 360
     - T  T  A  E  E  A  G  I  G  D  T  P  S  L  E  D  E  A  A  G
 361 - CACGTGACCCAAGCTCGCATGGTCAGTAAAAGCAAAGACGGGACTGGAAGCGATGACAAA - 420
     - H  V  T  Q  A  R  M  V  S  K  S  K  D  G  T  G  S  D  D  K
 421 - AAAGCCAAGGGGGCTGATGGTAAAACGAAGATCGCCACACCGCGGGGAGCAGCCCCTCCA - 480
     - K  A  K  G  A  D  G  K  T  K  I  A  T  P  R  G  A  A  P  P
 481 - GGCCAGAAGGGCCAGGCCAACGCCACCAGGATTCCAGCAAAAACCCCGCCCGCTCCAAAG - 540
     - G  Q  K  G  Q  A  N  A  T  R  I  P  A  K  T  P  P  A  P  K
 541 - ACACCACCCAGCTCTGGTGAACCTCCAAAATCAGGGGATCGCAGCGGCTACAGCAGCCCC - 600
     - T  P  P  S  S  G  E  P  P  K  S  G  D  R  S  G  Y  S  S  P
 601 - GGCTCCCCAGGCACTCCCGGCAGCCGCTCCCGCACCCCGTCCCTTCCAACCCCACCCACC - 660
     - G  S  P  G  T  P  G  S  R  S  R  T  P  S  L  P  T  P  P  T
 661 - CGGGAGCCCAAGAAGGTGGCAGTGGTCCGTACTCCACCCAAGTCGCCGTCTTCCGCCAAG - 720
     - R  E  P  K  K  V  A  V  V  R  T  P  P  K  S  P  S  S  A  K
 721 - AGCCGCCTGCAGACAGCCCCCGTGCCCATGCCAGACCTGAAGAATGTCAAGTCCAAGATC - 780
     - S  R  L  Q  T  A  P  V  P  M  P  D  L  K  N  V  K  S  K  I
 781 - GGCTCCACTGAGAACCTGAAGCACCAGCCGGGAGGCGGGAAGGTGCAGATAATTAATAAG - 840
     - G  S  T  E  N  L  K  H  Q  P  G  G  G  K  V  Q  I  I  N  K
 841 - AAGCTGGATCTTAGCAACGTCCAGTCCAAGTGTGGCTCAAAGGATAATATCAAACACGTC - 900
     - K  L  D  L  S  N  V  Q  S  K  C  G  S  K  D  N  I  K  H  V
 901 - CCGGGAGGCGGCAGTGTGCAAATAGTCTACAAACCAGTTGACCTGAGCAAGGTGACCTCC - 960
     - P  G  G  G  S  V  Q  I  V  Y  K  P  V  D  L  S  K  V  T  S
 961 - AAGTGTGGCTCATTAGGCAACATCCATCATAAACCAGGAGGTGGCCAGGTGGAAGTAAAA - 1020
     - K  C  G  S  L  G  N  I  H  H  K  P  G  G  G  Q  V  E  V  K
1021 - TCTGAGAAGCTTGACTTCAAGGACAGAGTCCAGTCGAAGATTGGGTCCCTGGACAATATC - 1080
     - S  E  K  L  D  F  K  D  R  V  Q  S  K  I  G  S  L  D  N  I
1081 - ACCCACGTCCCTGGCGGAGGAAATAAAAAGATTGAAACCCACAAGCTGACCTTCCGCGAG - 1140
     - T  H  V  P  G  G  G  N  K  K  I  E  T  H  K  L  T  F  R  E
1141 - AACGCCAAAGCCAAGACAGACCACGGGGCGGAGATCGTGTACAAGTCGCCAGTGGTGTCT - 1200
     - N  A  K  A  K  T  D  H  G  A  E  I  V  Y  K  S  P  V  V  S
1201 - GGGGACACGTCTCCACGGCATCTCAGCAATGTCTCCTCCACCGGCAGCATCGACATGGTA - 1260
     - G  D  T  S  P  R  H  L  S  N  V  S  S  T  G  S  I  D  M  V
1261 - GACTCGCCCCAGCTCGCCACGCTAGCTGACGAGGTGTCTGCCTCCCTGGCCAAGCAGGGT - 1320
     - D  S  P  Q  L  A  T  L  A  D  E  V  S  A  S  L  A  K  Q  G
1321 - TTG - 1323
     - L
```

Figure 1.2: **Human tau40**. The complete sequence of full length tau (htau40). The highlighted sequence (yellow) is the second repeat.

For a polypeptide, its stable amyloid fibril state competes with its monomeric folded state (when a folded state exists), or with other nonaggregated states (Tycko, 2011). The relatively stable and remarkably protease resistant amyloid fibrils represent the end point of the protein misfolding process. Tau filaments belong to the class of amyloid fibrils whose formation is driven by hydrophobic interactions. The amyloid fibrils formed due to these misfolding processes are implicated in many neurodegenerative diseases **(Figure 1.3)**. Neurodegenerative diseases in which tau filaments are implicated are collectively referred to as tauopathies (Lee, Goedert, & Trojanowski, 2001).

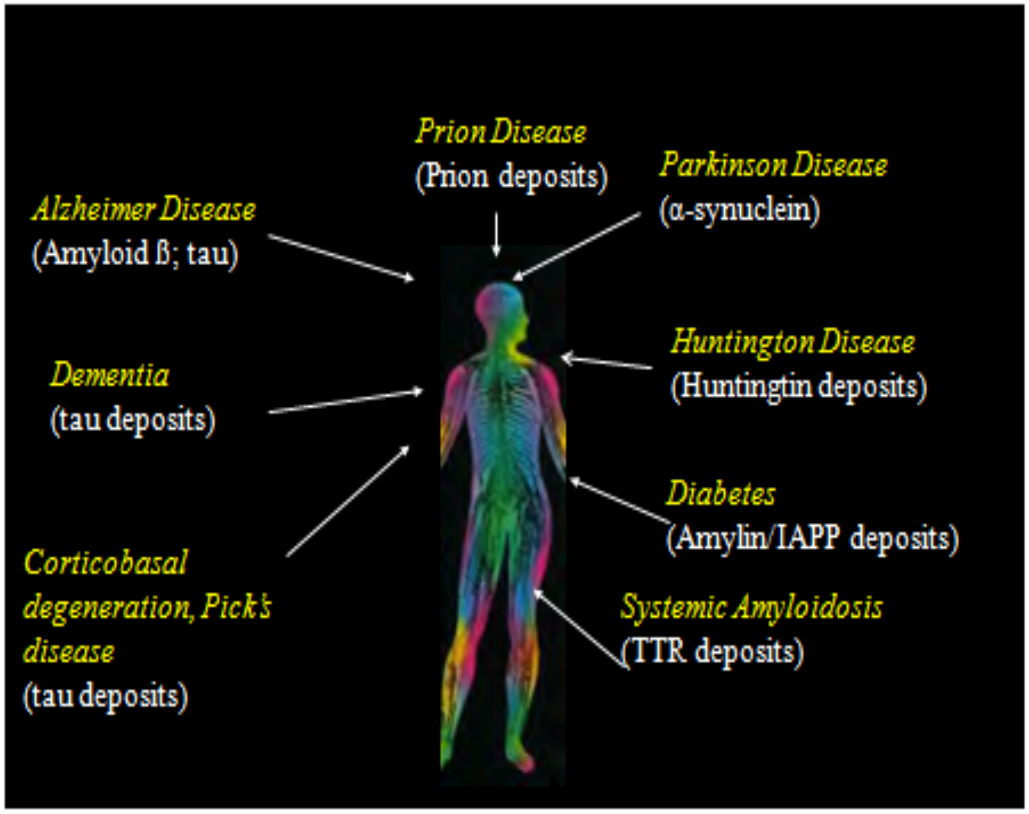

Figure 1.3: **Major classes of amyloid diseases.** Tau and other proteins that are implicated in major amyloid diseases.

1.2 Tauopathies

The neurodegenerative diseases are characterized by distinct brain lesions that have in common the formation of filamentous deposits of abnormal proteins. In heterogeneous dementias and some movement disorders, it is characterized neuropathologically by prominent intracellular accumulations of abnormal filaments formed from the microtubule associated protein tau **(Table 1)**.

Table 1: Diseases in which tau inclusions have been described (M. Goedert & Spillantini, 2011)

Alzheimer's disease
Amyotrophic lateral sclerosis/parkinsonism-dementia complex
Argyrophilic grain disease
Chronic traumatic encephalopathy
Corticobasal degeneration
Diffuse neurofibrillary tangles with calcification
Down's syndrome
Familial British dementia
Familial Danish dementia
Frontotemporal dementia and parkinsonism linked to chromosome 17 caused by MAPT mutations
Gerstmann–Sträussler–Scheinker disease
Guadeloupean parkinsonism
Mytotonic dystrophy
Niemann–Pick disease, type C
Non-Guamanian motor neuron disease with neurofibrillary tangles
Pantothenate kinase-associated neurodegeneration
Pick's disease
Postencephalitic parkinsonism
Prion protein cerebral amyloid angiopathy
Progressive subcortical gliosis
Progressive supranuclear palsy
SLC9A6-related mental retardation
Subacute sclerosing panencephalitis
Tangle-only dementia
White matter tauopathy with globular glial inclusions

Tau pathology is the hallmark of >20 neurodegenerative diseases, (Lee et al., 2001). In frontotemporal dementia and parkinsonism linked to chromosome 17 (FTDP – 17) mutations in the tau gene have been linked to the disease (Goedert & Spillantini, 2011). The majority of tauopathies, however, develops sporadically.

Alzheimer's disease (AD), a major dementia, is characterized by the presence of two different types of deposits in the brain, senile plaques and neurofibrillary tangles (NFTs). The main component of senile plaques is the β amyloid peptide whereas tau protein is bundled into NFTs (Goedert & Spillantini, 2006; Grundke-Iqbal et al., 1986).

NFTs which consist of paired helical filaments (PHFs) and straight filaments are composed predominantly of abnormally hyperphosphorylated tau proteins (Goedert et al., 1988). Hyperphosphorylation is believed to be an early event in the pathway that leads from soluble to insoluble and filamentous tau protein (Braak et al., 1994). However it is unclear whether phosphorylation is sufficient for assembly of tau monomers into filaments.

The advancing age of a person, generally 65 years or older, is a risk factor for AD and other dementias, but the occurrence of neurodegenerative disease is not a normal part of aging (alz.org). Neurodegenerative diseases have been shown not only to affect people in their old age but also in their young age. Brain autopsies of players of football, hockey and other games where the brain experiences increased incidences of concussion, the presence of NFTs of tau protein have been reported. This disease has been classified as Chronic Traumatic Encephalopathy. Autopsies of players as young as 21 years have

shown the presence of NFTs in the brain (Los Angeles Times, 2011; McKee et al., 2009; Omalu et al., 2011; Omalu et al., 2011; The New York Times, 2011).

1.3 Architecture of Tau Filaments

Straight filaments and PHFs (15-20 nm diameter) isolated from brain tissue have a cross-β structure in which β-strands run perpendicular to the long fiber axis and are spaced ~4.7 Å apart (Berriman et al., 2003) (**Figure 1.4**). This structural feature is a common denominator of filaments belonging to the amyloid class (Sunde & Blake, 1997), which are self-assembled aggregates made from proteins with diverse amino acid sequence (Sunde & Blake, 1998). In an amyloid fibril, two to six protofilaments (2-5 nm in diameter) twist around each other to form a supramolecular structure (Serpell et al., 2000). AFM measurements have shown that the fibrils form unbranched structures with diameters ranging up to ~25nm. The fibrils themselves can again form large bundles.

The precursor proteins of these fibrils have no general sequence or 3- dimensional (3D) structural homology in their native, soluble forms, but they all assemble into a cross-β-fiber structure, with β-strands perpendicular and β-sheets parallel to the long fiber axis.

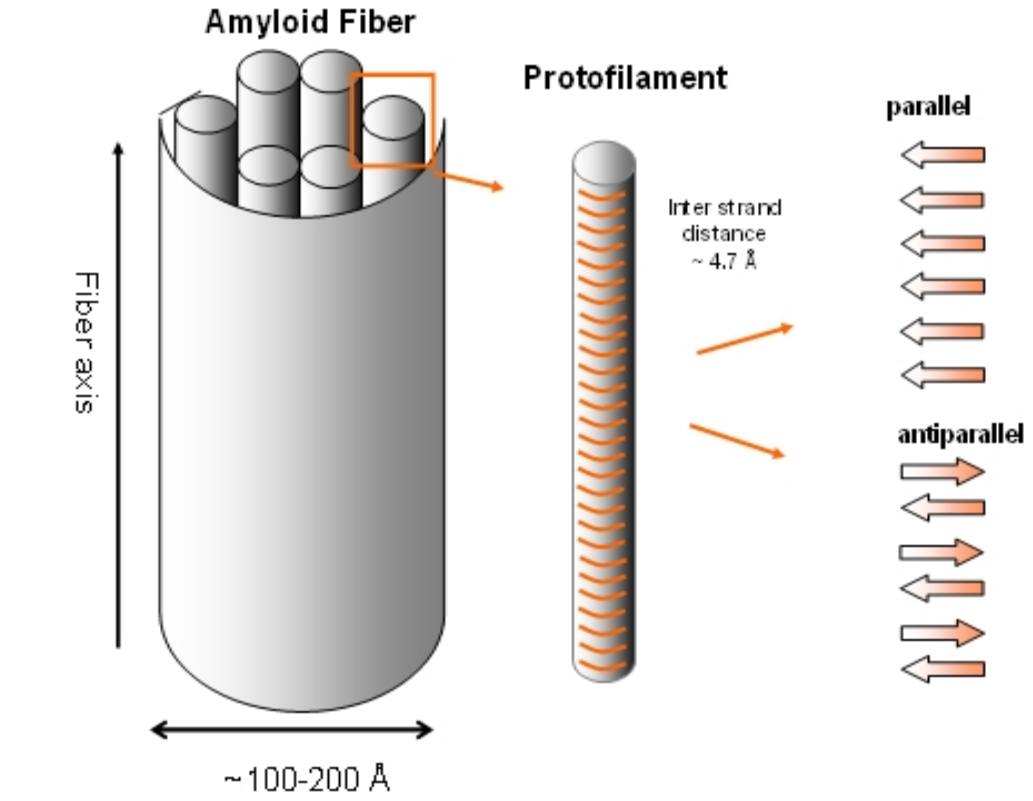

Figure 1.4: Schematic structure of amyloid fiber. Arrangement of protein monomers in β-pleated sheet structure in a protofilament either in parallel or anti parallel β-sheet structure. The protofilaments twist together to form supramolecular structures called fibrils.

When two or multiple sheets are present, they have a predominantly parallel in-register arrangement of β-strands and usually antiparallel arrangement of β-strands is seen in peptides that form single β- sheets depending on the amino acid sequence (Margittai & Langen, 2008).

The antiparallel β-strands are sometimes seen in aggregates formed by smaller peptides, but the parallel in-register arrangement of β-strands in β-sheets is seen in most of the amyloid fibrils. Tau filaments show parallel in-register arrangement of β-strands (Margittai & Langen, 2004). Aggregates of other protein filaments of Aβ (Paravastu,

Petkova, & Tycko, 2006), IAPP (Jayasinghe & Langen, 2004), α-synuclein (Chen et., 2007), β_2-microglobulin (Ladner et al., 2010), HuPrP (Cobb et al., 2007) Rnq1 (Wickner et al., 2008) also show parallel in-register arrangement.

Studies of β-amyloid fibrils have shown that fibrils with similar morphological appearance can vary greatly in molecular design; and gross morphology and fine structure need not be correlated (Petkova et al., 2005). Therefore, despite the shared similarities described amongst tau filaments in the previous paragraph, they may be different at the molecular level.

1.4 Importance of study of structural polymorphism in tau filaments

Even though tau filaments have been implicated in neurodegenerative diseases, their role has been controversial (Brunden et al., 2008). In particular, it has been debated whether filaments might have an altogether protective function by preventing individual tau molecules from partitioning into toxic oligomers (Bretteville & Planel, 2008).

It has been suggested that the cytotoxicity of fibrils could be due to the number of misfolded forms including non-fibrillar oligomers (Chiti & Dobson, 2006). The importance of mature amyloid fibrils as etiological agents in AD and other amyloid diseases, as opposed to nonfibrillar oligomers observed at earlier stages of peptide incubation has been in dispute (Kayed et al., 2003; Lashuel et al., 2002). One principal argument against a primary role for mature fibrils in AD has been the absence of a robust correlation between the severity of neurological impairment and the extent of amyloid deposition (Kirkitadze et al., 2002). Studies have shown that certain amyloid morphologies may be more pathogenic than others in the affected organs of amyloid

diseases, which would weaken the correlation between disease symptoms and total amyloid deposition (Petkova et al., 2005). As a result, the structural study of fibrils gains importance.

There are various reasons why the study of structural polymorphism in tau filaments is important. Studies in human, mouse and *in vitro* have revealed a direct link between amyloid-β and tau in causing toxicity in Alzheimer's disease (Hardy & Selkoe, 2002; Ittner & Götz, 2010). Tau protein is predominantly found in axons, and under some physiological conditions, it has also been seen to localize in dendrites albeit in lower amounts (Hirokawa, 1982). It mediates dendritic signaling and causes β-amyloid toxicity in dendrites (Ittner & Götz, 2010). In tissue culture studies, transfer of tau filaments to neighboring cells has been seen (Frost et al., 2009). Recent findings have suggested that tau filaments could play an important role in the propagation of the misfolded state of tau from one cell to the next (Lee et al., 2010). In addition, injections of insoluble tau into mouse brain resulted in the spread of misfolding through different brain regions (Clavaguera et al., 2009). Also it has been recently shown that tau pathology *in vivo* could spread through synapses of nerve cells (Liu et al., 2012).

The above mentioned properties of tau filaments are reminiscent of those observed in prion proteins (Prusiner, 1998). In the prion field it has been shown that the same prion protein due to different conformational states could result in different transmissible states (Prusiner, 1998). Although the overall evidence for prion-type mechanisms in tauopathies is scarce, it has lent a new urgency and relevance to better understand the structure of tau filaments.

There are currently 5.4 million cases of AD and related dementias in the U.S population (Alzheimer's association, 2011). The annual healthcare cost of this aging population is around $183 billion. It has been projected by 2050 that the number of people with AD and other dementias would be 13.2 million and the health care cost would be 1.1 trillion dollars. Therefore, neurodegenerative diseases are considered to be a major health issue (alz.org, 2011).

For the past two decades, drug development efforts for the major neurodegenerative disease AD have been focused on targets defined by the amyloid cascade hypothesis (Hardy & Higgins, 1992; Karran et al., 2011) with disappointing results. Tau-based strategies, in contrast have received little attention until recently, despite the presence of extensive tau pathology. The discovery of mutations within the tau gene that causes fronto-temporal dementia has demonstrated that tau dysfunction, in the absence of amyloid pathology, is sufficient to cause neuronal loss and clinical dementia (Medina, 2011). Investigation of the fundamentals of tau polymerization is indispensable for identifying inhibitory conditions or compounds preventing formation of PHFs which may allow the slowing down or even reverse the degeneration of neurons in tauopathies (Andronesi et al., 2008). Considering all these, understanding the structural polymorphism in tau filaments could be one of the starting points to come up with better drugs in the future.

My investigations into the structural polymorphism of tau filaments are organized as follows:

Chapter 2 studies have tried to understand assembly of 3R and 4R tau isoforms in filaments. Continuous wave electron paramagnetic resonance (CW EPR) spectroscopy in combination with site directed spin labeling (SDSL) was used to study the assembly of these isoforms.

Chapter 3 is related to the study of the recruitment of 3R and 4R tau isoforms into filaments. For this purpose, an intrinsic fluorescence assay using the environment sensitive dye acrylodan was developed.

Chapter 4 is related to the study of the structure of tau filaments at the residue level using Double electron-electron resonance spectroscopy (DEER).

Chapter Two: Determination of Composition of Tau Filaments

2.1 Introduction

In the adult human brain, all six isoforms (**Figure 1.1A**) are present and the ratio of 3R and 4R tau isoforms is ~one to one (Lee et al., 2001). Antisera raised against synthetic peptides corresponding to different human tau isoforms have demonstrated that multiple tau protein isoforms (both 3R and 4R) are incorporated into the neurofibrillary tangles of AD (Goedert et al., 1989a; Goedert et al.,1992a; Greenberg et al.,1992). The relative proportions of the tau isoforms observed in AD PHFs are similar to those that are observed in normal adult human brain. Also different pathogenic mutations alter the biochemical properties and stoichiometry of tau isoforms and this has been shown by analysis of brains of FTDP-17 patients (Hong et al., 1998; Trojanowski & Lee, 1994). All these studies led us to the question, whether the 3R and 4R isoforms segregate into homogeneous filaments or coassemble to form heterogeneous filaments. To understand this phenomenon, tau aggregation was studied *in vitro*.

2.1.1 Aggregation of tau filaments *in vitro*.

The exact mechanism responsible for assembly of soluble tau protein into insoluble filaments in brain cells is not yet known. The monomeric tau proteins are highly soluble and form a double hairpin loop, a paperclip like structure folded in the

vicinity of the repeat region (Jeganathan et al., 2006), forming through transient intramolecular contacts (Mukrasch et al., 2009). These interactions, together with the overall positive charge of the protein, greatly inhibit aggregation. As a consequence a negatively charged cofactor (heparin) is used to accelerate aggregation.

Heparin is a copolymer of alternating uronic acid and amino sugar residues, with sulfated esters in various positions **(Figure 2.1)**. The ionized carboxylate and sulfate groups give it a high negative charge. The *in vitro* aggregation of non-phosphorylated tau protein into filaments is based on the electrostatic interaction of negatively charged heparin with the positively charged tau monomers (Calamai et al., 2006). The characteristics of these *in vitro* assembled filaments closely resemble tau filaments from AD brain (Goedert et al., 1996) . Other polyanions, for example, RNA, DNA, and arachidonic acid have also been shown to cause aggregation of tau into filaments (Calamai et al., 2006; Frost et al., 2009; Goedert et al., 1996). Studies have shown that heparin becomes integrated into the rigid core region of the PHF, probably by providing charge compensation for the lysine-rich stretches that form upon the stacking of the repeat regions (Sibille et al., 2006). Also these polysulfonated sugars have been seen in the plaques of many amyloid diseases (Strohmeyer et al., 2002). Binding of heparin to Aβ, IAPP and α-synuclein is at a higher affinity than with their monomer states. These observations indicate that recognition depends on the quaternary structure of the aggregates and therefore heparin is seen in the rigid interiors of the amyloid fibrils (Alexandrescu, 2005). This view is different from the observation made by some other

researches that heparin is not associated with tau filaments, but is only required to catalyze aggregation (Friedhoff et al., 1998; Jeganathan et al., 2008).

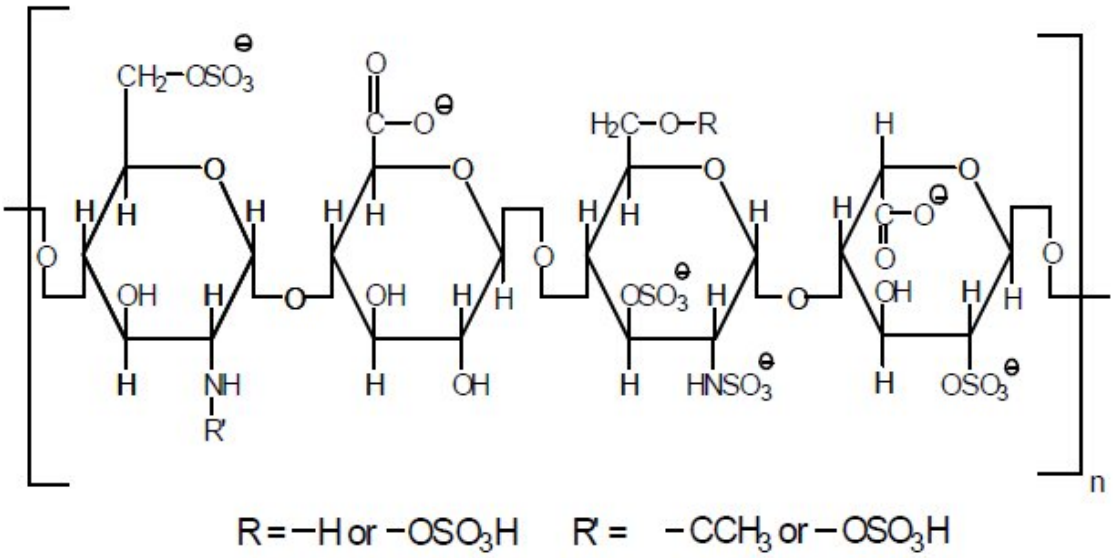

Figure 2.1: **Partial heparin structure.** (Sigmaaldrich.com)

When tau monomers self-aggregate into filaments, the microtubule binding repeat (MTBR) region has shown to be protease resistant (Goedert et al., 1988; Novak et al., 1993; Wischik et al., 1988), thus establishing itself to be part of the structured core. The N- and C-terminal regions by contrast remain largely disordered, forming a fuzzy coat (Wischik, et al., 1988). Charge and conformational changes are of uttermost importance near the second (R2) and third (R3) MTBR that are thought to be involved directly in the nucleation of the aggregation (Friedhoff et al., 1998). Therefore to accelerate aggregation

of tau monomers into filaments, N and C termini are removed which is exemplified by the 4R and 3R constructs K18 and K19 **(Figure 1.1B)** (Barghorn & Mandelkow, 2002).

2.1.2 Structure determination of tau filament.

Nuclear magnetic resonance spectroscopy and X-ray crystallography, which have been used to determine protein structures at high resolution are inadequate to solve structures of proteins with low solubility and those that do not form crystals. Analysis of tau filaments, which are aggregates, has been challenging due to their large size and low solubility. SDSL with CW EPR spectroscopy, which monitors structure at the backbone level, fills part of this gap and has been very useful in studying the structures of filaments (Hubbell et al., 1996; Huber et al., 2001; Margittai & Langen, 2004).

2.1.2.1 EPR spectroscopy.

EPR spectroscopy involves the study of energy differences due to the interaction of an unpaired electron in the sample with a magnetic field, B_0. This effect is called the Zeeman Effect. The electron acts like a bar magnet when it is placed in a magnetic field because of its magnetic moment. Since energies are quantized, a single unpaired electron has only two allowed energy states. It has a state of lower energy; when the moment of the electron, μ, is aligned with the magnetic field and a higher energy state when μ is aligned against the magnetic field **(Figure 2.2)**. The two states are designated by the projection of the electron spin, m_s, on the direction of the magnetic field. Because the electron is a spin ½ particle, the parallel state has m_s= -1/2 and the antiparallel state has m_s = +1/2. The difference between the energies of these two states is caused by the interaction between the electron spin and the magnetic field.

The energy, $\Delta E = h\nu$ is required to cause a transition between two spin states

$\Delta E = h\nu = g\,\mu_B B_0$ and $\mu_B = eh/2m_e$

Where g is the g-factor, μ_B is the Bohr magneton which is the natural unit of the electron's magnetic moment, h is the Planck's constant, e is the electron charge and m_e is the mass of the electron and the change in spin state is $\Delta m_s = \pm 1$.

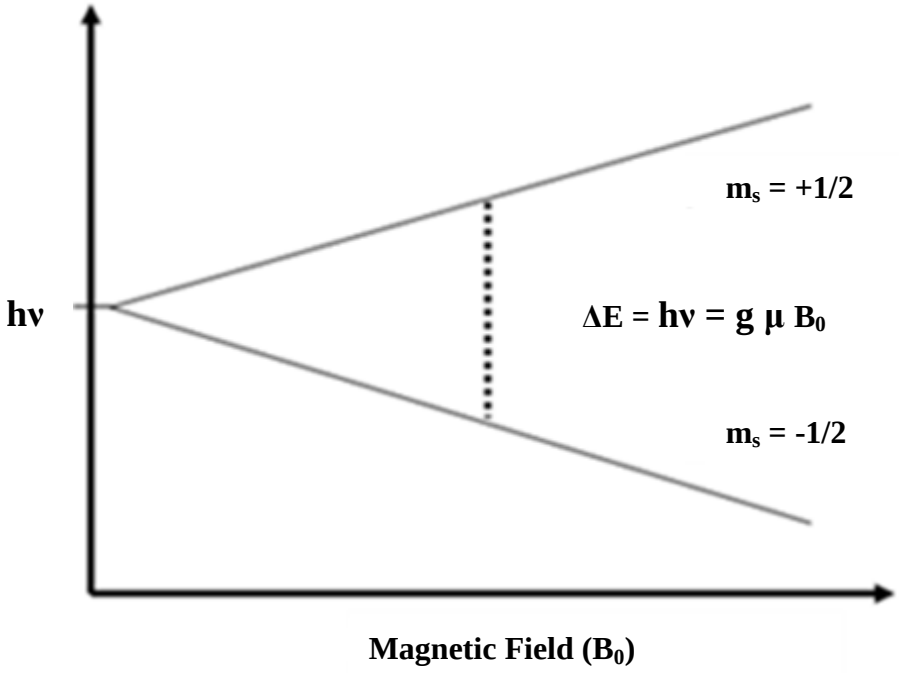

Figure 2.2: Zeeman energy level splitting. The energies of the two spin states of an unpaired electron diverge when the magnetic field is scanned. The magnetic field for which energy difference between the two electrons spin states is equal to hν for the spectrometer, absorption of energy by the spins takes place which is called as resonance.

In **Figure 2.2**, it is shown that in the absence of a magnetic field the two spin states are degenerate and energies of the spin states diverge linearly as the magnetic field is increased. To obtain an EPR spectrum, the electromagnetic radiation frequency (microwave) is held constant and the magnetic field scanned. When the energy difference between the two spins states matches the energy of the applied radiation, absorption occurs **(Figure 2.2).** The field for resonance is not a unique "fingerprint" for identification of a compound because spectra can be acquired at different microwave frequencies (Eaton et al., 2009). However, the g value is independent of the magnetic field.

2.1.2.2 Hyperfine interactions.

Additional information about the species that contains the unpaired electron can be obtained from nuclear hyperfine interactions. The nuclei of the atoms in a molecule or complex often have magnetic moments, which produce a local magnetic field at the electron. The interaction between the electron and the nuclei is called the hyperfine interaction. It gives a wealth of information about the sample such as the identity and number of atoms in molecule or complex that have a magnetic moment; as well as the electron spin density at those nuclei. When an electron spin interacts with a spin ½ nucleus such as hydrogen, the EPR absorption signal splits into two signals (Eaton et al., 2009).

2.1.2.3 Spin label, EPR spectrum of Tau filaments.

For the study of protein structure and dynamics, SDSL in combination with EPR has been systematically developed (Columbus & Hubbell, 2002; Hubbell et al., 1998;

Hubbell et al., 1996; Hubbell et al., 2000a) and this has also proved to be an effective tool in the investigation of tau filaments (Margittai & Langen, 2004; Margittai & Langen, 2006a) and other amyloid fibrils (Margittai & Langen, 2008). The spin label reports faithfully on the conformation of the protein backbone regardless of the size of the investigated species. Nitroxide scanning of a large set of spin labeled protein is done to determine secondary structure (Hubbell et al., 1996). The introduction of the nitroxide side chain is done by a common procedure in which cysteine – substitution mutagenesis is followed by derivatization of the reactive cysteine with a sulfhydryl-selective nitroxide reagent. The reactive native cysteines are first replaced by a suitable non-reactive amino acid. Introduction of this spin label side chain at single sites in the structure results in a remarkably small degree of structural perturbation (Hubbell et al., 1996). For our studies nitroxide label, [1-oxyl-2,2,5,5-tetramethyl-Δ^3 – pyrroline-3-methyl]methanethio-sulfonate (MTSL) was used **(Figure 2.3)** (Berliner et al., 1982). MTSL attached to the cysteine residue has a free electron on the nitroxide group that can be detected in a magnetic field. The four neighboring methyl groups in the C2 and C5 positions of the pyrroline ring dramatically stabilize the radical, making MTSL a reliable reporter over extended periods.

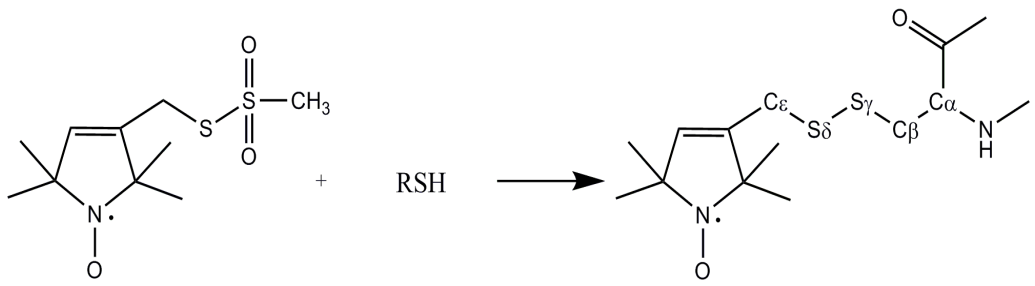

Figure 2.3: Spin labeling of cysteine by nitroxide label. Derivatization of the –SH group of cysteine side chain with MTSL radical by disulfide linkage.

EPR spectrum.

For filament studies, CW EPR measurements at X-band (9.2 – 9.9 GHz) are done, where the incident wavelength is kept constant while the magnetic field is swept. The absorption of electromagnetic radiation is influenced by the nuclear spin of the nitrogen in MTSL resulting in three line EPR spectra. When an electron spin interacts with a spin 1 nucleus (I=1), such as ^{14}N, then the number of hyperfine lines is three (2I+1=3) in the absorption and its first derivative displays. The first derivatives are more commonly depicted than the absorption spectra because of improvement in signal to noise ratio (Eaton et al., 2009). The parameters that are typically extracted from CW EPR measurements include mobility, accessibility, distance and polarity.

Mobility.

In the EPR spectrum, the line shape provides valuable information on the mobility of the label and the local structure (Mchaourab et al., 1996). Line shapes reflect motion, motional anisotropy, environmental polarity, and hydrogen bonding. A line shape denotes an array of interacting parameters and cannot be reduced to a simple descriptive number

reflecting local structure (Altenbach et al., 1990). When the nitroxide label is attached to an unfolded site in the protein, it results in a spectrum with three sharp and narrowly spaced lines with large amplitude **(Figure 2.4 A)**. On the contrary, attachment to an immobilized site results in broad lines, large separation of outer resonances and small amplitude **(Figure 2.4 B)**. When the label is attached to surface-exposed secondary structures and tertiary contact sites, complex lineshapes are seen because of increase in immobilized sites. The spectral features mentioned reflect the mobility of the label. These features are quantified in terms of (1) spectral breadth (the inverse second moment $<H^{-2}>$ and (2) inverse central linewidth ΔH_0^{-1}. These quantifications allow in categorizing individual sites according to various backbone structures (Margittai et al., 2001; Margittai & Langen, 2008; Mchaourab et al., 1996).

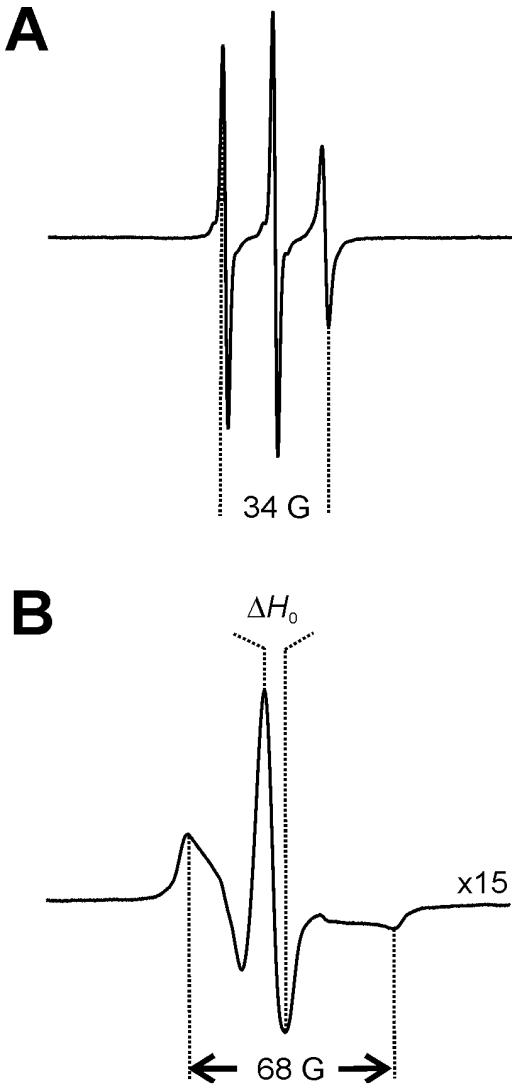

Figure 2.4: EPR lineshapes. (A) Three line spectra with amplitudes are observed when the spin labels are attached to mobile regions. (B) Broad spectra with small amplitudes are seen when spin labels are attached to immobilized regions. The central linewidth is given as ΔH_0. For comparison, the spectrum in (B) is amplified 15-fold. Outer resonance separations are given in gauss (G).

Spin exchange.

The dipolar interactions in slow-motion regime (rigid lattice conditions) causes line broadening of the EPR spectrum because of the proximity of two spin labels (0.7-2 nm). Apart from dipolar interactions, spin exchange due to orbital overlap between multiple paramagnetic centers is also seen (Altenbach et al., 2001; Molin et al., 1980). In this type of spin-spin interaction, the spectral features depend on the number of centers and the spatial arrangement between them. However, spin exchange is not usually observed in SDSL, as multiple spin label contacts are required. But in amyloid fibrils, spin exchange plays an important role.

The appearance of spin exchange narrowed spectra is understood by observing the line shapes for radicals. The EPR spectrum of a nitroxide label shows three sharp lines with an intensity ratio of 1:1:1. Spin exchange results in collapse of the hyperfine lines and narrowing of the spectra as a result of increase in exchange frequency **(Figure 2.5)**. The increased interactions between paramagnetic molecules are seen at high spin label concentrations and reduction of distances between them.

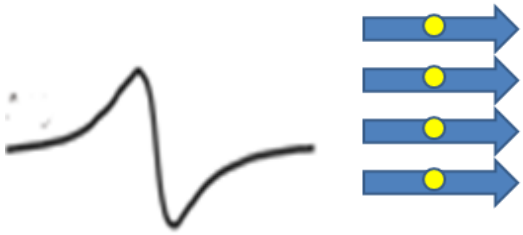

Figure 2.5: Spin Exchange and structural interpretation. Recombinant tau with a single cysteine at position 310 attached with paramagnetic label MTSL. After fibril formation in the presence of heparin and incubation for a period of 12 days, under agitation, EPR measurements were taken. A single-line EPR spectrum is observed because of spin exchange due to stacking of spin labels (yellow) in a parallel in-register arrangement of β strands. The scan width for the spectrum is 150 G.

Biradicals and higher-order radicals with small molecular weights tumble rapidly in solution and as a result averaging of dipolar interactions is seen (Hanson et al., 1996). Crystals and amyloid fibrils do not tumble on EPR time scale and EPR spectra in these systems show spin exchange phenomenon. The spin exchange frequency is $> 10^8$ s^{-1} and it is also retained at lower temperatures (Margittai & Langen, 2004).

Correlation between exchange narrowing of EPR spectrum and tau filament structure reported by SDSL.

The single-line EPR spectrum was first observed in tau filaments, a signature of arrangement of β-strands in parallel and also in-register (Margittai & Langen, 2004). In tau filaments, parallel in-register arrangement of β-strands is seen when identical amino acids are stacked on top of each other along the length of the fiber axis **(Figure 2.5)**. CW EPR studies have also shown that filaments of β-amyloid (Torok et al., 2002), α -synuclein (Chen et al., 2007), IAPP (Jayasinghe & Langen, 2004), β2 microglobulin

(Ladner et al., 2010) and HuPrP (Cobb et al., 2007) also have parallel in-register structure.

At the beginning of this project EPR investigations on the structure of tau filaments had already been done for the 2nd repeat (Margittai & Langen, 2006a) and until amino acid 320 in the 3rd repeat (Margittai & Langen, 2004). In continuation, the complete structural study of the repeat region in 3R and 4R tau was done using SDSL and CW EPR. After this, the same techniques were utilized to understand the composition of tau filaments when mixtures 3R and 4R tau monomers form filaments. The findings of this study have direct implications for the structures of filaments observed in AD and other tauopathies.

2.2 Methods

2.2.1 Site directed mutagenesis.

DNA fragments containing full length tau (htau40) and fetal tau (htau23) were generated by PCR amplification with primers containing *NcoI* and *XhoI* restriction sites. The templates used for these reactions were htau40 in pRK172 (provided by Dr. Goedert at the Medical Research Council Laboratory, Cambridge, UK) and htau23 in pBluescript (provided by Dr. Matt Farrer at the Mayo Clinic, Jacksonville, FL). The fragments were cloned into *NcoI* and *XhoI* restriction sites of prokaryotic expression vector pET-28b and site directed mutagenesis of htau40 (C291S, C322S) and htau23 (C322S) were performed to remove the two native cysteines (Margittai & Langen, 2004). The replacement of cysteine residues with serine residues was shown not to cause any effect on the morphology of tau filaments (Gamblin, et al. 2000). Subsequently the fragments of K18

and K19 were generated in the second set of PCR amplification process from htau40 and htau23 respectively and cloned into *NcoI/XhoI* restriction sites of pET-28b. Using the QuikChange®II Site-Directed Mutagenesis Kit method from Strategene/Agilent Technologies, site-directed mutagenesis was performed to introduce single cysteines in cysteine free htau40 and htau23. The mutant primers for the PCR reaction were ordered from IDT (Integrated DNA Technologies). For the PCR reaction setup, in the PCR tube (0.2 ml, Fisherbrand), 5 µl of 10 X Reaction Buffer (provided in the strategene kit), mutant plasmid 4 µl (5 ng/µL), dNTP (1 µl),*PfuUltra* High Fidelity DNA polymerase (2.5 U/ µl), mutant primers forward and reverse (0.4 µM) were added and the reaction volume was made up to 50 µl using H_2O. The MJ Mini^{TM} Personal Thermal Cycler (BIO-RAD) instrument was used to perform PCR reactions. The PCR temperature parameters are provided in **Table 2**. For the PCR cycling, initial denaturation was done at 95°C. For the annealing of the mutant primer to the DNA template, temperatures were varied from 55-60°C and for the elongation 68°C temperature was used. After PCR amplification, it was important that the parent strand be removed. Parent strand which is methylated was removed by digestion by *DPN1* enzyme (10 U/ µl) which specifically recognizes the methylated sites. The PCR product was incubated with the *DPN1* enzyme (1µl) for 2 hrs at 37°C for the digestion. For better transformation results, the salts in the PCR product were removed by using a purification kit from Genscript (Quickclean 5M PCR Purification kit) **(Appendix B)**.

Table 2
Polymerase Chain Reaction parameters used for tau mutagenesis

Segment	Number of cycles	Temperature(°C)	Time
1	1	95	45 seconds
2	17	95	45 seconds
		55-60	1 minute
		68	12 minutes

Transformation

Transformation of the mutant plasmid was done in XL1 Blue Supercompetent cell lines (Strategene kit). For the transformation 14-ml BD Falcon Polypropylene round bottom tubes were used. To 20 µl of XL1 Blue competent cell lines (Strategene kit), 2 µl of the amplified DNA (PCR product) was added and incubated on ice for 30 minutes. After 30 minutes, heat shock at 42°C was given to cells for 50 seconds. To the cells 800 µl of LB medium was added and incubated in a shaker for 45 minutes at 37°C. The cells were plated onto kanamycin LB agar plates and incubated at 37°C for 24 hrs. The plates were checked for colonies and stored at 4°C.

2.2.2 Plasmid purification, *NcoI* and *XhoI* digestion, DNA sequencing.

A single colony from the kanamycin agar plate was picked and added to 50 ml LB medium, and 30 mM of kanamycin was added to it. The bacteria were allowed to grow for 17 hrs, cells were pelleted and plasmid purification was done using Qiagen® Plasmid Midiprep Kit **(Appendix B)**.

A Cary-100 Bio UV-Vis spectrophotometer from Varian was used to measure the DNA concentration of the purified plasmid. The formula used was Unknown(µg/ml) = A_{260} x 50 µg/ml X dilution factor, where the concentration of pure double stranded DNA, 50 µg/ml shows an absorbance at A_{260} = 1.0.

To check for the correct mutant tau gene size, digestion with *NcoI* and *XhoI* restriction enzymes was performed. For this, 15 µl reaction volume was used. In the PCR tubes, 1500 ng of mutant DNA was mixed with 1.5 µl 10 X BSA, 1.5 µl 10 X NEBuffer 2, 0.5 µl *NcoI* (10,000U/ml), *XhoI* (20,000U/ml) [reagents from NEW ENGLAND *Biolabs®Inc*.]. The samples were incubated at 37°C for 50 minutes. After the digest, the samples were mixed with 4 µl sample buffer (*BIO-RAD* Nucleic Acid Sample Buffer 5X) and agarose gel electrophoresis was carried out in the presence of 250 µl 1X TBE buffer mixed with 10 µl of *EtBr*. For the gel, 1% agarose was used. For the full length tau fragments, *BIO-RAD* EZ Load™ 1 kb Molecular Ruler and for truncated versions, K18 and K19, *BIO-RAD* EZ Load™ 100 bp Molecular Ruler was used to identify the fragments. Agarose gels were viewed under UV light (BIORAD trans illuminator). Based on the correct size of the DNA fragments, mutant plasmids were given for DNA sequencing at University of Colorado Health Science (CU Cancer Center DNA sequencing and Analysis service). Samples submitted to the sequencing facility had 2500 ng of plasmid DNA and 30 pmoles/µl primer concentration. For DNA sequencing, primers T7 promoter (5'-TAATACGACTCACTATAGGG-3') and T7 terminator (5'-GCTAGTTATTGCTCAGCGG-3') from IDT ReadyMade Primer were used.

2.2.3 Expression and purification of tau proteins.

Expression of tau proteins was done in *Escherichia coli (E.coli)* strain BL21 (DE3)**.** An overnight start culture was prepared of *E.coli*. To 50 ml of the LB broth, 30 mM kanamycin was added and a single colony of *E.coli* (having the required tau mutant) was picked and added to the broth. The overnight start culture was incubated at 37°C for 16-17 hrs. To 1.5 L of autoclaved LB broth, 75 µM of kanamycin and 15 ml of the start culture was added and incubated at 37°C in a shaker until the bacterial growth reached an optical density between 0.8-1. After this, 1.0 mM of IPTG was added to each flask to induce protein expression. The *E.coli* expression phase was for about 3.5 hrs. The bacterial cells were spun down at 6000 x g for 20 minutes. The bacterial pellet was taken up in resuspension buffer (20 mM Pipes, pH 6.5; 500 mM NaCl, 1 mM EDTA, 50 mM β-mercaptoethanol) and kept at -80°C for further processing. Tau protein is extremely heat stable (100°C, 5 minutes) (Weingarten et al., 1975). The heat stability and the high isoelectric points of tau protein were utilized in the purification process (M. Margittai & Langen, 2004).The cells were ruptured by heating at 80°C for 20 minutes and then sonicated for 60 sec using Fisher scientific sonifier (150 T series) at amplitude 3.

The samples were immediately centrifuged at 15,000 x g for 30 minutes. To the supernatant, ammonium sulfate (55-60% m/V) was added to precipitate the proteins. After 1 h of salting out, the precipitate was centrifuged at 15,000 x g for 10 minutes. Resuspension of the precipitate was carried out in H_2O with 2 mM Dithiothreitol (DTT) added to it. The solution was sonicated for 30 seconds, syringe filtered using Life Sciences Acrodisc® Premium 25 mm Syringe filter with GxF/0.45 µm GHP membrane

and further diluted with H_2O (2 mM DTT) before loading onto the column to bring down the conductivity of the solution. The instrument used for purification of tau protein was AKTA design GE Healthcare Fast protein liquid chromatography (FPLC). Tau proteins were purified using cation exchange chromatography based on their isoelectric points. The buffers used for cation exchange chromatography were Buffer A and Buffer B with 20 mM Pipes (pH6.5) in them. The low pH of the buffer helps to increase the positive charge of the tau protein. Proteins were loaded onto the Mono S column (GE Healthcare) and eluted by applying NaCl gradient (Barghorn & Mandelkow, 2002). The program used for purifying proteins by ion exchange and gel filtration is given in **Appendix D**. Protein fractions were analyzed on SDS-PAGE with BIORAD® SDS-PAGE broad range marker as the standard. To 6 µl of the elution fraction 2 µl of the 4X sample buffer (SB) was added and loaded onto 15% SDS-PAGE gel for truncated tau and 12% SDS-PAGE gel for full length tau. For the separation of the proteins a Mini PROTEAN II electrophoresis chamber (BIORAD) was used. The gel was stained using Coomassie blue and destained using Destain solution **(Appendix A)**. The correct protein fractions were pooled and then stored at -80°C after the addition of 5mM DTT. To further purify the tau protein samples, gel filtration (Superdex 200 column) was carried out using Tris buffer (pH 7.0). Protein fractions were collected and precipitated overnight at 4°C by adding an equal volume of methanol with 5 mM DTT to the pooled fractions of full length tau. To the truncated K18 and K19, three fold excess of acetone with 5 mM DTT was added. The samples were pelleted and redistributed into equal aliquots. After centrifugation of the

protein aliquots at 15,000 x g for 10 minutes, protein pellets were stored at -80°C in methanol (2 mM DTT) for full length tau and acetone (2 mM DTT) for K18 and K19.

2.2.4 Spin labeling and filament assembly of tau proteins.

The organic solvent was removed from the stored protein pellets (4-6 mg). The pellets were solubilized in 200 µl GndHCl and reacted with an ~10 fold molar excess of either paramagnetic label MTSL or nonparamagnetic [1-acetyl-2,2,5,5-tetramethyl-Δ^3 – pyrroline-3-methyl]methanethio-sulfonate (Gross et al., 1999). Both the chemicals were purchased from Toronto Research Chemicals, Downsview, Canada. To attach the labels to the single cysteine, proteins were incubated for 1 h at 25°C in the dark. The proteins were passed over PD-10 desalting columns (GE Healthcare) using elution buffer (EB) to remove all denaturant and unreacted labels. Protein concentration of htau40 and htau23 were measured in 6 M GndHCl by UV absorption at 276 nm **(Appendix C)** while K18 and K19 concentration measurements were done using BCA assay (Pierce) **(Appendix E)**.

To set up the proteins for filament formation, 20-30 µM of protein was mixed with heparin (molecular mass ≈5,000 Da, Celsus, Cincinnati, OH) at a protein to heparin molar ratio of 4:1. The full length and the truncated versions were incubated at 25°C under constant stirring for 12 and 3 days, respectively. For all mixing experiments, final protein concentrations were 50-60 µM and the protein: heparin molar ratio of 4:1 was maintained. After filament formation, they were pelleted by ultracentrifugation at 100,000 x g for 30 minutes and finally washed with EB.

2.2.5 Measurement of spin labeled filaments by EPR spectroscopy.

2.2.5.1 EPR measurement parameters.

Protein pellets were transferred into borosilicate capillaries (0.6-mm inner diameter X 0.84 mm outer diameter, VitroCom, Mountain Lakes, NJ). Measurements were carried out in a Bruker EMX spectrometer fitted with an ER 4119HS resonator. The experimental parameters for taking the spectra were sweep width 150 G. The microwave bridge parameters attenuator 12 dB, incident microwave power 12 milliwatts were used. In the signal channel, the receiver gain was set at 5.02×10^3, modulation frequency at 100 kHz, modulation amplitude for filaments was set at 3 G and for monomers it was set at 1.5 G. The modulation phase was set at 0 deg. The offset was 0%, time constant 81.92 msec, conversion time 20.48 msec, sweep time 41.49 sec, harmonic 1, resolution 2048 were set.

Data analysis was done using the software "A labview program for multicomponent CW EPR spectra" by Christian Altenbach, University of California, Los Angeles. Spectra were normalized to the same number of spins using double integration. A minor background originating from <0.5% soluble tau was subtracted from all spectra.

2.2.6 Negative stain electron microscopy.

To view the tau filaments using electron microsope, carbon coated copper with 250 mesh grids (EM grid) (Electron Microscopy Sciences) were used. The EM grids were placed for 40 seconds on 10 µl drops of tau filaments (3-4 µM). The EM grids were removed and adsorbed onto the filter paper before placing them on 10 µl drops of 2% uranyl acetate for 40 seconds. The grids were subsequently air-dried on filter paper for 10

minutes. All images were taken with Phillips/FEI Tecnai-12 electron transmission microscope operating at 80 keV equipped with a Gatan 2k x 2k CCD camera at University of Colorado, School of Medicine, Cell and Developmental Biology Department.

2.3 Results

2.3.1 Defining the stable ordered core in filaments of htau40.

Previous investigations on the conformation of tau filaments have revealed that the third repeat of tau consists of a highly ordered core with parallel, in-registered arrangement of β – strands (Margittai & Langen, 2004). These studies had been done up to residue 320, which is the first half of the 3rd repeat. To look at the residues beyond 320 and to understand the structure, the naturally occurring cysteine at position 322 was labeled with paramagnetic nitroxide label MTSL. The cross-linking of the nitroxide label through a thiol linkage to the protein resulted in a new side chain R1 **(Figure 2.6 A)**. Before starting SDSL, the native cysteines were removed and replaced with serines to maintain the selectivity of the approach (Todd et al., 1989).

When this labeled monomeric protein was measured, it produced an EPR spectrum of three sharp lines (hyperfine splitting of EPR spectrum because of nitrogen atom) characteristic of intrinsically disordered regions **(Figure 2.6 B**, left panel**)**. After the induction of tau monomers to form filaments with heparin and 12 days of incubation under agitation at room temperature (25°C), EPR measurement showed a single line spectrum **(Figure 2.6 B**, right panel**)**. This spectrum is the signature feature for parallel, in-register arrangement of β-strands (Margittai & Langen, 2008; Margittai & Langen,

2004). The results showed that the ordered core region extends beyond the previously published region (Margittai & Langen, 2004).The presence of filaments was confirmed by negative stain electron microscopy **(Figure 2.6 C)**.

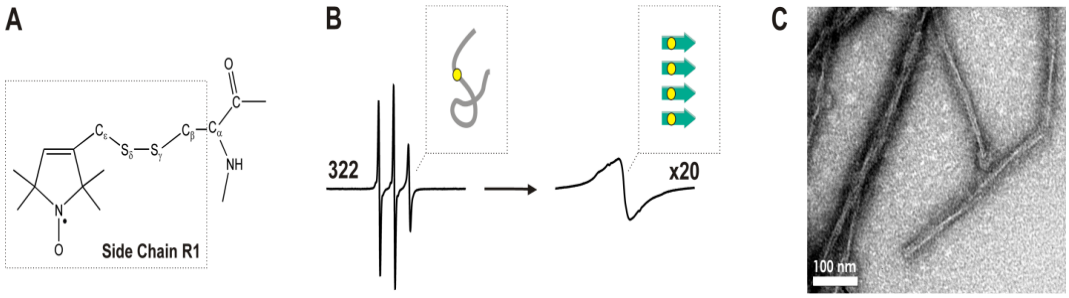

Figure 2.6: Structural analysis of htau40 spin-labeled at position 322. (A) Labeling of a cysteine in the protein with the paramagnetic label (1-oxy-2,2,5,5-tetramethyl-D-pyrroline-Δ3-methyl)-methanethiosulfonate results in the side chain R1. (B) Monomeric tau, labeled at position 322, produces a spectrum with three sharp lines (left) characteristic for random structure (left insert). Formation of filaments results in a spectrum with a single line indicative of crystal-type order with parallel, in-register arrangement of β-strands (right insert). (C) Negative stain electron microscopy reveals twisted filaments with 15-20 Å diameter. Bar = 100nm (Siddiqua & Margittai, 2010)

After seeing the parallel in-register structure at position 322, starting from position 321 to 358, single cysteine residues, introduced by site-directed mutagenesis were spin labeled. The CW spectra of labeled monomeric proteins showed three sharp lines, which indicated a predominance of random structure **(Figure 2.7)**. These findings demonstrate that tau is an intrinsically disordered protein which is in good agreement with previous studies (Cleveland et al., 1977; Schweers et al., 1994). After the addition of heparin, filaments were allowed to form from tau monomers. When the CW EPR spectra of the filaments were measured, significant changes in the line shape of the spectra were observed. Based on the observed EPR spectra, the tau filament could be divided into two

distinct regions **(Figure 2.8 A)**. The first region (residues 321-336), which extends to the end of repeat 3, gives rise to single-line spectra which makes this region a part of the highly ordered core. The second region (residues 337-358) which is a part of the 4th repeat produces spectra with single lines (e.g., 348), three lines (e.g., 346), or mixtures of both single and three lines (e.g., 357).

Such spectral heterogeneity was previously observed in the 2nd repeat of the full length tau (htau40) where single amino acid substitutions had caused a conformational switch between stacked and disordered conformations. Based on this, it was concluded that the 2nd repeat is less stable and an independent domain (Margittai & Langen, 2006a). In line with the parallel, in-register arrangement of β-strands in the 2nd repeat, introduction of β-branched residues promoted folding whereas the introduction of charged residues prevented folding.

The 4th repeat showed a similar trend. The substitution of a charged amino acid, for example, Asp-348 with cysteine and cross linking with the spin label resulted in a single-line spectrum (representing ordered structure), whereas substitution of hydrophobic amino acid (Val-350) produced a three-line spectrum (representing disordered structure). Replacement of the amino acids with cysteines in the 3rd repeat region inadvertently resulted in a single line spectrum. The signal amplitude increases linearly with increasing amounts of mobile component (Margittai & Langen, 2006a; Margittai & Langen, 2006b). An amplitude plot **(Figure 2.8 B)** shows low mobility for residues in the 3rd repeat and varied mobility for residues in the 4th repeat. These data, combined with previous observations (Margittai & Langen, 2004), reveal a stable, highly

ordered core structure of the 3rd repeat which is flanked by marginally stable regions that can switch between conformationally distinct states.

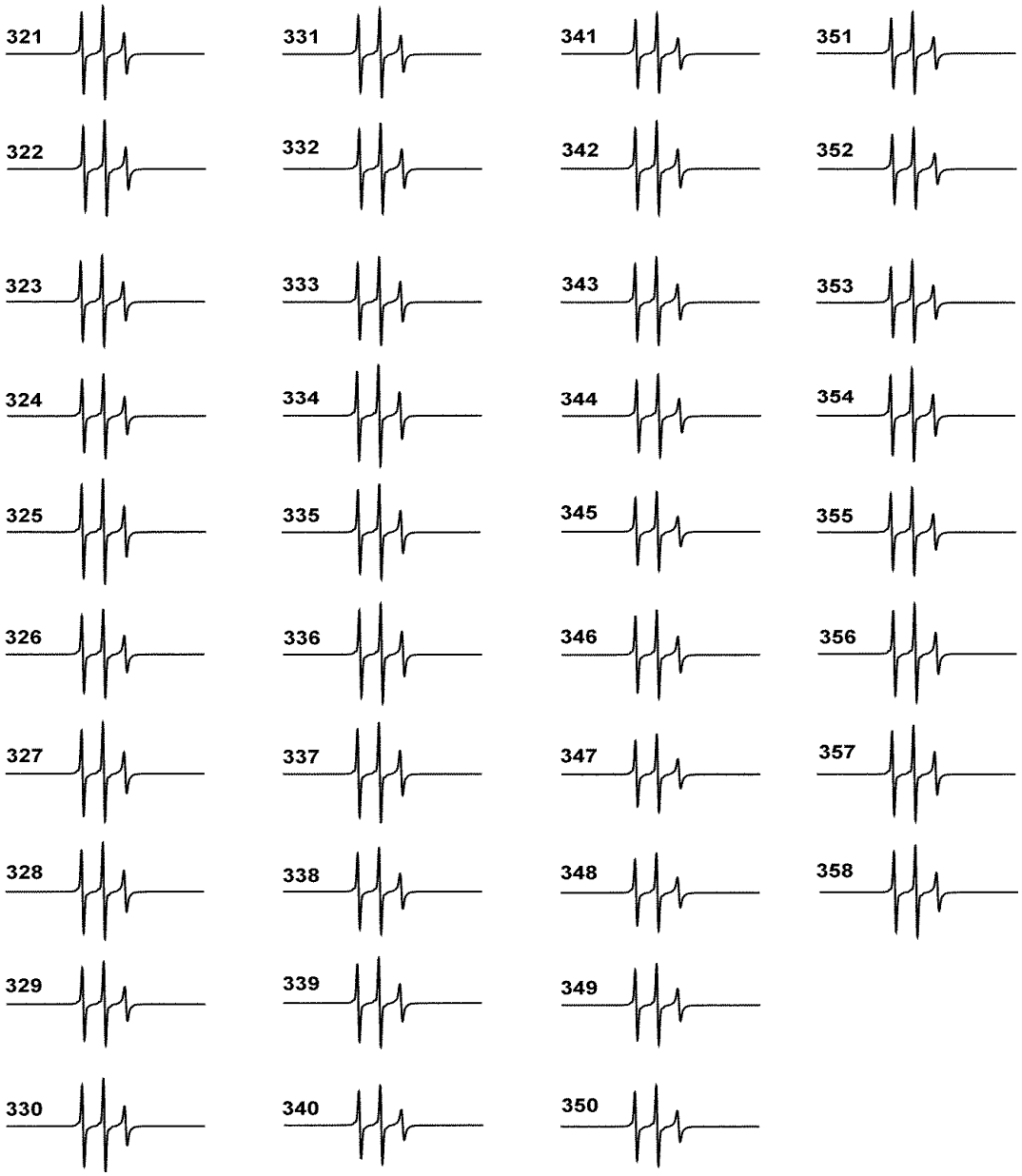

Figure 2.7: EPR spectra of htau40 monomers. Single cysteine mutants of htau40 (residues 321-358) were labeled with paramagnetic probe MTSL. All spectra were taken at 150 G and normalized to the same number of spins. All spectra show three sharp lines, which indicate a random coil structure (Siddiqua & Margittai, 2010).

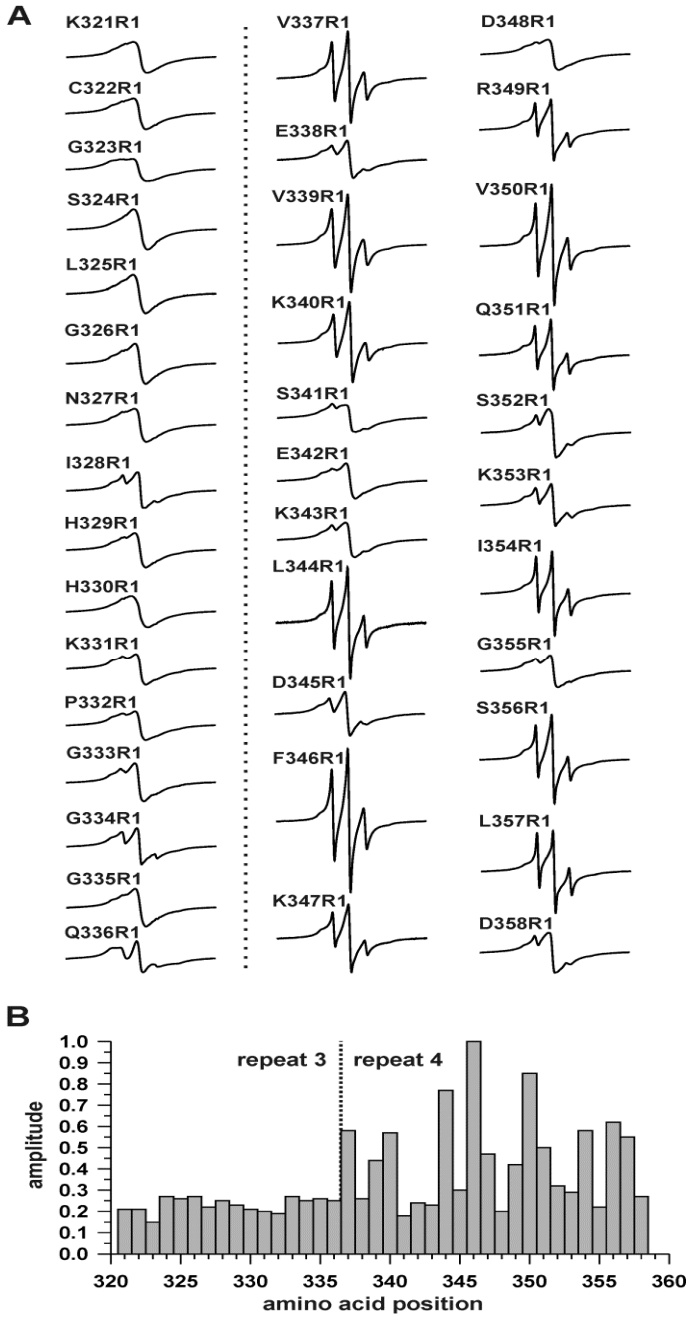

Figure 2.8: EPR analysis of spin-labeled htau40 filaments. (A) Residues 321-358 were individually replaced by the side chain R1. All spectra were taken at 150 G and normalized to the same number of spins. The *dotted line* between the *left* and *middle columns* marks the boundary between repeats 3 and 4. (B) The amplitudes of all EPR spectra are plotted against the respective residue numbers. All amplitudes are normalized to spectrum F346R1, which has the highest amplitude (Siddiqua & Margittai, 2010).

2.3.2 Preservation of core structure in htau23 and smaller tau fragments.

Investigations thus far have focused solely on the largest isoform htau40 which has four microtubule binding repeats. To understand whether the fetal tau htau23 (three microtubule binding repeats) has similar ordered core structure, six different cysteine positions in the 3rd repeat (positions 309, 310, 311, 317, 322 and 326) were spin labeled. All monomeric proteins produced EPR spectra with three sharp lines **(Figure 2.9)**. This observation is in good agreement with the current data which shows that soluble tau is intrinsically disordered. The filament formation from monomeric tau was carried out by addition of heparin and then incubating the sample for 12 days. Filaments were harvested by centrifugation and transferred into EPR capillaries for measurement. EPR spectra of the spin labels at the six investigated positions were all single line **(Figure 2.10**, left column**)**, indicating parallel, in-register arrangements of β-strands.

The smaller fragments of tau, K18 and K19 have been used in the past as valuable models of tau aggregation (Barghorn & Mandelkow, 2002). To understand whether the smaller fragments reveal similar structural arrangement, the same set of single cysteine mutants were created and spin-labeled. The spin-labeled proteins in their monomeric form showed three sharp lines in their EPR spectrum and the filaments showed a single line spectrum **(Figure 2.10,** middle & right column**)**. These results are similar to full length tau isoforms. This indicates that the parallel, in-register arrangement of β-strands is an intrinsic feature of the repeat region and maybe a common theme in all filaments of isoforms and constructs containing the stable 3rd repeat.

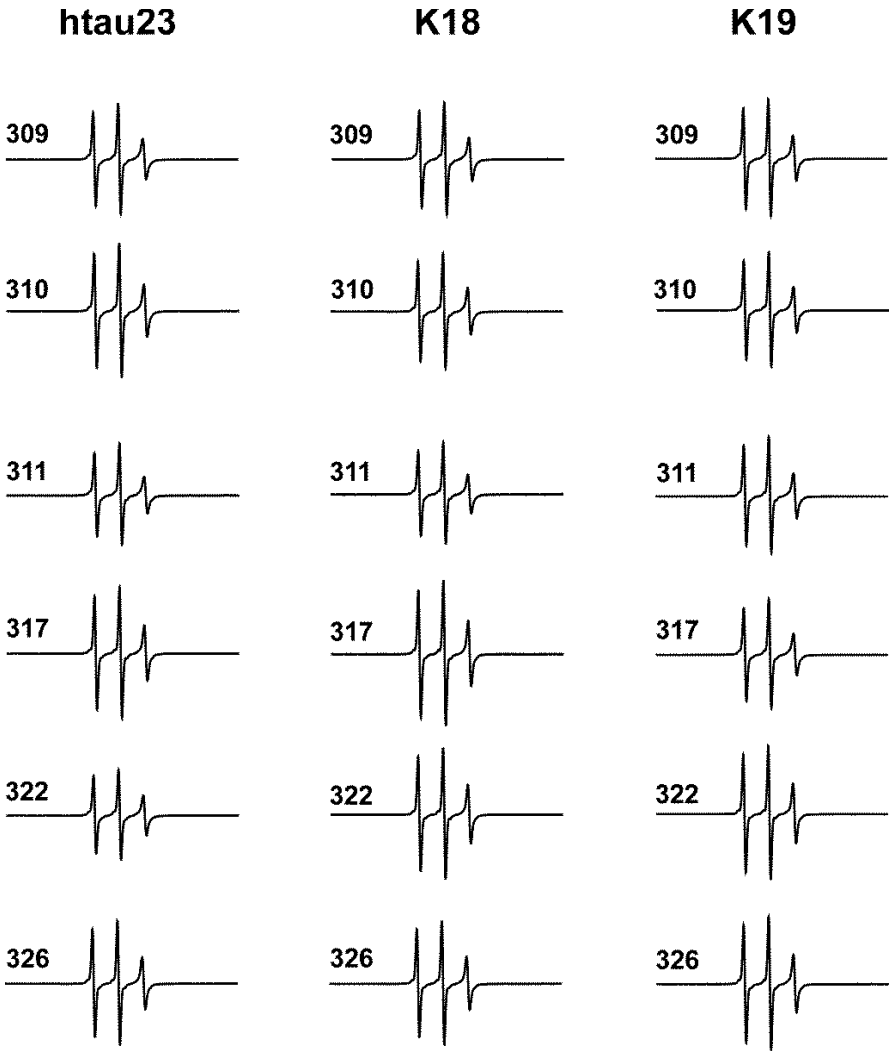

Figure 2.9: EPR spectra of htau23, K18 and K19 monomers. Single cysteine mutants in the 3rd repeat were labeled with paramagnetic probe MTSL. All spectra were taken at 150 G and normalized to the same number of spins. All spectra show three sharp lines which indicate a random coil structure (Siddiqua & Margittai, 2010).

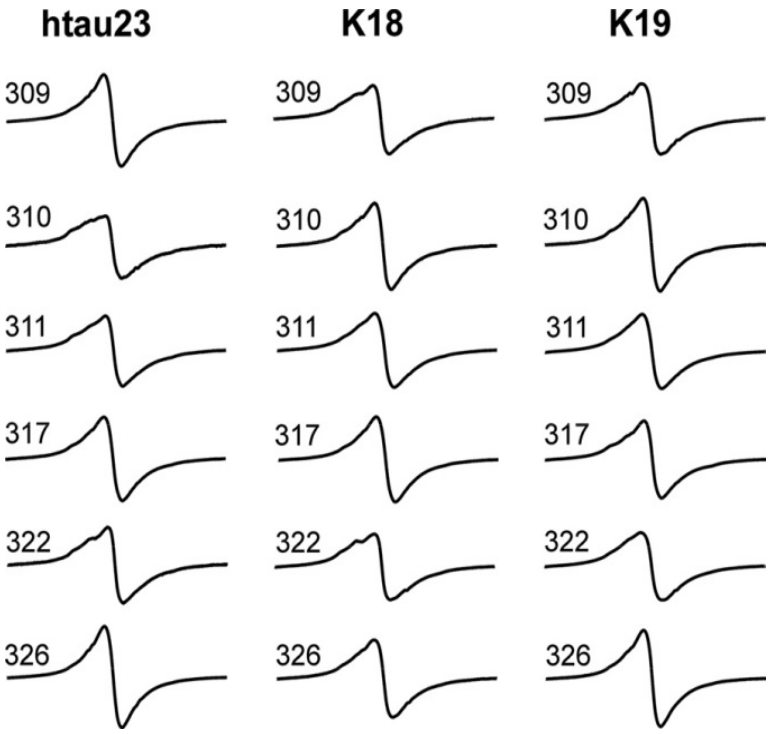

Figure 2.10: EPR spectra of filaments of htau23, K18, and K19. Residues in the third repeat of htau23, K18, and K19 were replaced by cysteine attached to the paramagnetic side chain R1. Spectra of all filaments were recorded at 150 G scan width and normalized to the same number of spins (Siddiqua & Margittai, 2010).

2.3.3 3R and 4R tau combine to form heterogeneous filaments.

The above data shows that the filaments formed from 3R and 4R tau are structurally similar. The question that arose from this was whether these constructs could assemble into mixed filaments. To answer this question, in the first step, a paramagnetic label at position 310 of K18 was attached. A nonparamagnetic label (which produces no EPR signal) at position 310 of K19 was attached which resulted in a R1' side chain (Gross et al., 1999). The two proteins were subsequently mixed at different molar ratios and heparin was added for fibrillization. After 3 days of incubation at 25°C under agitation condition, all filaments were pelleted at 100,000 x g and transferred into EPR

capillaries. At low spin concentration (10% R1), a three – line EPR spectrum was observed **(Figure 2.11 A**, red trace**)** with outer peak separation of 68 G. Such a spectrum is typical for an immobilized site with little interaction between spin labels (Margittai & Langen, 2006a; Margittai & Langen, 2006b). At intermediate spin concentration (60% R1), the spectrum broadened and the amplitude of the central peak decreased **(Figure 2.11 A**, green trace**)**. These changes are due to dipolar interactions between labels, which are effective at distances between 0.8 and 2.5 nm (Hubbell et al., 2000b). At high spin concentration (100% R1), a single-line spectrum with increased amplitude was observed **(Figure 2.11 A**, black trace**)**. This spectrum is due to spin exchange between labels in close contact (Margittai & Langen, 2008). The observation of a three-line EPR spectrum at low spin concentration (10% R1) suggests that K18 had coassembled with K19. Segregation into separate filaments can be excluded as this would have retained the contacts between individual spin labels resulting in a single-line spectrum. To obtain a more comprehensive picture of the coassembly between K18 and K19, a titration series was performed in which the concentration of K18R1 was successively increased from 5 to 100%. The EPR spectra of filaments were taken and amplitudes of the central lines were plotted as a function of the mole percent of K18R1 **(Figure 2.11 B)**. The amplitude changes are similar to those that had been previously observed in other spin dilution experiments (Margittai & Langen, 2004; Margittai & Langen, 2008). Depending on the type of spin interaction that dominates at a particular dilution, different amplitudes are obtained: 1) large amplitudes for no interaction, 2) small amplitudes for dipolar coupling, and 3) slightly elevated amplitudes, and loss of hyperfine splitting, for spin exchange

(Figure 2.11 A). These changes occur gradually as the concentration of paramagnetic label increases and the average distance between individual labels decrease. Various spacing between labels in the differently composed filaments **(Figure 2.11 B**, insets I-III**)** can explain these amplitude changes. An amplitude plot that is similar to the one depicted here is obtained when instead of K18, K19 is attached to the paramagnetic label **(Figure 2.12)**. This suggests that K18 and K19 have similar probabilities of integrating into the filaments. To identify the core structure of heterogeneous filaments, equimolar ratios of paramagnetically labeled K18 and K19 were mixed. A single-line EPR spectrum was observed **(Figure 2.11 C)**, suggesting a crystal-type order with parallel, in-register arrangement of β-strands. Electron micrographs confirmed the presence of twisted and bundled filaments **(Figure 2.11 D)**. As expected, no amorphous aggregates were observed for sample with single line EPR spectrum (Margittai & Langen, 2004).

In the adult brain full length versions of tau isoforms htau40 and htau23 are present. To look at their ability to coassemble, the same labeling strategy of K18/K19 constructs was used. The htau40 was paramagnetically labeled while htau23 was labeled with non paramagnetic label. The assembled filaments produced similar spectra to those of the smaller constructs **(Figure 2.11 E, compare with 2.11 A)**. Accordingly, the amplitude plot obtained from a titration series of these isoforms revealed the same overall features **(Figure 2.11 F)** as the one obtained for K18 and K19 **(Figure 2.11 B** and **Figure 2.12)**. Furthermore, filaments formed from an equimolar mixture of paramagnetically labeled htau40 and htau23 produced a single-line spectrum **(Figure 2.11 G)**. The presence of filaments and absence of amorphous aggregates was confirmed by negative

stain electron microscopy **(Figure 2.11 H)**. These results demonstrate that regardless of construct size, 3R and 4R tau coassemble into heterogenous filaments with a core containing parallel, in-register arranged β-strands (Margittai & Langen, 2006a).

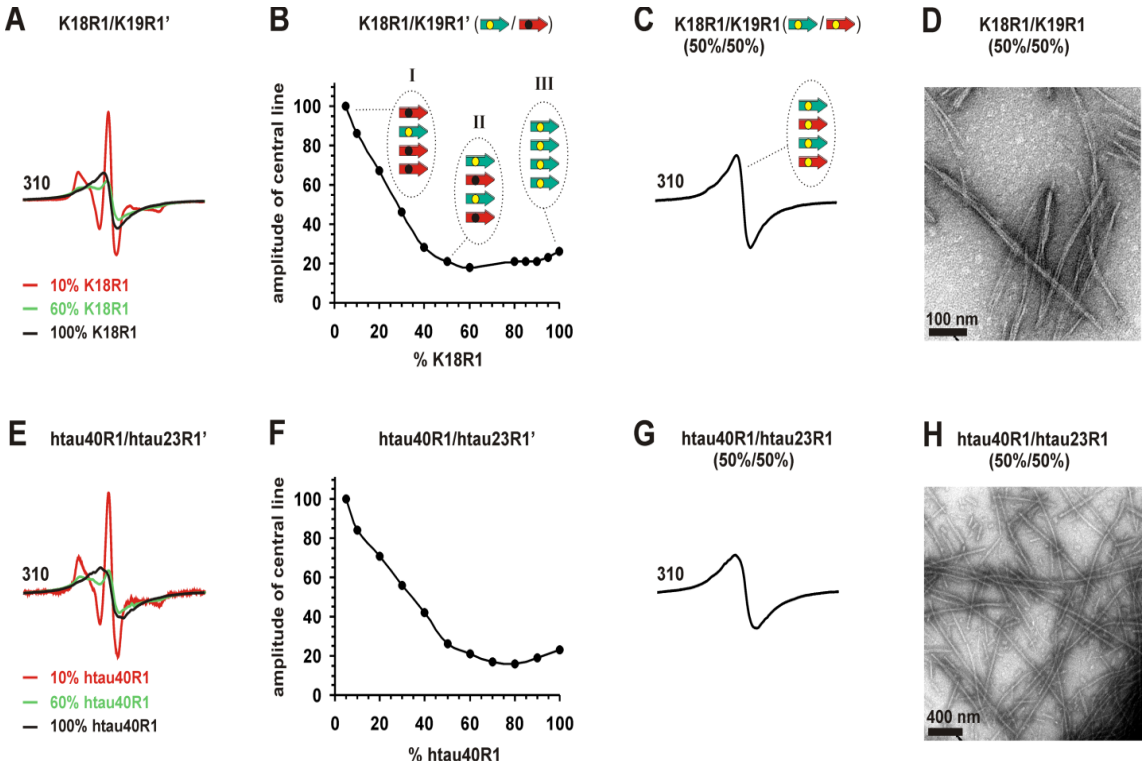

Figure 2.11: Coassembly of 3R and 4R tau. (A) EPR spectra of tau filaments coassembled from K18R1 (paramagnetic) and K19R1' (nonparamagnetic). The following mole percentages were used: 1) 10% K18R1/90% K19R1' (red trace), 2) 60% K18R1/40% K19R1'(green trace), and 3) 100% K18R1 (black trace). In both constructs, labels were attached to position 310. (B) The amplitudes of the central lines of the EPR spectra in A together with those of additional dilutions are plotted as a function of the mole percent of K18R1. Regions in the plot in which spectra are dominated by no spin interactions, by dipolar coupling, or by spin exchange are interpreted in terms of different β-strand combinations (insets I–III). K18R1 = green arrow, yellow dot; K19R1' = red arrow, black dot. (C) Spectrum of filaments formed from 50% K18R1 and 50% K19R1 (labels attached to position 310). The inset provides a structural interpretation. K18R1 = green arrow, yellow dot; K19R1 = red arrow, yellow dot. (D) Electron micrograph of heterogeneous filaments (K18R1/K19R1). Bar = 100 nm. (E) EPR spectra of filaments formed from htau40R1 and htau23R1' (all labels attached at position 310). Dilutions have same color coding as in A. (F) Amplitudes of central lines from filaments formed at different dilutions of htau40R1 and htau23R1'. (G) Spectrum of filaments formed from 50% htau40R1 and 50% htau23R1. All spectra were taken at 150 G and normalized to the same number of spins. (H) Electron micrograph of htau40R1/htau23R1 filaments. Bar = 400 nm (Siddiqua & Margittai, 2010).

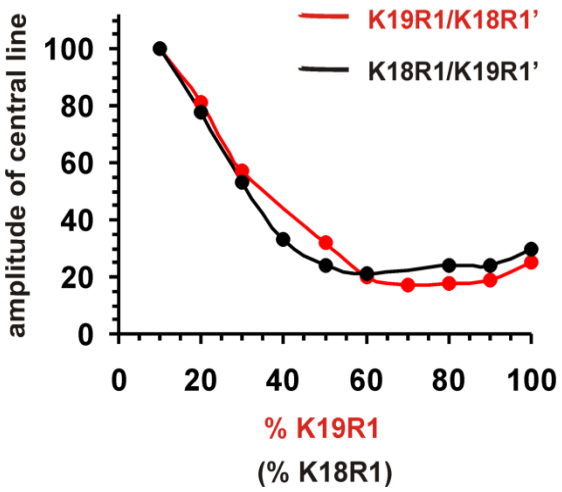

Figure 2.12: Coassembly of K19R1 and K18R1' into heterogeneous filaments. Filaments were coassembled from K19R1 and K18R1'. EPR spectra were collected and amplitudes of central lines were plotted as a function of the mole percent of K19R1 (red trace). For comparison, the amplitudes from spectra of filaments formed from different ratios of K18R1 and K19R1' (see Figure 2.12B) are also plotted (black trace). The amplitude derived from the spectrum of filament from K19R1/K18R1' (10%/90%) is arbitrarily set at 100 (Siddiqua & Margittai, 2010).

2.4 Discussion

Tau filaments are the pathological hallmark of numerous tauopathies. In most diseases, filaments are composed of either 3R or 4R tau, but in AD, filaments contain all isoforms. The isoform composition of tau filaments was determined twenty years ago (Goedert & Spillantini, 2006; Greenberg et al., 1992) but it was not clear whether the 3R and 4R isoforms in AD form homogeneous or heterogeneous filaments (Adams, et al., 2010). This information is important as either aggregate could imply fundamentally different mechanisms of tau fibrillization. This study involved obtaining molecular insights into the structure of different tau filaments and to address the question of single-filament composition. First, it was demonstrated that homogeneous filaments of both 3R and 4R tau share a highly ordered core structure that coincides with the third repeat and is

characterized by parallel in-register arrangement of β-strands. This conformation is preserved regardless of whether full-length isoforms (htau40 and htau23) or smaller constructs (K18 and K19) are used. Second, when 3R and 4R tau are present in the same sample they coassemble into heterogenous filaments. This was seen for both the full length tau and the truncated versions of tau. Because the heterogeneous filaments contain the same ordered third repeat core structure as their homogeneous counterparts, the third repeats of 3R and 4R tau must be able to replace each other. Together, these results suggest that at least three fundamentally different types of tau filaments exist: 1) filaments of 3R tau, 2) filaments of 4R tau, and 3) filaments of 3R/4R tau **(Figure 2.13)**. This classification is based on composition and places emphasis on the core-forming repeat regions.

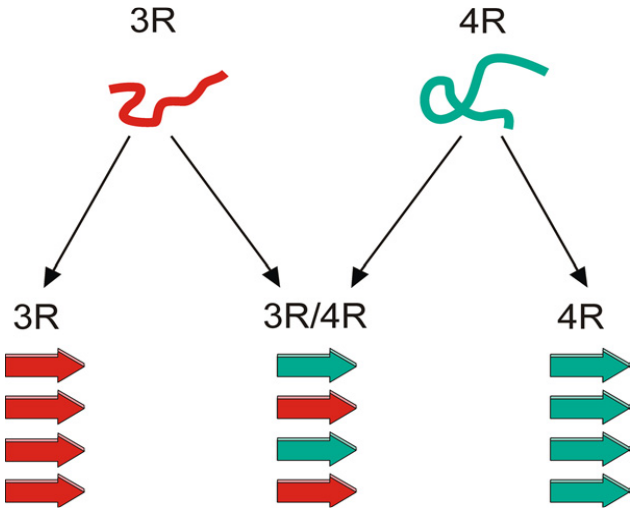

Figure 2.13: Types of tau filaments. 3R tau (*red*) and 4R tau (*green*) assemble into at least three different types of filaments: 1) homogeneous filaments of 3R tau, 2) homogeneous filaments of 4R tau, and 3) heterogeneous filaments of 3R and 4R tau. All filaments have in common a parallel, in-register arrangement of β-strands in repeat 3 (Siddiqua & Margittai, 2010).

Each 3R and 4R tau can represent three different isoforms that are defined by the inclusion or exclusion of the two inserts in the N-terminal region **(Figure 1.1)**. This region is in the unstructured periphery of the filament and may not contribute to the stable core (Wischik et al., 1988). It is evident from the experimental data that each filament type can be further classified into subtypes composed of different isoforms at various ratios. Dilution experiments have shown that 3R and 4R tau coassemble at different ratios tested. As a consequence, a staggering number of filaments exist based on composition alone. Despite a shared parallel, in-register arrangement of β-strands, all three types of filaments must vary in conformation. This is because the second repeat of 4R tau contributes to the filament core (Li et al., 2002; Margittai & Langen, 2006a). Its presence or absence results in different packing interactions for each filament type. For example, in heterogeneous 3R/4R filaments, the second repeat cannot solely pack against itself. Hence, 4R tau will assume different conformations depending on whether it is incorporated into homogeneous or heterogeneous filaments. Conformational plasticity of 4R tau was seen when htau40 assumed different structures grown onto wild type filaments as opposed to mutant filaments (Frost et al., 2009). Conformational plasticity is a common property of amyloid proteins resulting in structurally distinct fibrils of homogeneously composed proteins (Colby et al., 2009; Kodali, et al., 2010a; Paravastu et al., 2008; Petkova et al., 2005; Tanaka et al., 2004a). It is likely that similar structural polymorphisms exist for each type of tau filament. Compositional diversity and conformational plasticity allow for a plethora of tau filament structures that may exceed those of other amyloid fibrils.

Ample experimental evidence suggests that phenotypic diversity in prion diseases is encoded in different misfolded conformations of the same protein (Bessen & Marsh, 1994; Collinge et al., 1996; King & Diaz-Avalos, 2004; Tanaka et al., 2004a; Telling et al., 1996). Fragmentation and growth properties of different fibrils have provided a physical basis of how protein conformation could determine phenotype (Colby et al., 2009; Tanaka et al., 2006). As pointed out before, the filaments in different tauopathies have characteristic compositions of 3R and 4R tau. Filaments in Pick's disease contain 3R tau. Filaments in progressive supranuclear palsy and corticobasal degeneration contain 4R tau. Filaments in AD incorporate both 3R and 4R tau. Since 3R and 4R tau coassemble in heterogeneous filaments, in AD, the filaments could be different from those of 3R and 4R tauopathies. It was previously shown that filaments in AD contain roughly equimolar ratios of 3R and 4R tau (Goedert et al., 1992a). This ratio reflects the expression pattern of tau in the adult human brain (Goedert et al., 1989a; Goedert et al., 1992a; Goode et al., 2000). Hence, the majority of individual filaments in AD brain may be composed of evenly mixed 3R and 4R isoforms. However, because the expression patterns of tau isoforms can vary between different neuronal subpopulations (Goedert et al., 1989a), the specific composition of individual tau filaments could vary in a cell-specific manner. The free interchangeability of 3R and 4R tau allows for a broad spectrum of heterogeneous filaments with diverse physical and biological properties.

Even though the repeat region in tau may determine the stability of filaments (Jeganathan et al., 2008), the N-terminal inserts could still influence the interactions with cellular components. Here, we demonstrate that 3R and 4R tau can coassemble into

heterogeneous filaments, expanding the number of possible filament structures. If future experiments corroborate interneuronal spreading of tau misfolding in a prion-like fashion (Goedert et al., 2010), the large compositional and conformational diversity of tau filaments could be an important contributor to the large phenotypic diversity of tauopathies.

Apart from composition of 3R and 4R in tau filaments, the recruitment of 3R and 4R monomers into filaments could also cause conformational diversity. The next chapter deals with the recruitment process of 3R and 4R into filaments and how it enhances the conformational diversity of tau filaments.

Chapter Three: Variations in Seeded Recruitment of 3R and 4R Tau Monomers into Filaments

3.1 Introduction

As already mentioned, in the adult human brain 3R and 4R tau coexist at an equimolar ratio (Goedert et al., 1989a) and this ratio is also reflected in the tau proteins found in the filamentous inclusions of Alzheimer's disease (Goedert et al., 1992a). Abundant tau inclusions, in the absence of β-amyloid deposits, define Pick's disease, progressive supranuclear palsy, corticobasal degeneration and other diseases. In contrast to AD, filaments in progressive supranuclear palsy contain only 4R tau and filaments in Pick's disease contain only 3R tau (Buée & Delacourte, 1999). The molecular basis for this difference in tau deposition in neurodegenerative diseases is not yet understood and maybe understanding the recruitment of 3R and 4R tau monomers into filaments would give a clue of why this difference in deposition of 3R and 4R is seen in various diseases.

3.1.1 Nucleated versus seeded tau filament formation.

In vitro assembly of tau filament formation (as that of other amyloid fibrils) depends on the assembly of a critical nucleus onto which individual monomers can grow **(Figure 3.1)**. This nucleation event requires the cooperative interaction of a few monomers to form oligomers which constitutes an initial lag phase in the formation of filament. Also this nucleation event is concentration dependent. After the nucleation

process, filament elongation is a fast process. The nucleation event marks the rate – limiting step of fibril formation that can be circumvented by the addition of seeds (Friedhoff et al., 1998; Nonaka et al., 2010). These *in vitro* aggregation features makes this fibril assembly broadly similar to that of amyloid fiber aggregation in AD or other aggregation processes in different neuronal disorders (Friedhoff et al., 1998).

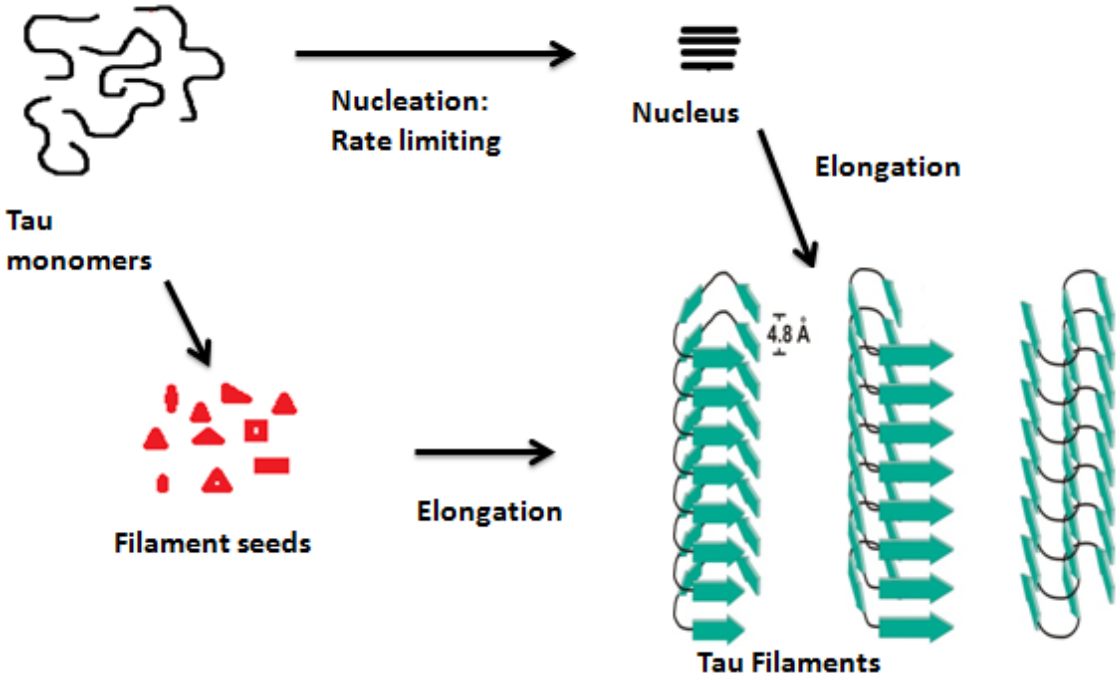

Figure 3.1: Nucleated versus seeded formation of tau filaments *(Not drawn to scale).*

3.1.2 Spread of tau filaments.

There are various reasons for studying seeded *in vitro* reactions. Studies have shown that filaments can transfer among neighboring cells in tissue culture (Frost et al., 2009). The injection of brain extract from mutant P301S tau-expressing mice into the

brain of transgenic wild-type tau-expressing animals was shown to induce the assembly of wild-type human tau into filaments and the spread of pathology from the site of injection to neighboring brain regions (Clavaguera et al., 2009). Also studies in mice have shown that cognitive impairment becomes manifested when tau inclusions reach the hippocampus from other regions of the brain. These abundant neocortical tau inclusions and extracellular β-amyloid deposits found in mouse brain resembles the pathology seen in AD (Clavaguera et al., 2009).

Recent studies have shown that the introduction of minute quantities of misfolded tau filaments into tau-expressing cells rapidly recruits large amounts of soluble tau into filamentous inclusions resembling NFTs. This efficient recruitment of tau monomers into filaments suggests a "seeding"-recruitment process as a highly plausible mechanism underlying NFT formation *in vivo* (Guo JL & Lee VM, 2011). The spontaneous uptake of tau filaments into cells is most likely mediated by endocytosis, suggesting a potential mechanism for the propagation of tau lesions in tauopathy brains (Guo JL & Lee VM, 2011).

Analysis of diseased brain tissues of humans have shown that in the disease process neuronal tau inclusions first appear in the transentorhinal cortex, from where they spread to the hippocampus and neocortex (Braak & Del Tredici, 2011). The spreading of tau filaments is reminiscent of the (interneuronal) spreading of prions, which raises the important question of whether prion-like mechanisms are responsible for tau pathogenesis (Goedert et al., 2010; Prusiner, 1998). Prion diseases, unlike tauopathies, are infectious. However, infectivity and interneuronal transmissibility of prions are

thought to be based on a single molecular principle: recruitment of monomeric proteins onto the filament ends. Understanding this recruitment process for tau may provide important molecular insights into the interneuronal spreading of tauopathies.

3.1.3 Study of recruitment of tau monomers into filaments

To study the recruitment of 3R and 4R tau monomers by seeds of tau filaments, truncated versions of full length isoforms K18 and K19 were used **(Figure 1.1)**. As the aggregation kinetics of K18 and K19 is faster than that of full length htau40 and htau23, the former constructs have been used as model systems for the aggregation of 3R and 4R tau (Barghorn & Mandelkow, 2002).

3.1.3.1 Study of tau aggregation.

Previous studies on aggregation kinetics of proteins into amyloid fibrils have been done using Thioflavin T assay (Khurana et al., 2005). This assay uses thioflavin T (ThT), a thiobenzaldehyde dye which associates rapidly with aggregated fibrils of synthetic peptides and gives rise to a new excitation (ex) (absorption) maximum at 450 nm and enhanced emission (em) at 482 nm, as opposed to the 385 nm (ex) and 445 nm (em) of the free dye (Levine III, 1993). This change is dependent on the aggregated state as monomeric or dimeric peptides do not show this effect (Levine III, 1993). Also thioflavin T, has been visualized bound along the fibrils using atomic force microscopy (Khurana et al., 2005).

For our studies of kinetics of aggregation of tau monomers into filaments a fluorescence assay using acrylodan was standardized. Acrylodan is an environment sensitive dye and its behavior in solvents is explained in the following section.

3.1.3.2 Monitoring of General solvent effects on Acrylodan by Fluorescence Spectroscopy.

The general solvent effects on acrylodan fluorophore can be explained by a Jablonski diagram **(Figure 3.2)**.

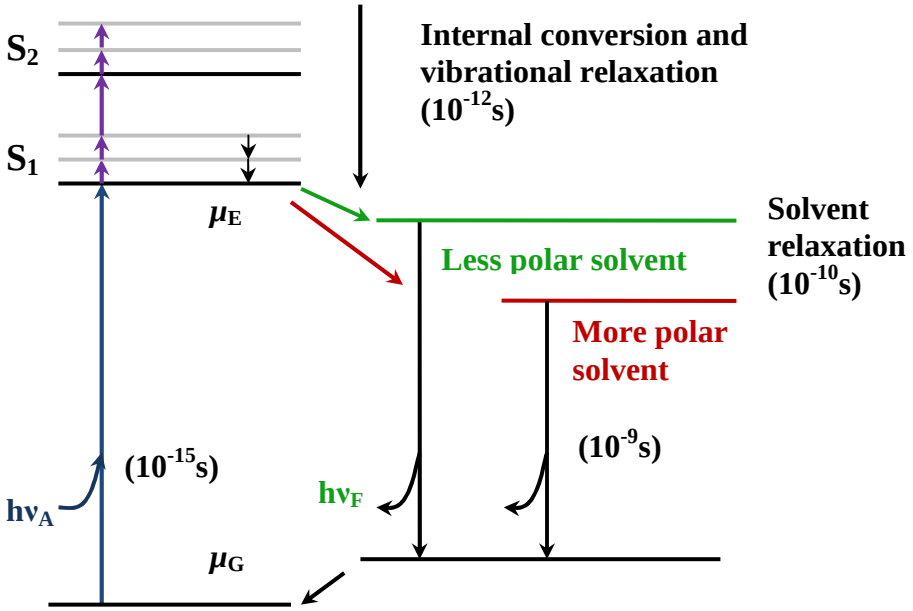

Figure 3.2: Jablonski diagram for fluorescence with solvent relaxation.

Fluorescence is the emission by a fluorophore of a photon from the lowest excited state S_1 to the ground state S_0. Emission of a photon occurs with a certain energy E and which can be observed at a certain wavelength λ_{em}. Because of the vibrational levels fluorescence is seen at longer wavelengths than the first singlet absorption. Solvents also have an effect on the position of the fluorescence band and many studies on biomacromolecules have exploited this fact. One aspect of the solvent effect is the General solvent effect which depends on the polarizability of the solvent, and increasing

the dielectric constant usually shifts the fluorescence to longer wavelength **(Figure 3.2)**. General solvent effects involve the interaction of the permanent dipole moment of the molecule in both the ground and excited states with the reactive field induced in the surrounding solvent.

The Franck-Condon principle states that during electronic transitions nuclei do not move, but the electrons of the solvent molecules redistribute themselves around the new excited state dipole. Also, because of the long lifetime of the excited state (10^{-8} s), before the emission of the fluorophore, the solvent molecules reorient to their equilibrium position around the excited state of the fluorophore **(Figure 3.3).**

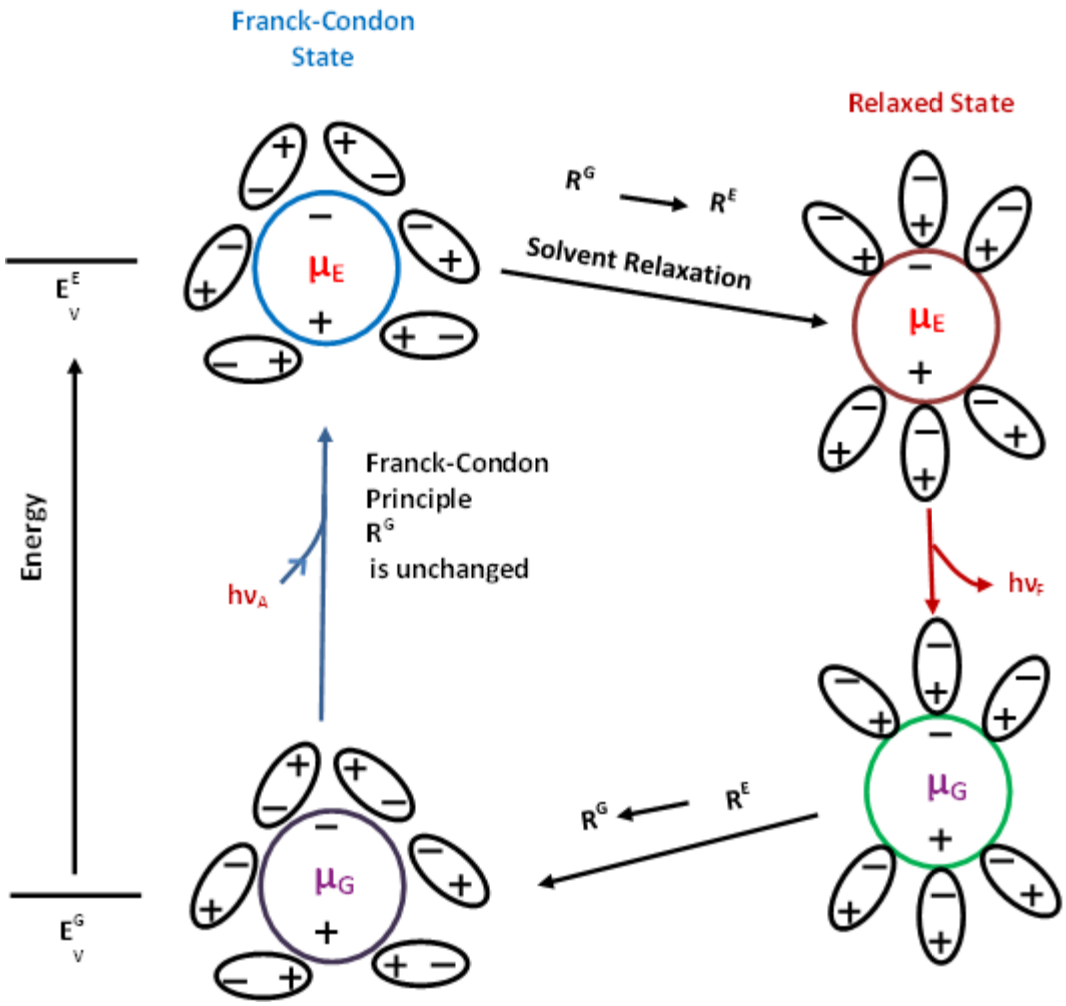

Figure 3.3: Dipole in a dielectric medium. The effects of electronic and orientation reactions fields on the energy of a dipole in a dielectric medium, $\mu_E > \mu_G$, where μ_E and μ_G are the excited and ground-state dipole moments respectively of the electrons.

The dipole moments of the ground (μ_G) and excited-state (μ_E) and the reactive fields around these dipoles describe the interaction of a fluorophore with solvent. Solvent reorientation (R^G and R^E) and electronic motions define these fields **(Figure 3.3)**. E_v describes the energy levels of the fluorophore in the vapor state. The electronic reaction field which is induced by the excited state dipole causes the decrease of the absorption

transition energy. This occurs because the electrons in the solvent follow the rapid change in the electron distribution within the fluorophore as shown in **Figure 3.3**. On the contrary, the orientation of the solvent molecules, during the absorption of light does not change.

Tau filament aggregation was studied by attaching the acrylodan fluorophore to the cysteine residue in the monomer. Since the acrylodan fluorescence emission is highly sensitive to its local environment, when bound to a protein it exhibits changes in both intensity and emission wavelength that reflect the degree of solvent exclusion and the effective dielectric constant of the environment of the fluorophore (Hibbs et al., 2004; Wearsch et al., 1998).

3.2 Methods

3.2.1 Site directed mutagenesis, protein expression and purification.

Site directed mutagenesis, protein expression and purification were done using the protocols given in chapter 2 sections 2.2.1, 2.2.2 and 2.2.3.

3.2.2 Seed production.

In a 2 ml eppendorf vial, 1500 µl of 25 µM cysteine free K18 and K19 (or a combination of 12.5 µM K18 and 12.5 µM K19) were mixed with a twofold molar excess of heparin (50 µM) (average molecular mass of 5000 Da, Celsus, Cincinnati, OH) and allowed to grow under agitation at room temperature (25°C) for 3 days. Subsequently, the filaments (500 µl) were kept on ice for half an hour and then sonicated on ice for 20 seconds using Fisher Scientific Sonifier (150 T Series) at power setting 3. The seed morphology was verified by negative stain electron microscopy **(Figure 3.4)**. For

multiple steps of seeded reactions, filament formation was allowed for 1 h and then they were sonicated to produce seeds for the next reaction.

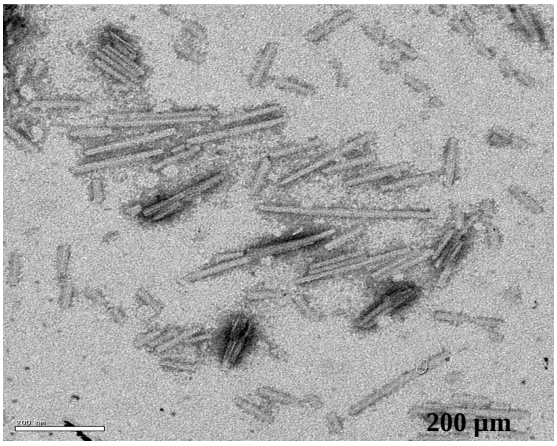

Figure 3.4: **Electron micrograph of filament seeds**. The filament seeds are produced by ultrasonic shearing of seeds.

3.2.3 Seeding assay and fluorescence detection.

3.2.3.1 Acrylodan assay.

The following mole percentages were used for all reactions: 2% acrylodan-labeled tau, 98% cysteine-free tau. The final concentration of monomeric proteins K18 and K19 was 10 µM. For the fibrillization process 2 fold molar excess of heparin to tau was added. Initiation of the seeding reactions was done by the addition of 3 mol% seeds. Experiments that required multiple cycles of seeding and elongation contained higher concentration of monomers (25 µM) and larger mole percentages of seeds (8%). After one hour of fibrillization, each reaction was sonicated to produce seeds for the next reaction cycle. The final seeding step in this multicycle procedure contained 3 mol% seeds and 10 µM monomers. All reactions were monitored in a Fluorolog 3 system (Horriba, Jobin). Temperatures were controlled at 37°C using a solid state Pelletier

element. The fluorophore was excited at 360 nm and single emission spectra were measured from 400-600 nm with excitation and emission slit widths set at 5 nm.

3.2.3.2 Thioflavin T seeding assay.

The filament formation was monitored by the change in ThT fluorescence upon ThT binding to tau filaments (Maskevich et al., 2007; Naiki et al., 1989). Reactions were carried out in a HEPES buffer (100 mM NaCl, 10 mM HEPES, pH 7.4) at 37°C, with 5μM ThT. Tau (10 μM K18 or K19) was pre-incubated for 5 min at 37°C, whereupon reactions were initiated with 3 mol% of respective seeds. All reactions contained two fold molar excess of heparin (average MW = 5000) to monomeric tau. Fluorescence was measured using a Fluorolog 3 spectrofluorometer (Horiba Jobin Yvon), with the excitation wavelength set at 440 nm and the emission wavelength set at 480 nm. The excitation and emission slit widths were 5 nm.

3.2.4 Negative stain electron microscopy.

The method used here has already been mentioned in Chapter 2 section 2.2.6. The tau filament concentration used was 10 μM.

3.3 Results

3.3.1 Seeds of 3R/4R Tau Nucleate the Formation of 3R and 4R Tau filaments.

In the previous chapter we showed that the mixing of 3R and 4R tau monomers causes them to coassemble into heterogeneous filaments rather than segregate into separate filaments. Whether these coassembled filaments can effectively seed the

propagation of individual 3R and 4R tau monomers is not known. For the studies, acrylodan was cross-linked to a single cysteine **(Figure 3.5 A)** at position 310 in the third repeat of K19. This site was chosen as it is located in the core of the filament (Andronesi et al., 2008; Margittai & Langen, 2004) and as such is expected to have different polar environments in monomers versus filaments. Furthermore, spin-labeling of the site had no measurable effect on overall structure as shown in chapter 2. The reaction with acrylodan resulted in a new side chain, henceforth referred to as A1. For the filament formation, the labeled protein was mixed with a 50-fold molar excess of cysteine-free K19. The fluorophore labeled sample was excited at 360 nm and the emission spectrum was measured from 400 – 600 nm. The emission spectrum had a maximum at 523 nm **(Figure 3.5 B)** which is characteristic of a solvent exposed site (Wearsch et al., 1998). This result is in agreement with tau being an intrinsically disordered protein (Cleveland et al., 1977; Schweers et al., 1994).

The addition of seeds that were produced by ultrasonic shearing of K18/K19 filaments and heparin (2 fold molar excess to the protein) initiated the aggregation of tau monomers. Upon completion of the fibrillization process, the emission spectrum blue shifted to 462 nm **(Figure 3.5 B)**, indicating label exposure to a more hydrophobic environment (Wearsch et al., 1998). The reciprocal of the wavelength for the emission maximum was plotted as a function of time revealing elongation kinetics of K19 **(Figure 3.5 C)**. Similarly, when K18 was allowed to grow on K18/K19 seeds the elongation kinetics were similar to K19 on K18/K19 seeds. In the absence of seeds, aggregation of neither K18 nor K19 on K18/K19 seeds was seen. The presence of filaments in the

seeded reactions was confirmed by negative stain electron microscopy **(Figure 3.5 D, E)**. Together, these findings suggest that the filaments of 3R/4R tau serve as seeds for the formation of 3R and 4R tau filaments.

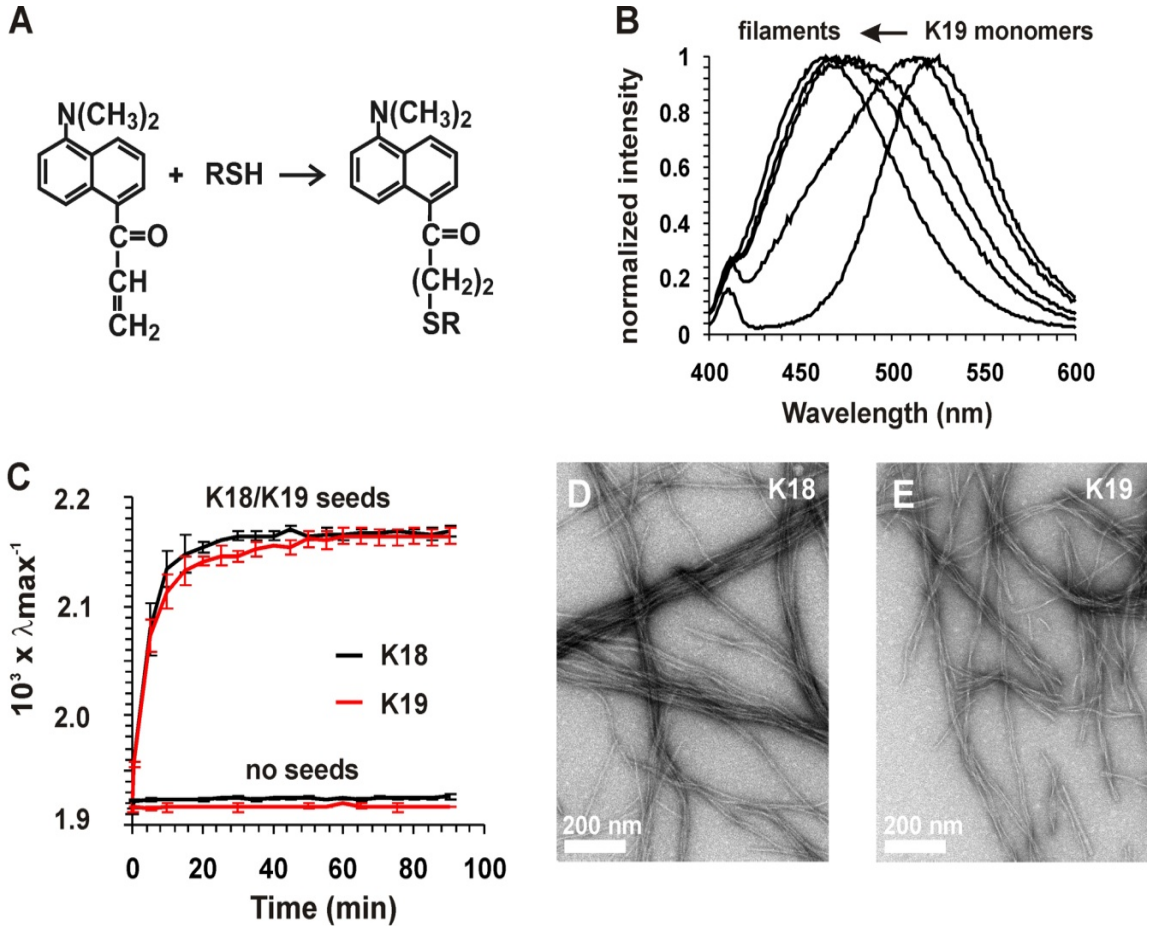

Figure 3.5: Seeds of K18/K19 effectively template growth of K18 and K19. (A) Scheme of acrylodan labeling of cysteine side chain. (B) Addition of 3% K18/K19 seeds to a mixture of monomers of 98% K19 and 2% K19_310A1 (total concentration: 10 µM) results in a time-dependent blue shift in the emission maximum. Traces from right to left represent reactions after 0, 0.5, 5, 10, and 80 min. Excitation: 360 nm, Emission: 400-600nm. (C) The reciprocal of wavelength plotted as a function of time reveals the progression of K19 (red trace) and K18 (black trace) aggregation. In the absence of seeds no changes are observed. Values represent mean ±s.d (n = 3 experiments). (D, E) Electron micrographs of K18 and K19 filaments produced through K18/K19 seeded reactions (Dinkel et al., 2011).

3.3.2 Cross-seeding barrier prevents growth of 3R tau onto 4R tau seeds.

When compared to K18, K19 lacks the 2nd microtubule binding repeat **(Figure 1.1B)**. To determine whether this variation affects the filament conformation, the seeding properties of K18 and K19 filaments were tested. In the first set of experiments, the elongation kinetics of K18 and K19 on K18 seeds was monitored. The acrylodan fluorophore was attached to position 310 of both K18 and K19 to report the fibrillization process. A 50-fold molar excess of K18 and K19 cysteine-free protein was mixed with K18_310 A1 and K19_310 A1 respectively. The results showed that K18 grew on K18 seeds while K19 did not grow on K18 seeds **(Figure 3.6A)**. An increase in the concentration of seeds by 3- or 5-fold did not lead to incorporation of K19 monomers on K18 seeds, which indicates a robust conformational barrier **(Figure 3.7 A)**. The attachment of label to different positions of the K19 was checked to see whether this conformational barrier was due to labeling at position 310 **(Figure 3.7 B)**. These labeled K19 monomers (317, 322) also failed to form filaments. Electron micrographs confirmed this seeding behavior as filaments were observed for K18 **(Figure 3.6 B)**, but not for K19 **(Figure 3.6 C)**. In the next step, seeds from K19 were produced, and K18 and K19 allowed to grow on them. Both K18 and K19 grew on K19 seeds but the incorporation of K19 monomers was markedly more efficient **(Figure 3.6 D)**. The filamentous nature of the aggregates was confirmed by electron microscopy **(Figure 3.6 E, F)**. In order to verify the seeding properties of K18 and K19 independently, all experiments were carried out using an extrinsic thioflavin T based assay **(Figure 3.8 A, B)**. The same asymmetric barrier was observed. Furthermore, replacement of the truncated monomers with full-

length versions of tau (htau23 and htau40) produced similar seeding characteristics, albeit with slower kinetics **(Figure 3.9 A, B)**. Combined, these data suggest that conformational differences between filaments of 3R and 4R tau allow growth of 4R tau onto 3R tau seeds but prevent the growth of 3R tau on 4R tau seeds.

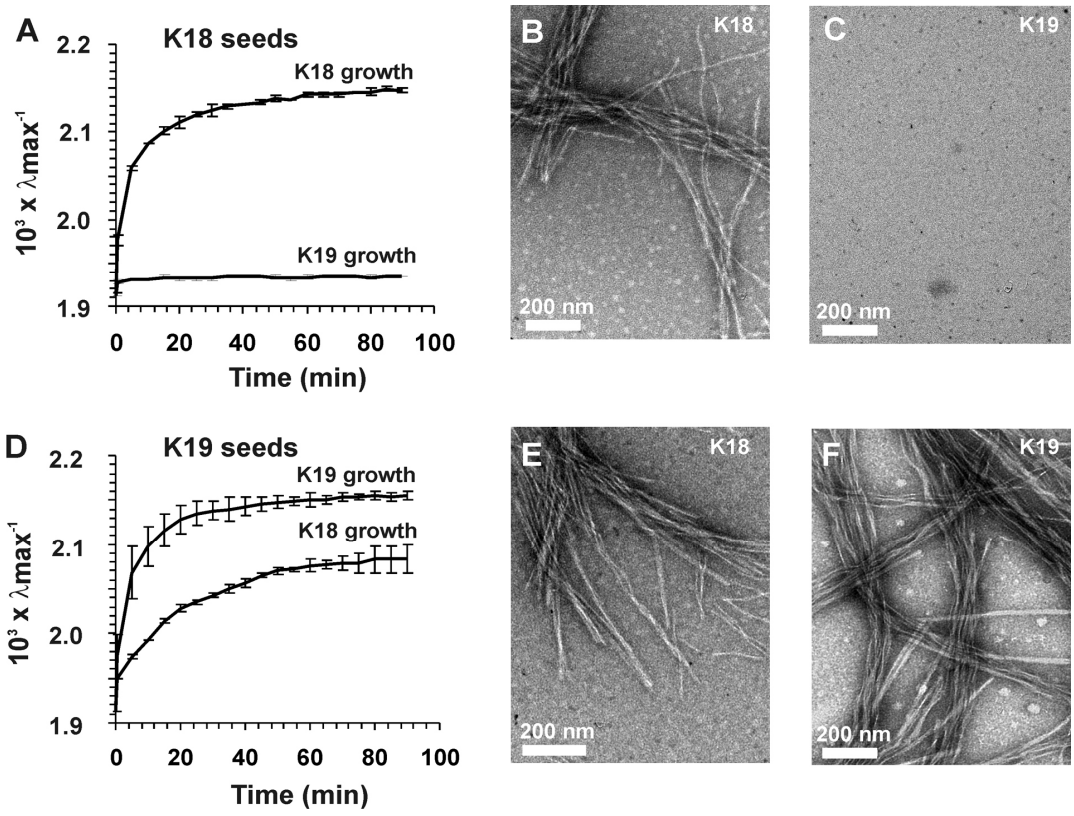

Figure 3.6: Asymmetric barrier for K18 and K19 cross-seeding. (A) Aggregation of K18 monomers (98% K18, 2% K18_310A1) and K19 monomers (98% K19, 2% K19_310A1) in the presence of 3% K18 seeds. (B) Electron micrograph of K18 filaments seeded with K18. (C) Electron micrograph of K19 grown onto K18 seeds. (D) Aggregation of K19 monomers (98% K19, 2% K19_310A1) and K18 monomers (98% K18, 2% K18_310A1) in the presence of 3% K19 seeds. (E) Electron micrograph of K18 grown onto K19 seeds. (F) Electron micrograph of K19 grown onto K19 seeds. Protein concentrations were 10 μM. All values represent mean ±s.d. (n = experiments) (Dinkel et al., 2011).

A

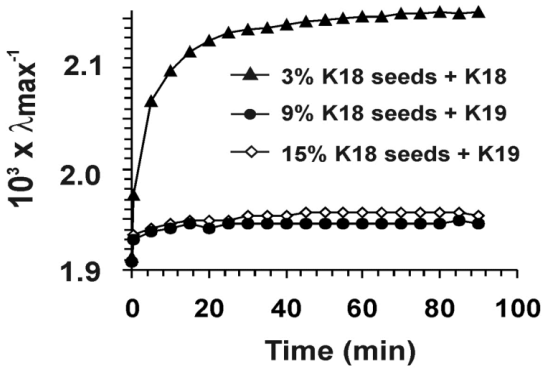

B

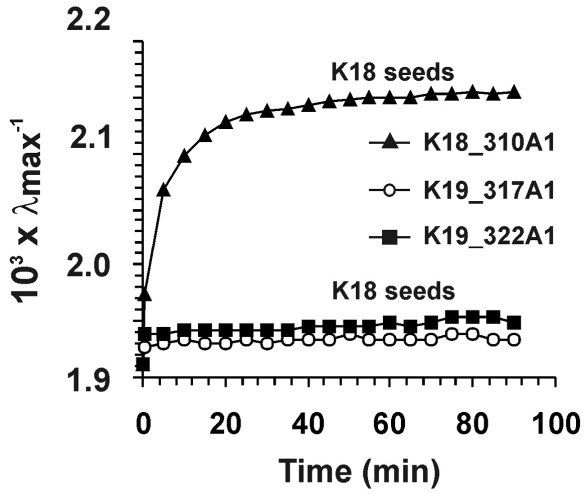

Figure 3.7: Robust asymmetric barrier for K18 and K19 cross-seeding. (A) A robust barrier prevents growth of K19 monomers onto K18 seeds. Circles = 9% seeds, diamonds = 15% seeds. Growth of K18 monomers onto 3% K18 seeds (triangles) is reproduced from figure 3.6 A and shown for comparison. In all samples acrylodan is attached to position 310. (B) K19 aggregation monitored through acrylodan-labeled constructs K19_317A1 (circles) and K19_322A1 (squares) indicates that regardless of the position that is labeled, K19 does not grow onto K18 seeds. Growth of K18 onto K18 seeds (triangles) is depicted for comparison. In all cases 3% seeds are added to 10 µM monomers (Dinkel et al., 2011).

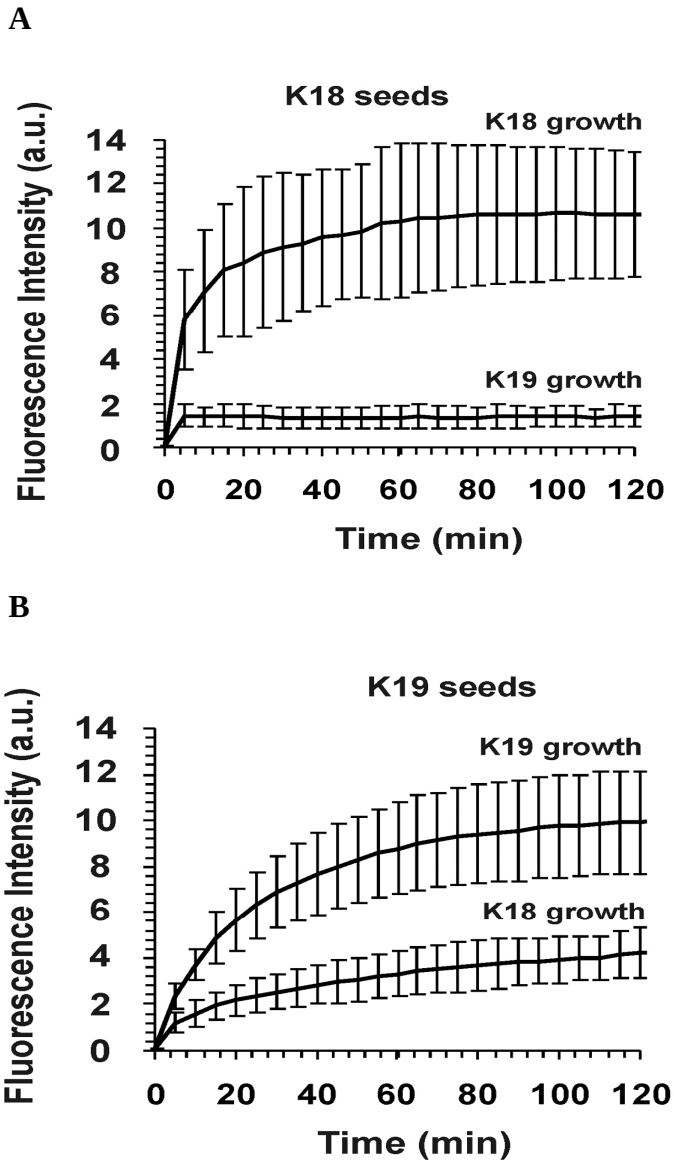

Figure 3.8: Seeded filament growth monitored with Thioflavin T (5 µM).
(A) Changes in fluorescence intensity indicate that K18 monomers grow onto K18 seeds, but K19 monomers do not. (B) ThT fluorescence reveals growth of K19 monomers onto K19 seeds and reduced growth of K18 monomers onto K19 seeds. In all ThT experiments, 3% seeds are added to 10 µM monomers. All values in A, B represent mean ± s.d. (n = 3 experiments) (Dinkel et al., 2011).

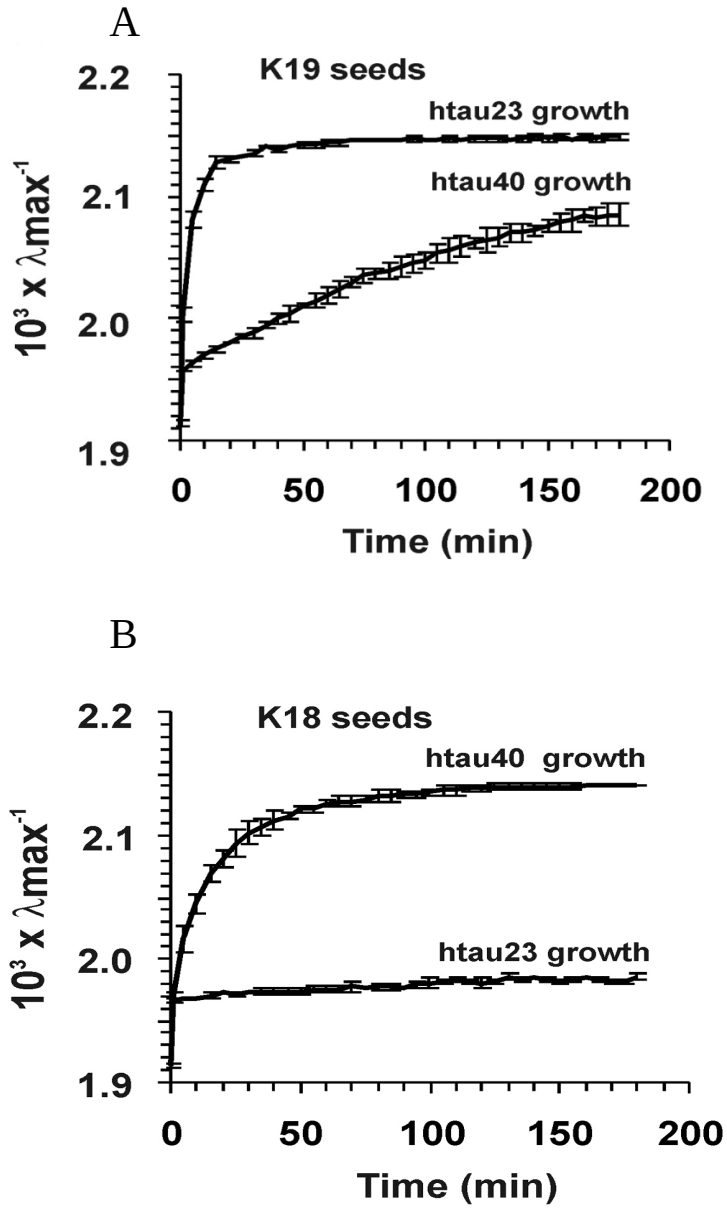

Figure 3.9: Full length aggregation kinetics of htau40 and htau23. (A) Aggregation of htau23 monomers (98% htau23, 2%htau23_310A1) in the presence of 8% K19 seeds or 8% K18 seeds. (B) Aggregation of htau40 monomers (98% htau40, 2% htau40_310A1) seeded by addition of 8% K18 seeds or 8% K19 seeds. Monomer concentrations are 20µM. All values in A, B represent mean ± s.d. (n = 3 experiments) (Dinkel et al., 2011).

3.3.3 Cross-seeding gives rise to a new type of 4R tau filament.

The observation that 4R tau can grow onto 3R tau seeds raised the question of whether the resulting filaments have the ability to seed 3R tau. Such a property would be expected if the monomers of 4R tau assumed the conformation of the seeds of 3R tau. In order to address this question, a three step seeding experiment was carried out **(Figure 3.10 A)**. In the first step K18 monomers were grown on K19 seeds. In the second step three cycles of seeding and elongation produced an enriched population of K18 filaments. In the third step seeds of these K18 filaments were added to K19 monomers. Remarkably, the K18 seeds had the ability to seed the formation of K19 filaments **(Figure 3.10 B,** top trace**)**. As a result of the multistep procedure the concentration of K19 seeds was reduced from 2.0 X 10^{-6}M in the first reaction to 3.1 X 10^{-11}M in the final reaction. At this final seed concentration K19 does not accelerate aggregation, therefore the growth of K19 monomers was not affected by any residual K19 seeds. The presence of filaments was confirmed by EM **(Figure 3.10 C)**. Importantly, when the initial seeds in the multistep seeding procedure were composed of K18, seeding of K19 in the final step did not occur **(Figure 3.10 B,** bottom trace**)**. Corresponding results were obtained when the full length tau was used in the final elongation step **(Figure 3.11 A, B)**. These observations are important as they demonstrate that the same protein, K18, can produce filaments with different seeding properties, depending on the initial template, and furthermore that these properties can be propagated over multiple generations.

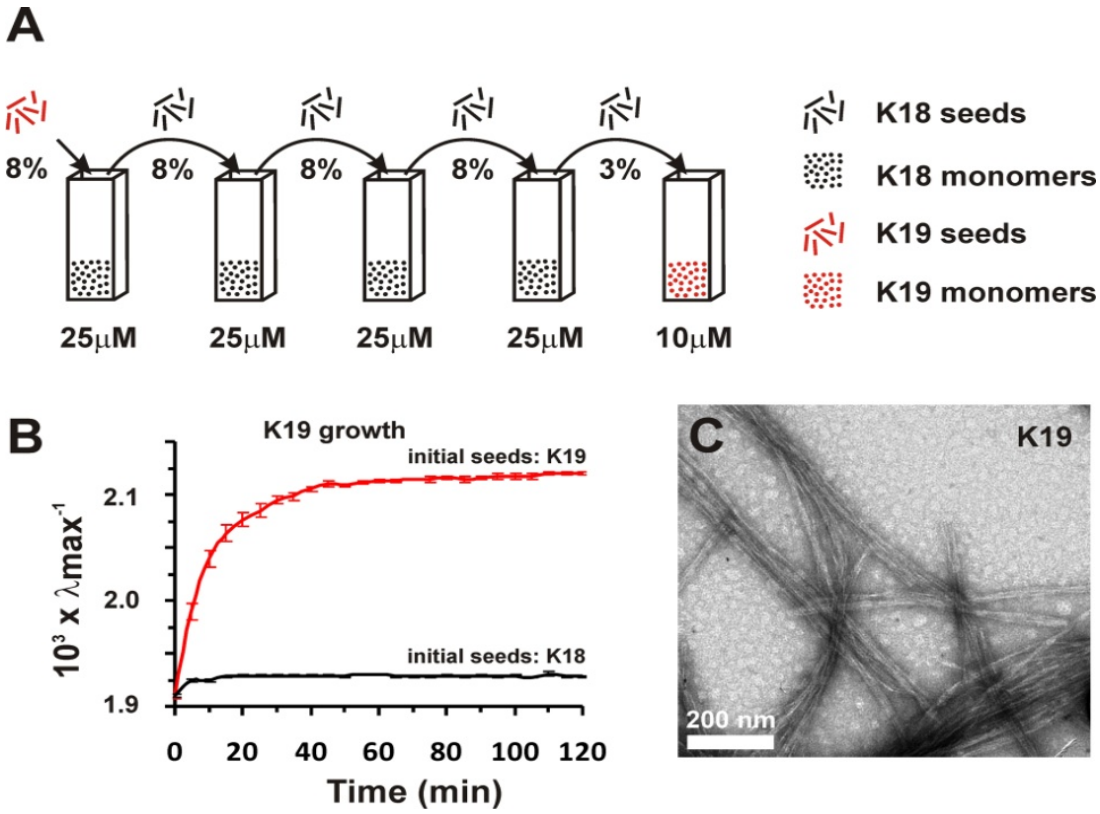

Figure 3.10: Tau filament diversification. (A) Experimental design of multicycle seeding reactions. Each time seeds from the previous reactions were used to form new filaments. (B) Aggregation of K19 monomers (98% K19, 2% K19_310A1) in the presence of 3% K18 seeds (last step in A) monitored as a change in the reciprocal of emission wavelength over time (top trace). When instead of K19 seeds K18 seeds were present in the initial step, no aggregation was seen (bottom trace). (C) Electron micrograph representing the end point of the top trace in (B) (Dinkel et al., 2011).

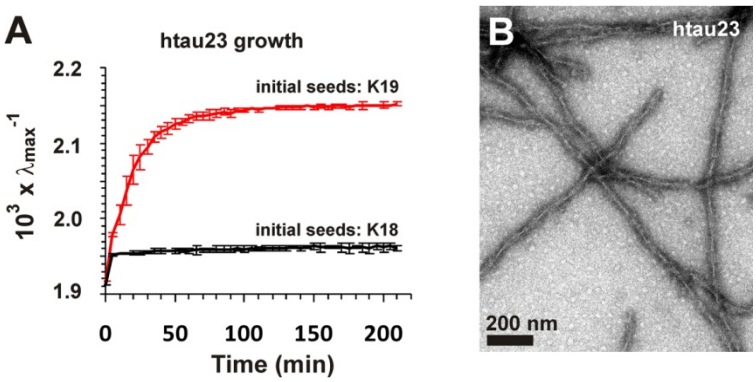

Figure 3.11: Tau filament diversification in full length tau. A multi-cycle seeding procedure as outlined in Fig. 3.10 A is used with the only difference that seeds (8 mol %) in final reaction are added to htau23 (20 μM) instead of K19. (A) Aggregation of this reaction (98% htau23, 2% htau23_310A1) is monitored as a change in reciprocal emission wavelength over time (red). When initial seeds in this five-step procedure are K18 and not K19 filaments, aggregation does not occur (black trace). (B) Electron micrograph representing the end point of the red trace in A (Dinkel et al., 2011).

3.4 Discussion

The identification of three compositionally distinct types of tau filaments that share a common core with parallel, in-register arrangement raised the question of whether these filaments could be conformationally distinct. In filaments, variations in packing interactions could impart different biophysical properties to them. To identify differences between the three types of filaments their seeding characteristics were studied. Recent evidence suggests that caspase-cleaved fragments (De Calignon et al., 2010), and other truncated forms of tau (Wang et al., 2007), may play a critical role in the initiation of filament formation. These smaller forms accelerated kinetics and therefore seeds may serve as templates onto which full-length isoforms bind (De Calignon et al., 2010; Wang et al., 2007). For seeds, the constructs K18 and K19 were chosen, which are truncated

versions of tau that contain the core-forming repeat region (Figure 1.1B). The following key observations were made irrespective of whether truncated (K18 and K19) or full-length versions of tau (htau23 and htau40) were used for filament growth (summarized in **Figure 3.12**): First, seeds of 3R tau and 3R/4R tau recruit both types of isoforms. Second, seeds of 4R tau recruit 4R tau and 3R/4R tau, but not 3R tau, establishing an asymmetric barrier. Third, conformational templating of 4R tau onto 3R tau seeds abolishes this barrier giving rise to a new type of tau filament. These results indicate the existence of at least four conformationally distinct types of filaments.

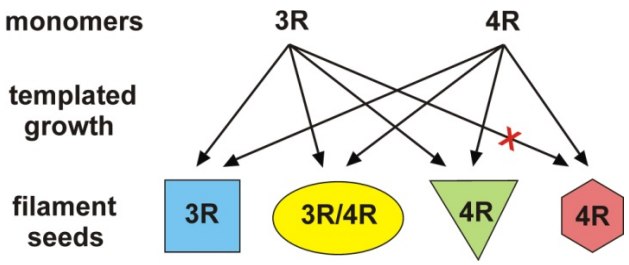

Figure 3.12: Templated filament growth of tau. Monomers of 3R and 4R tau (top) can grow only on the ends of 3R (blue), 3R/4R (yellow) and 4R filaments (green and pink) if their sequence is compatible with the conformation of the seed (arrows). Structural incompatibility gives rise to a seeding barrier (crossed out arrow) (Dinkel et al., 2011).

Conformationally distinct fibrils are a hallmark of prions and are thought to be the basis for strain (or phenotype) variations in mammals (Colby et al., 2009; Legname et al., 2006) and yeast (King & Diaz-Avalos, 2004; Tanaka et al., 2004a). Strain identity is thought to be maintained by imprinting the conformation of the prion fibril onto the soluble prion proteins via seeded conversion (Castilla et al., 2008; Jones & Surewicz, 2005). Prion proteins that vary in sequence may also be recruited giving rise to the

transmission of prions from one species to another or, in the case of polymorphisms, the transmission within species (Collinge, 2001). This process can lead to the emergence of new strains as exemplified by the appearance of variant Creutzfeld Jacob's disease, which has been linked to the transmission of bovine prions to humans (Collinge et al., 1996). If the primary structure of the variant is incompatible with the conformation of the seed, a transmission barrier occurs. The seeding barrier that prohibits 3R tau from growing onto 4R tau seeds is reminiscent of such a barrier, suggesting that the primary structure of 3R tau is incompatible with the conformation of 4R tau seeds. The primary structure of 4R tau, however, is compatible with the conformation of 3R tau seeds, leading to the emergence of a new type of filament. An asymmetry in seeding specificity, similar to that observed for 3R and 4R tau, has been described for the tau disease mutant P301L (Aoyagi et al., 2007). While the seeds of this mutant recruited its respective monomers, wild type monomers were not recruited. Wild type seeds, on the other hand, were able to recruit both mutant and wild type tau. Whether P301L that had been grown onto the wild type seeds resembled a new type of filament that was able to seed wild type tau has not been addressed. Regardless, these findings demonstrate that the coexistence of different tau isoforms and the presence of tau mutants could have intricate effects on the propagation.

On the basis of their seeding properties, we have identified four conformationally distinct types of filaments **(Figure 3.12)**. It is likely that additional types of filaments exist. Previous experiments have demonstrated that 4R tau can adopt different conformations when grown onto distinct seeds (Frost et al., 2009; Colby et al., 2009),

revealing a structural plasticity of tau akin to that of other amyloid proteins (Colby et al., 2009; Kodali et al., 2010a; Paravastu et al., 2009; Petkova et al., 2005; Tanaka et al., 2004a). The *in vitro* conditions that were used for filament formation arguably do not recapitulate the complex biochemical environment in the human brain. Cofactors, chaperones, and post-translational modifications could affect filament formation in a cell-dependent manner. In fact, in the case of prions it has been shown that different cell lines can favor different prion strains (Mahal et al., 2007) and that selective pressures can cause the amplification of new strains and the disappearance of old ones (Li et al., 2010). Despite their deficiencies, our *in vitro* experiments have demonstrated that tau filaments have the ability to seed, propagate, and diversify and that conformational barriers can determine isoform recruitment. Our experiments suggest that the initial nucleation event may have a profound effect on subsequent filament formation. Nuclei that contain 3R and 4R tau could establish templates that recruit all isoforms. Such a type of recruitment could be important in AD where all isoforms are deposited (Goedert et al., 1992a). Nuclei that contain only 4R tau could establish templates that recruit only 4R tau. Importantly, such a conformational barrier could explain the preferential deposition of 4R tau in progressive supranuclear palsy, corticobasal degeneration, and other 4R tauopathies. Although our *in vitro* experiments do not explain the preferential deposition of 3R tau in Pick's disease, it is possible that inefficient growth of 4R tau onto 3R tau seeds leaves these filaments prone to cellular clearance. Alternatively, an additional type of 3R tau filament may exist that is conformationally incompatible with 4R tau. Despite this lack of understanding, the molecular mechanisms that explain strain diversity, transmission

barriers, and strain emergence in prion diseases are clearly inherent in tau, suggesting that similar phenomena might exist in tauopathies.

Chapter Four: Study of Tau Conformers by DEER

4.1 Introduction

Amyloid fibrils may show polymorphism by (1) distinct modes of lateral association of protofilaments without significant variation in molecular structure (Jiménez et al., 2002) or (2) distinct morphologies can also result from significant variations in molecular structure at the protofilament level (Petkova et al., 2005). Studies in the previous chapter have shown that the seeds of K18 (4R) can recruit only 4R monomers while the seeds of K19 (3R) can recruit both 3R and 4R monomers. The 4R monomers do grow on K19 seeds albeit in slower manner when compared to the growth of 3R monomers on K19 seeds (3R). The conclusion of the study was that the 3R seeds were able to conformationally template 4R monomers. To study these conformationally different tau filaments at the molecular level, PELDOR or DEER (double electron-electron resonance spectroscopy) was utilized.

4.1.1 Double electron-electron resonance spectroscopy.

Solid state NMR has been used to study the structures of fibrils at the molecular level. Recent work in solid state NMR has demonstrated the feasibility of estimating electron-nucleus distances in proteins in the 1–2 nm range (Helmus, et al., 2008; Tycko, 2011) while DEER in favorable cases can measure up to 6 nm in proteins (Dockter et al.,

2009; Jeschke et al., 2005; Pannier, et al., 2000). Therefore when compared to solid state NMR, DEER is a better technique to pick up long range distance changes which could be a better reflection of structural changes in filaments.

DEER is a similar technique to Forster resonance energy transfer (FRET) (Yan, et al 2003). For protein – protein interaction studies by both FRET and DEER, the target molecules are labeled with pairs of fluorescent and paramagnetic labels respectively. The distances measured between the labels reflect conformational differences between proteins (Jeschke & Polyhach, 2007). Even though FRET is more sensitive than DEER (Banham et al., 2006), it requires large chromophores, which must be chosen according to the expected distance. Contrarily, DEER distance measurements can be performed between identical much smaller nitroxide labels and are precise over a broader range of distances (Jeschke, 2002; Jeschke et al., 2004). The CW EPR can also be used to measure distances between two nitroxide labels (Altenbach et al., 2001), but above 2 nm it is not very reliable (Berliner, 2000). Therefore above 2 nm, four pulse DEER is used (Milov et al., 1981; Pannier et al., 2000) .

Previously DEER spectroscopy has been applied for structural characterization of biomacromolecules such as membrane proteins (Dockter et al., 2009; Endeward et al., 2009; Jeschke et al., 2005), DNA (Ward et al., 2007) and RNA (Schiemann & Prisner, 2007; Schiemann, 2009). Distance measurements using DEER have also been done in filaments of α-synuclein (Karyagina et al., 2011) and hIAPP (human Islet Amyloid peptide) (Bedrood et al., 2011).

Here DEER in conjunction with SDSL was used to study the conformation of filaments. In the technique, SDSL is done with nitroxide labels and these labels are used for distance measurements. The observed distances are between the unpaired electrons at the end of the spin labels (Jeschke et al., 2006; Schiemann, 2009).

4.1.2 DEER measurements.

DEER measurements are based on alteration of the magnetic dipole-dipole interaction between two nitroxide spin labels by microwave pulses. Microwave pulses are used at two different frequencies, the observation frequency ($\nu_{observe}$) excites a set of spins in the EPR spectrum (spins X), and creates a spin echo signal. At the pumping frequency (ν_{pump}) a pulse excites another set of spins (spins Y), which alternates the sign of dipole-dipole interaction between spins X and Y. Hence the electron spin echo signal (DEER signal) depends on the magnitude of dipole-dipole interaction between X and Y spins and on pumping pulse time position and intensity (Fajer et al., 2007). The four pulse echo sequence which was used for DEER measurement is shown in **Figure 4.1**.

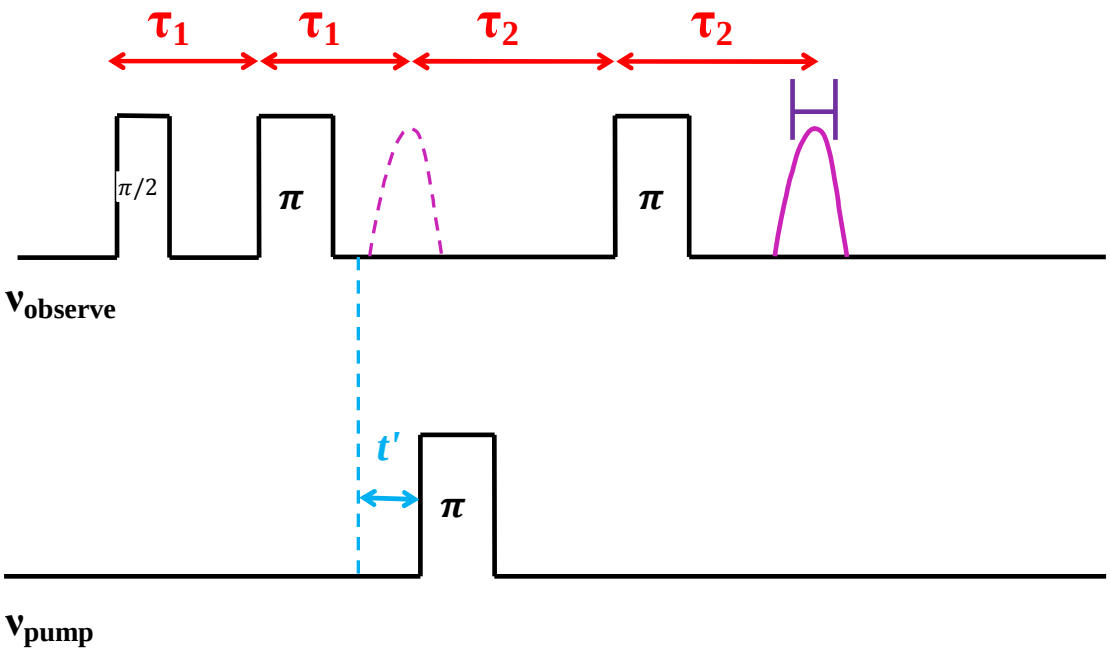

Figure 4.1: Four-pulse DEER sequence. A Hahn echo (dashed purple) is produced by a π/2 pulse followed by a π pulse at the observer frequency ($\nu_{observe}$). This echo is again refocused with a π pulse (purple). After the first observer π pulse, another set of spins are excited at pump frequency (ν_{pump}), at time *t'* (blue arrow). The τ1 and τ2 are kept constant while *t'* is sequentially stepped. When the two spins are coupled, stepping the pump pulse causes oscillation of the amplitude of refocused echo. The frequency of the oscillation is the dipolar coupling between both the spins.

The DEER signal *V(t)* contains contributions from the interaction between the two spins in one molecule but also from the interaction between spins on different molecules and is thus considered a product of two contributions

$V(t) = V(t)_{\text{intra}}\, V(t)_{\text{inter}}$

$V(t)_{\text{inter}}$ describes the decay due to the intermolecular interactions of unpaired spins and $V(t)_{\text{intra}}$ describes the periodic oscillations generated by the intramolecular interactions of pairs of spins (Milov et al., 1984; Schiemann, 2009). For the experiments in this study, intermolecular interactions were reduced by diluting the sample with protein that does not contain paramagnetic labels.

The pairwise dipole-dipole coupling between two spins is the basis for distance determination in DEER measurements. In the case of disordered system, the electron electron coupling (ω_{ee}) is given by the sum of dipole dipole coupling (ω_{dd}) and the exchange coupling J. In systems for which the point-dipole approximation is valid and for which the exchange coupling J can be assumed to be isotropic

$$\omega_{ee} = \omega_{dd}(3cos^2\theta - 1) + J$$

with

$$\omega_{dd} = \frac{g_A\, g_B\, \mu_B^2\, \mu_0}{4\pi h} \frac{1}{r^3}$$

Where g_A and g_B are the g values of the two spins, μ_B is the Bohr magneton, μ_0 is the permeability of free space, h is the Planck constant, r is the distance between the two spins and θ is the angle between the static field axis and the axis connecting the loci of the two electron spins. The distance measurement is based on the dependence of dipole-dipole couplings on the inverse cube of the distance.

To study the conformational differences between tau filaments, DEER measurements were compared for double mutants of K18 grown on K18 seeds, K19 grown on K19 seeds and K18 grown on K19 seeds.

4.2 Methods

4.2.1 Site directed mutagenesis, protein expression, and protein purification.

In the site directed mutagenesis, first a single cysteine was introduced as mentioned in Chapter 2 section 2.1.1 and this single cysteine DNA was used as a template to introduce another cysteine. As these double mutants were difficult to obtain, miniprep plasmid purifications were performed to sort the correct size of the required tau DNA. The correct DNA was transformed again in XL1Blue competent cells and then midiprep plasmid purifications were carried out to get higher yield for DNA sequencing. Then protein expression and purification were performed as mentioned in chapter 2.

4.2.2 Multistep production of seeds.

In the initial step, filaments were formed by mixing 25 µM of cysteine free K18 with 50 µM of heparin (average molecular mass of 5000 Da, Celsus, Cincinnati, OH) using elution buffer. After three days of agitation at 25°C, the filament sample was chilled and sonicated for 20 seconds to create seeds using Fisher Scientific Sonifier (150 T Series). The next round of filament reaction was set up by adding 10% seeds (from the first reaction) to 25 µM of K18 (cysteine free) and mixed with 50 µM of heparin. Filaments formation was carried out at 37°C for 1 h. This procedure was repeated four times and each time seeds from the previous reaction were used to form next set of

filaments. The final seeds (4^{th} cycle) were used in DEER sample preparation. The same was done to prepare K19 (cysteine free) seeds.

4.2.3 Sample preparation for DEER experiments.

For the preparation of filaments for DEER measurement, the MTSL labeled double mutant (procedure mentioned in chapter 2) was mixed with 50 fold excess of cysteine free K18 or K19, 5% seeds from the 4^{th} cycle of the multistep seeded reaction, and heparin (protein:heparin molar ratio of 4:1). The final protein concentration was 50µM and fibrillization was carried out at 37°C. Before preparing the DEER sample, the efficacy of seeds was checked by running a control acrylodan assay with and without seeds as mentioned in chapter 3. For the acrylodan assay, the reaction conditions were similar to those used for preparation of DEER sample. After 14 hrs, the formed filaments were pelleted at 100,000 x g and washed once with elution buffer. To the filament pellets, 20-50 µl of elution buffer was added to reconstitute the sample, which was then pelleted into a quartz capillary (1.1 mm inner diameter x 1.6 mm outer diameter) at 1000 x g. The buffer layer in the capillary tube above the sedimented filaments was completely aspirated out using a syringe. The capillary tube was flash frozen in liquid N_2 and stored at -80°C. DEER measurements were performed within seven days of making the sample.

4.2.4 Negative stain electron microscopy.

The EM grids of tau filaments were prepared as mentioned in chapter 2. The tau filament concentration used was 5 µM.

4.2.5 Setting up filaments of double mutants to confirm β parallel in-register structure.

Samples for CW EPR measurement for completely labeled K18 and K19 double mutants were spin labeled as described in chapter 2. Protein concentrations used were ~25μM. Filaments were prepared under agitation condition by mixing protein with heparin at a molar ratio of 4:1 and by incubating at 25°C for 3 days. Samples were pelleted at 100,000 x g for 30 minutes, washed with elution buffer, and transferred into borosilicate capillaries (0.6 mm inner diameter x 0.84 mm outer diameter).

4.2.6 EPR and DEER measurements

CW EPR measurements of samples were recorded with a Bruker EMX spectrometer fitted with an ER 4119HS resonator. Parameters for taking EPR spectrum are mentioned in chapter 2 section 2.2.5. Spectra were normalized to the same number of spins using double integration. From all spectra, a minor background arising from 0.5% soluble tau was subtracted.

DEER data were obtained at Q-band frequencies (34 GHz) with a Bruker Elexsys E580 spectrometer equipped with a 1-watt amplifier, a Bruker ER 5107 Q-band dielectric pulse resonator, and an Oxford CF 935 cryostat. Measurements were performed using four-pulse DEER experiment: $\pi/2(\nu_{obs}) - \tau_1 - \pi(\nu_{obs}) - t' - \pi(\nu_{pump}) - (\tau_1 + \tau_2 - t') - \pi(\nu_{obs}) - \tau_2 - echo$ **(Figure 4.1)** (Pannier et al., 2000; Dockter et al., 2009; Jeschke et al., 2005). For the experiment, the resonator was fully overcoupled (Q~100). All measurements were performed at a temperature of 80 K. The observer $\pi/2$ and π pulse lengths were optimized for each run and ranged from 30 - 40 ns and 60 – 80 ns

respectively. A pump pulse length of 40 ns was used. The τ_1 and τ_2 were kept constant and time *t*' was varied. Data analysis was performed for dipolar evolution times $t = t' - \tau_1 > 0$. The resonance magnetic field was set at the global maximum of the nitroxide EPR spectrum and the pump frequency, ν_{pump}, was set to the centre of the resonator dip. The observer frequency, $\nu_{observer}$, was 37 MHz higher than ν_{pump} and coincided with of the center of the spectrum (Fajer et al., 2007) **(Figure 4.2)**. The repetition time was calculated for each run as 1.2 times the T_1 relaxation time and 8-step phase cycling was used. The total measurement time for each sample was between 48 – 72 hours.

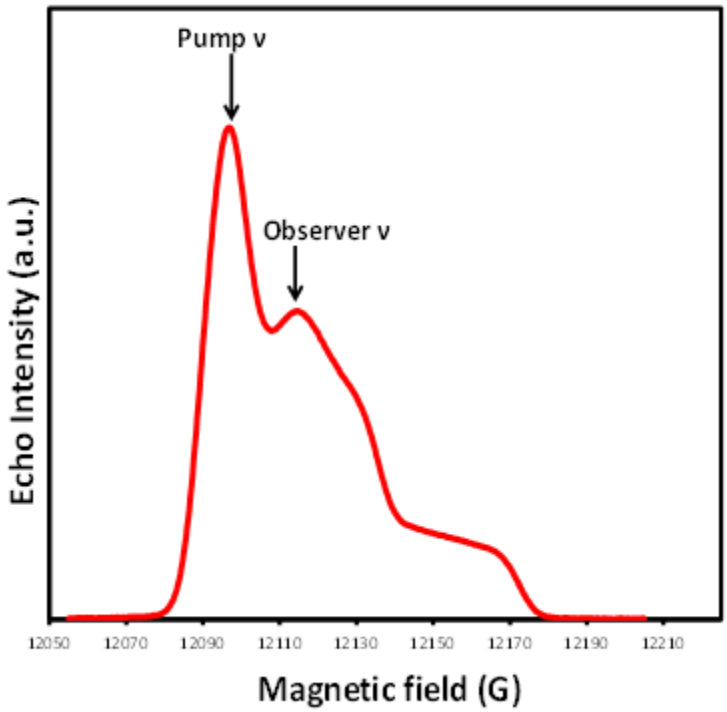

Figure 4.2: Field swept echo detected EPRspectrum. The pump frequency (ν_{pump}) and the observer frequency ($\nu_{observer}$) for nitroxide label in Q-band are shown for the double mutant K18 311/328 on K18 seeds.

4.2.7 DEER data analysis.

DEER data was analyzed using "DeerAnalysis2011" (Jeschke et al., 2006). The program DeerAnalysis2011 can extract distance distributions from dead-time free pulse ELDOR data (constant-time and variable-time pulse DEER).

Before distance distribution can be obtained from the dipolar evolution time, a background correction has to be performed. A background correction is performed to ensure that intermolecular distances are suppressed and only intramolecular distances are taken into account to find the distance distribution in the protein.

4.2.7.1 Homogenous background correction.

The general background function in this model is:

$$B(t) = \exp(-kt^{d/3})$$

Where k quantifies the density of the spins and d is the dimensionality of the homogeneous distribution. The distribution is homogeneous in d= 3 dimensions for proteins in solution and for membrane proteins it can be confined to d= 2 (Hilger et al., 2005; Zou & Mchaourab, 2010). For the current study 3D homogeneous background correction was used as it showed better background correction with singly labeled mutants. After the background correction, distances were extracted from the dipolar evolution curves using Tikhonov regularization (Jeschke et al., 2006; Jeschke & Polyhach, 2007).

4.2.7.2 Tikhonov regularization.

The data analysis was done by Tikhonov regularization which is a non biased (model independent) way of finding the distance distribution (Jeschke et al., 2006; Jeschke & Polyhach, 2007).

In Tikhonov regularization, the distance distribution is quantified by a regularization parameter α which is a compromise between smoothness (artifact suppression) and resolution of the distance distribution. The optimum distance distributions $P(r)$ are obtained by minimizing the sum of the functions η(α) andρ(α), where η(α) is the square norm of the second derivative of $P(r)$,which is a measure of smoothness multiplied by the regularization parameter α and ρ(α) is the mean square deviation between the simulated and experimental dipolar evolution time domain data. The larger α, lesser noise artifacts are introduced but also causes broadening of peaks in distance distribution. The optimum α is obtained by plotting log η(α) versus log ρ(α) which quantifies the mean square deviation and the smoothness. The L-curve (shape of the plot resembles alphabet “L”) for the data is implemented by doing Tikhonov regularization for a given set of regularization parameters (Chiang, et al., 2005) α = (0.001, 0.01, 0.1, 1, 10, 100, 1000, 10000, 100000).

4.3 Results

4.3.1 Conformational templating of 4R on 3R seeds.

We showed previously in chapter 3 that 4R was able to grow on 3R seeds, while 3R was unable to grow on 4R seeds. To study the conformational differences between the filaments when grown on different seeds, DEER was used. In this method double mutants were created in the repeat region of the tau monomer which forms β parallel in-register structure and is part of the core (Margittai & Langen, 2004) (chapter 2). The double mutants 4R (K18-311/322, 311/326, 311/328) and 3R (K19-311/322, 311/326, 311/328) were created by replacing amino acids at respective positions by cysteine residues (K311C, 322-natural cysteine, G326C, I328C). To make sure that the replacement of amino acids with cysteine residues in the double mutant did not disrupt the formation of filaments, the double mutant monomers were labeled with MTSL and set for filament formation. The measurement of filaments was performed using CW EPR, and single line spectra were observed for all double mutants **(Figure 4.3)**. This showed that the filaments of the double mutant had formed parallel in-register structure (Margittai & Langen, 2008).

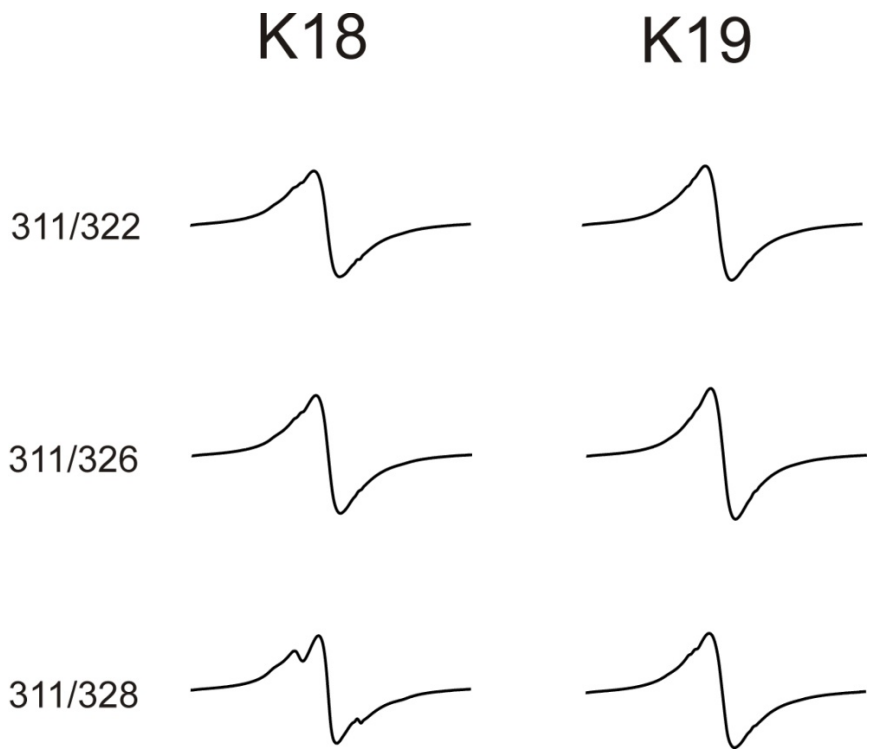

Figure 4.3: EPR spectra of completely labeled double mutants with MTSL. 311/322, 311/326 and 311/328 double mutants of K18 and K19, EPR spectra were taken. Spectra of all filaments were recorded at 150 G width and normalized to the same number of spins.

Next, samples for DEER were prepared by mixing 2% MTSL labeled double mutant with cysteine free protein. As the growth of filaments was a seeded reaction, seeds from the 4th cycle of multistep seeded reaction were used. Also, acrylodan assays performed with the same parameters which were used to prepare DEER samples showed the formation of filaments with the seeds of the 4th cycle from the multistep seeded reaction. The filaments were pelleted by ultracentrifugation, taken up in EB, transferred into quartz capillary and sedimented at 1000 x g. After this CW EPR measurements of the sedimented filaments were taken. Spectral broadening of the EPR spectra was not observed indicating that spin labeled monomers did not preferentially stack upon themselves, but incorporated evenly into the filaments **(Figure 4.4)**. Electron micrographs of all the mutants confirmed the presence of filaments **(Figure 4.5)**. The DEER samples were flash frozen and DEER measurements were carried out for all the samples, K18 311/322, K18 311/326, K18 311/328 on K18 and K19 seeds; K19 311/322, K19 311/326, K19 311/328 on K19 seeds.

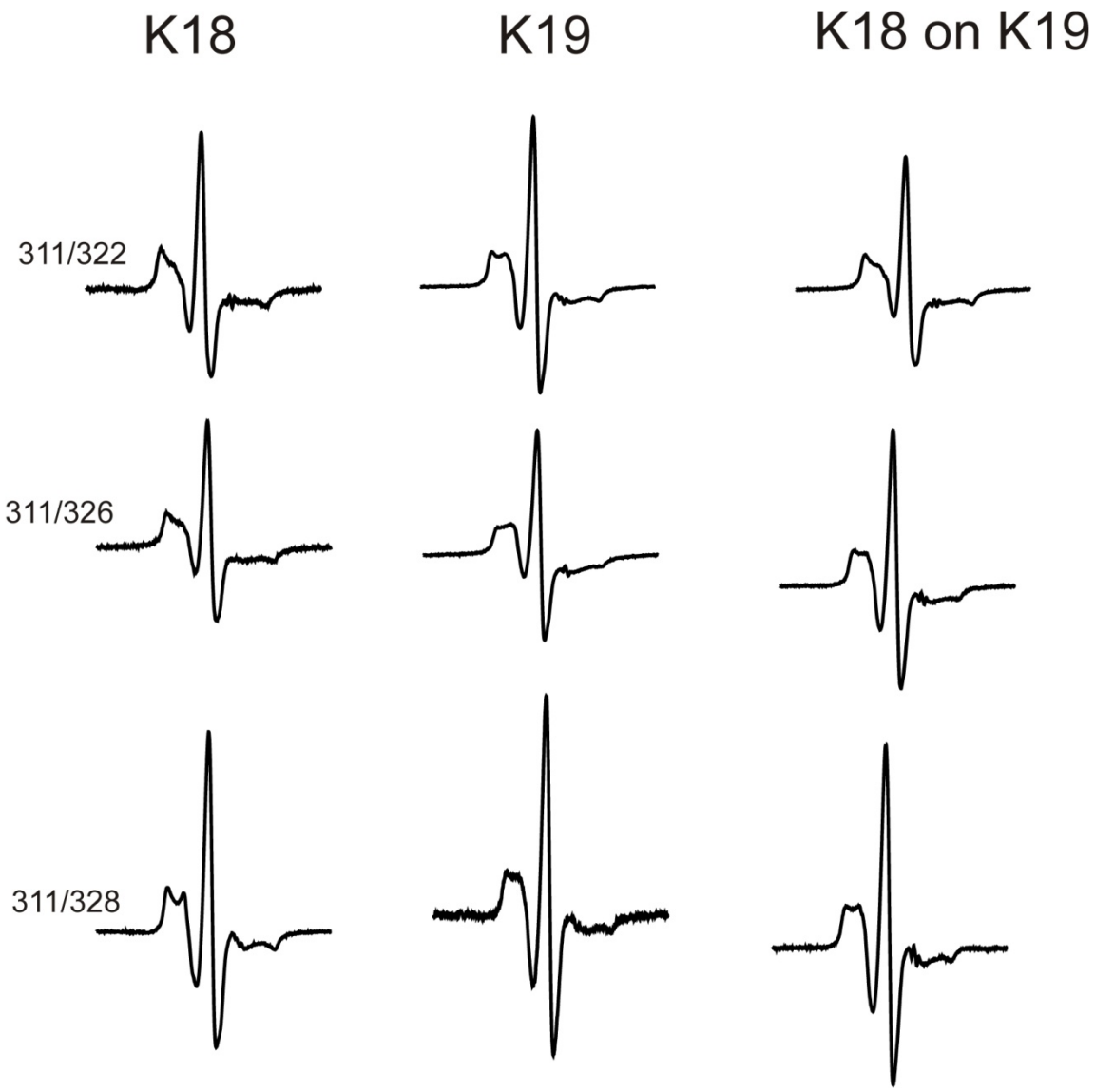

Figure 4.4: EPR spectra of diluted double mutants. Spectra of double mutants, 311/322, 311/326 and 311/328 of K18 grown on K18 seeds (left column), K19 on K19 seeds (centre column) and K18 on K19 seeds. 2% of the labeled double mutant was mixed with cysteine free tau protein. Spectra of filaments were recorded at 150 G scan width and normalized to the same number of spins.

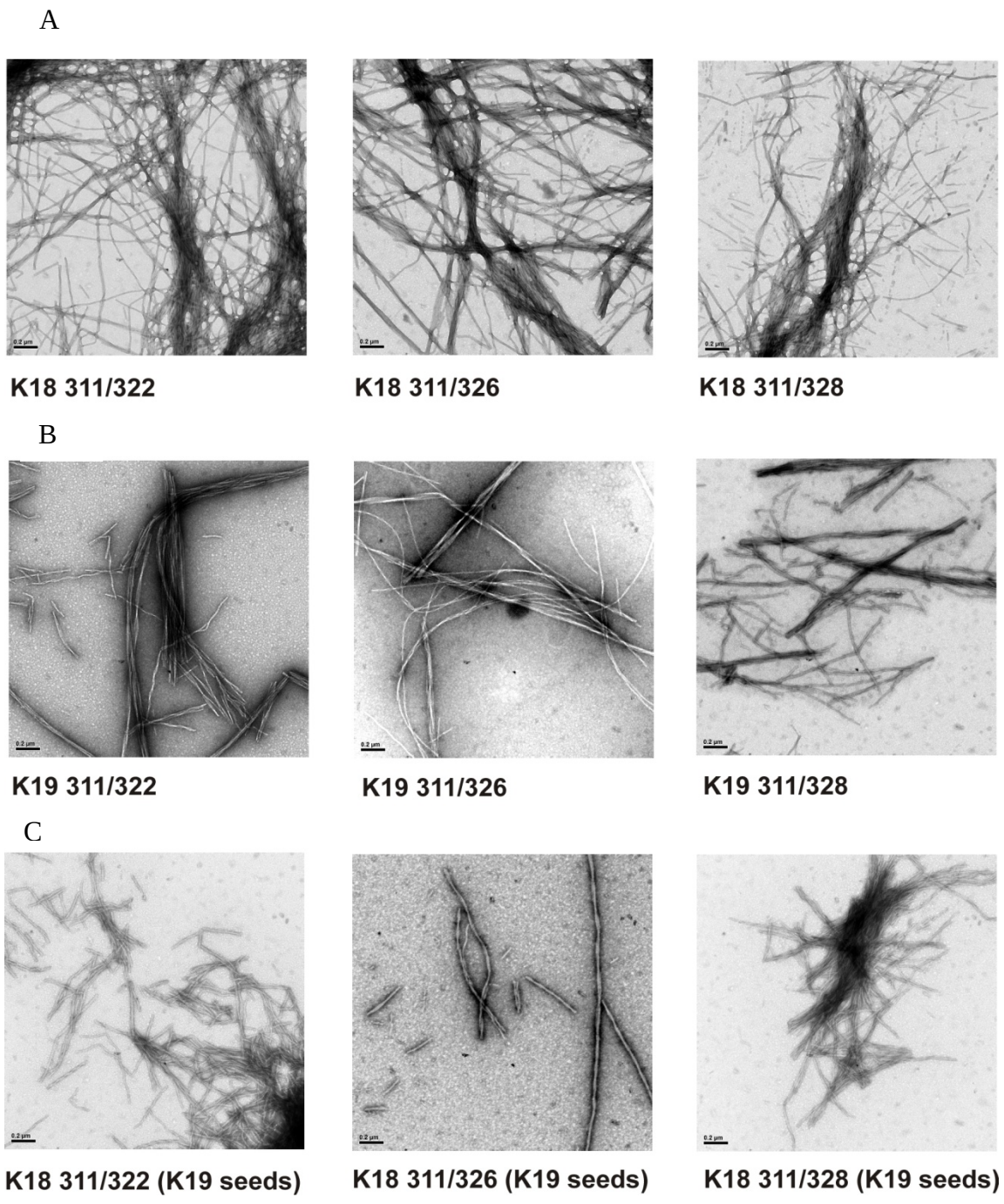

Figure 4.5: Electron micrograph of filaments. Double mutants 311/322, 311/326 and 311/328 (A) K18 grown on K18 seeds (B) K19 grown on K19 seeds (C) K18 grown on K19 seeds. Bar = 0.4 µm.

The dipolar oscillation traces of K18 311/322 on K18 (truncated 4R) (black trace) and K19 seeds (truncated 3R) (blue trace), K19 311/322 on K19WT seeds (red trace) were obtained from DEER measurements **(Figure 4.6 A)**. The dipolar oscillation traces of these three different filament growths matched with each other. The dipolar oscillation traces for 311/322 double mutant indicate similar spin-spin interactions for the three types of filaments, K18 on K18, K19 on K19 and K18 on K19 seeds. Similar spin-spin interactions between these double mutants indicate similar distances (Fajer et al., 2007).

Dipolar oscillation traces of K18 311/326 grown on K18 or K19 seeds and K19 311/326 grown on K19 seeds are shown in **Figure 4.6 B**. The results showed that when K18 311/326 was grown on K19 seeds, the dipolar oscillation trace was closer to the trace of K19 311/326 on K19 seeds rather than K18 311/326 grown on K18 seeds. The spin-spin interactions between 311 and 326 of K18 311/326 on K19 seeds were closer to that seen in K19 311/326 on K19 seeds. These results suggest that K18 311/326 on K19 seeds assumes a new conformation, similar to that of its seed. The same results were obtained when K18 311/328 was grown on K19 seeds **(Figure 4.6 C)**. Here, the spin-spin interactions were not as strong as seen when K18 311/328 was grown on K18 seeds. The weighted sum of the dipolar oscillation traces for singly labeled K19 for positions 311 and 326 **(Figure 4.6 B**, green trace**)** is similar to that of doubly labeled K19 311/326 and K19 311/328. This indicates a longer interspin distance for K19 311/326 and K19 311/328 doubly labeled mutants on K19 seeds when compared to K18 on K18 seeds for the same double mutant numbers. As a result, the data for 311/326 and 311/328 double mutants suggest that when K18 monomers were grown on K19 seeds, the K18 filaments

adopted the conformation of K19 seeds, which shows that K19 was able to conformationally template K18.

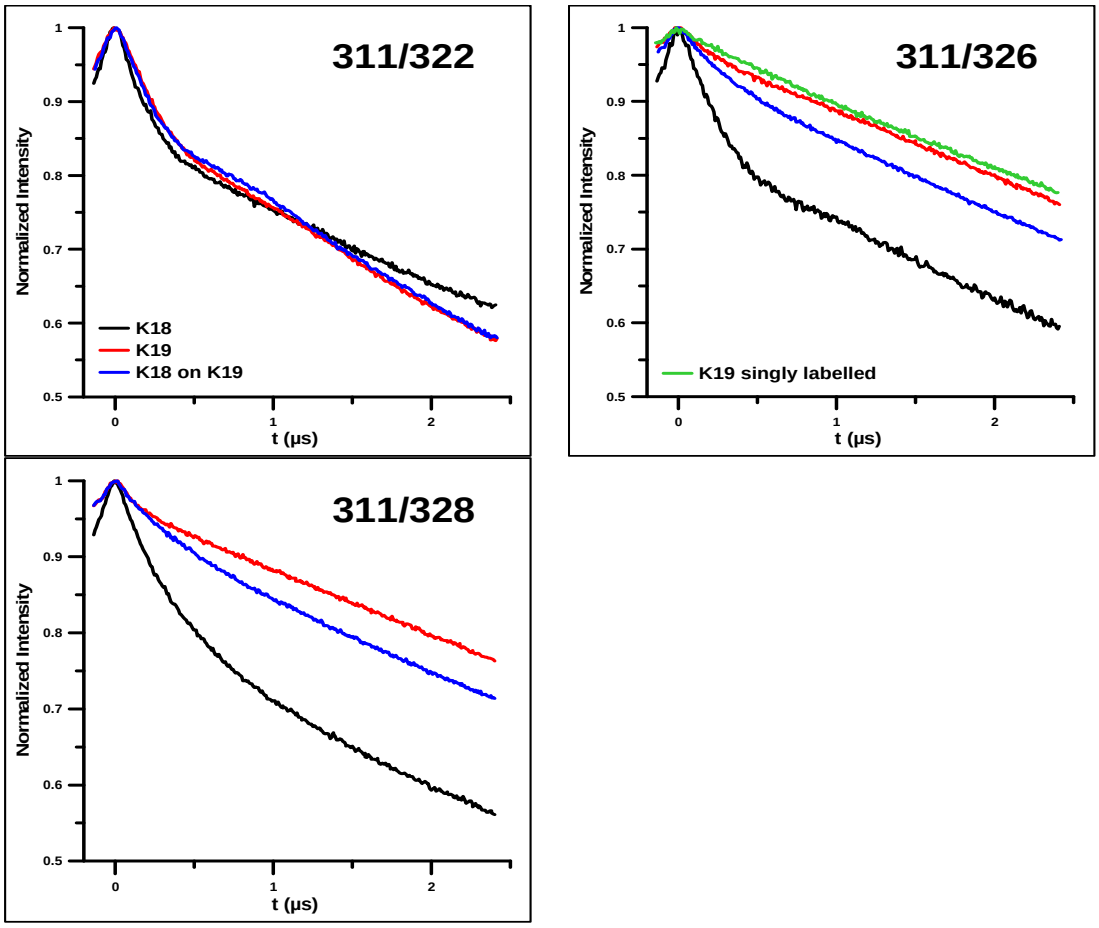

Figure 4.6: Dipolar oscillation curves of labeled mutants of tau filaments. (A) Dipolar oscillation curves taken for a T_2 of 2.5 μs. Double mutant 311/322 of K18 grown on K18 seeds (black), K19 grown on K19 seeds (red) and K18 grown on K19 seeds (blue). The curves for the three mutant filaments are the same. (B) Dipolar oscillation curves of 311/326 mutant of K18 grown on K18 seeds, K19 grown on K19 seeds and K18 grown on K19 seeds. The weighted sum of the dipolar oscillation curves for two singly labeled K19 311 and K19 326 is also shown (green). (C) The dipolar oscillation curves of 311/328 of K18 on K18 seeds (black trace), K19 on K19 seeds (red trace) and K18 on K19 seeds (blue trace).

4.3.2 3R and 4R tau form heterogeneous filaments.

When the dipolar oscillation curves were fit using Tikhonov regularization to obtain the distance distribution, multiple peaks suggest the presence of heterogeneous filament mixtures. While closely spaced peaks could be the result of different rotamers, peaks that are spaced over ~2.0-2.5 nm might represent different filament conformers.

4.3.2.1 Distance distribution for 4R double mutants.

The distance distributions between two spin labels in 4R were obtained by Tikhonov regularization. **Figure 4.7 A** shows the dipolar evolution data after the 3D homogeneous background correction (black trace) and the Tikhonov fit (red trace) corresponding to the distance distribution for the double mutants K18 311/322, K18 311/326 and K18 311/328 grown on K18 seeds. The dipolar Pake pattern obtained from the time trace after Fourier transformation is shown in **Figure 4.7 B** (black trace). After Fourier transformation of the data after background correction, the dipolar spectrum has the expected shape of a broadened Pake pattern and is well fitted by the dipolar spectrum corresponding to the distance distribution using Tikhonov regularization (red trace) **(Figure 4.7 A, B)** (Jeschke & Polyhach, 2007). The distance distributions when Tikhonov regularization parameter α was set at 100 is shown in **Figure 4.7 C**. Distance distributions in the K18 311/322 double mutant showed major component peaks at distances of 3.4 nm and 3.9 nm with a distribution width of 1.6 nm. For K18 311/326, the major component peak showed a distance of 3.6 nm with a distribution width of 1.2 nm while a minor component peak was at 5 nm with a distribution width of 0.9 nm. In K18 311/328 on K18 seeds, the major component peak was at 4.8 nm with a width of 1 nm

while minor component peaks were at 3.3 and 3.6 nm. The L-curves are also shown for the three double mutants **(Figure 4.8)**. The green marker in the L-curve highlights the regularization parameter $\alpha = 100$.

To make sure that the observed distance distributions were not due to noise artifacts, for K18 311/328, Tikhonov fits were done at different scan numbers (Jeschke et al., 2005; Jeschke et al., 2006). Here the minor peaks observed were $1/3^{rd}$ of the major peak. Even at lower scan numbers where the S/N is low, peaks were still seen at smaller distances of 3.4 nm and 3.9 nm apart from 4.8 nm (data not shown) confirming the formation of heterogeneous filaments. These results demonstrate that the Tikhonov distributions of the double mutants showed multiple distance distributions showing heterogeneity in the conformers of the filament mixture.

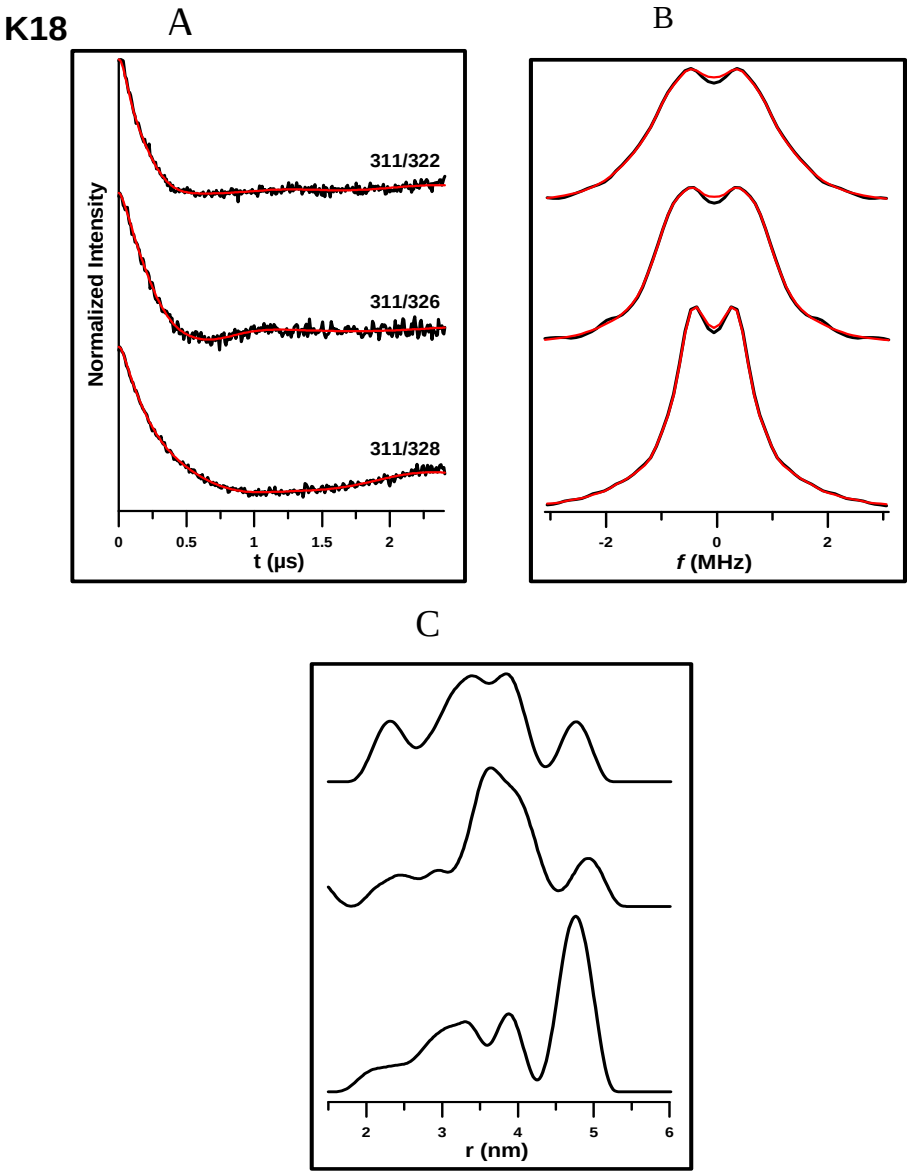

Figure 4.7: Distance distribution for filaments of K18 double mutants on K18 seeds. (A) Dipolar evolution curve due to the double MTSL labels in the filament (black trace), obtained by background correction, and the fit (red) corresponding to the distance distribution. The data are plotted in stacks. (B) Dipolar spectrum obtained by Fourier transformation of background corrected data (black) and fit to the spectrum corresponding to the distance distribution. (C) Distance distributions obtained by Tikhonov regularization with regularization parameter of $\alpha = 100$. Maximum heights for K18 311/322 = 3.4 and 3.9 nm, K18 311/326 = 3.6 nm and K18 311/328 = 3.4, 3.9 and 4.8 nm were observed.

4R on 4R seeds

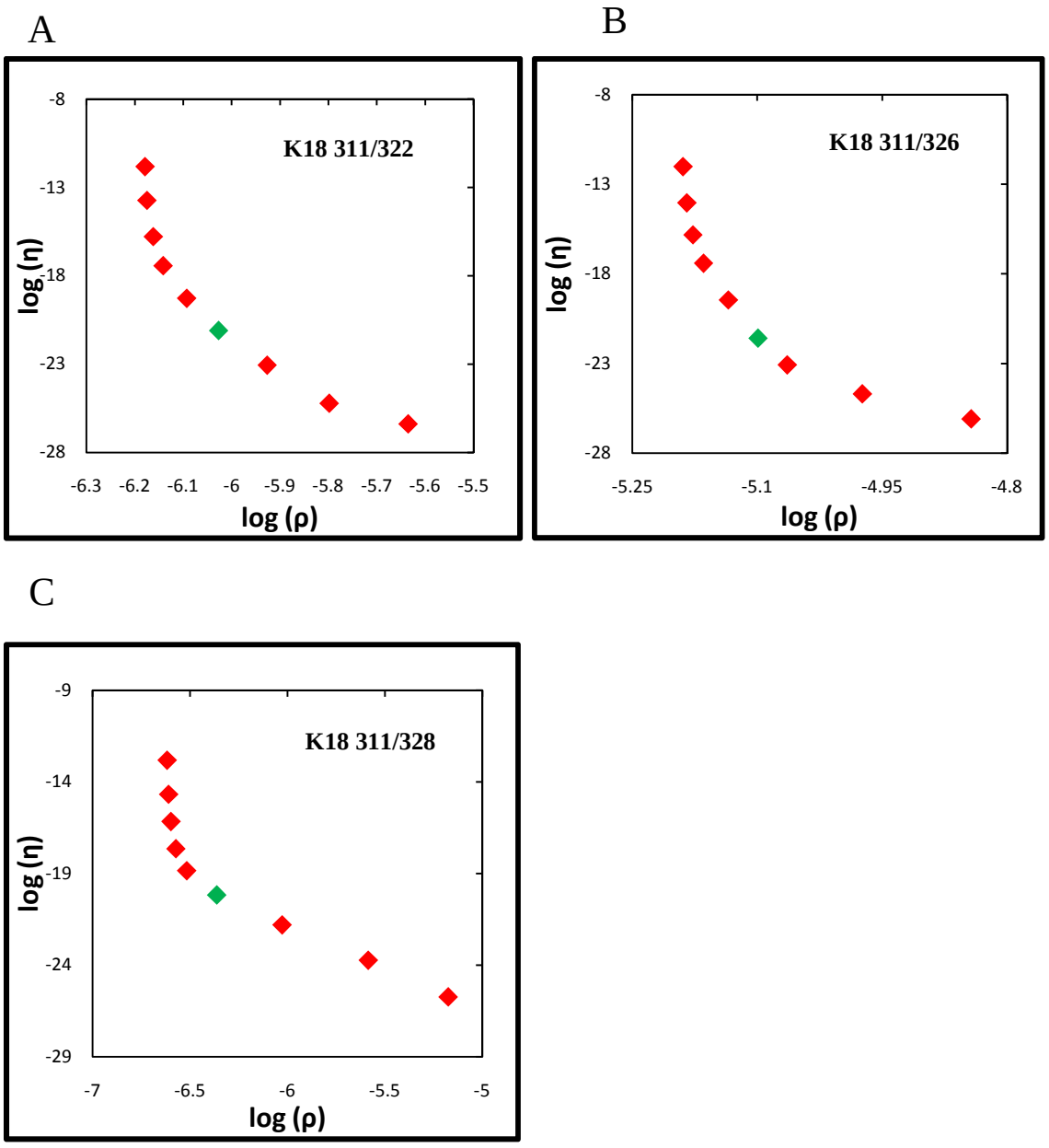

Figure 4.8: Tikhonov L curves of K18 on K18 seeds. (A) K18 311/322 (B) K18 11/326 (C) K18 311/328 templated on K18 (4R) seeds. The green data point corresponds to the regularization parameter α = 100 which was used to obtain the distance distribution.

4.3.2.2 Distance distribution of 3R double mutants.

Tikhonov regularization fit was done for the DEER data of K19 311/322 templated onto K19WT seeds **(Figure 4.9)**. The L-curve is shown in **Figure 4.11 A**. In the distance distribution, the major component peak was 3.9 nm and the width of this distribution was 1.7 nm. For K19 311/326 and K19 311/328, we were unable to do Tikhonov fits to obtain distance distributions from the dipolar evolution curves as the spin-spin coupling was weak. As mentioned above, the dipolar oscillation traces of K19 311/326 and K19 311/328 on K19 seeds were closer to the traces of the weighted sum of singly labeled K19 311 and K19 326. This clearly shows that the distance between the two labels is large.

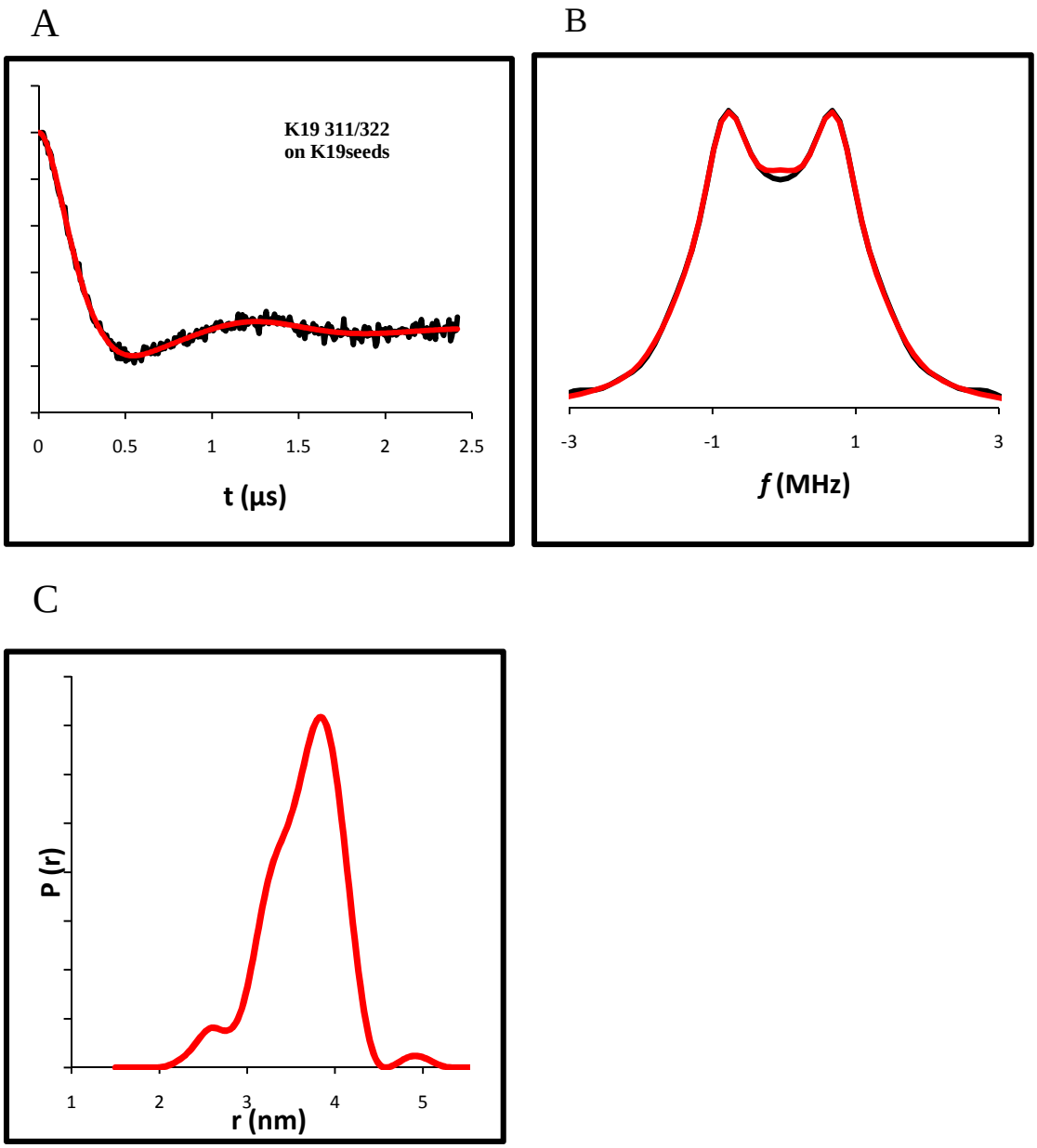

Figure 4.9: Tikhonov regularization fit for double mutant K19311/322 templated on K19 (3R) seeds. Dipolar evolution curves in time (A) and frequency (B) domains. (C) Resulting distance distribution with a major peak at 3.8 nm. Black traces are after background correction of the data while the red traces show fits after Tikhonov regularization.

4.3.2.3 Distance distribution of 4R double mutant on 3R seeds.

The Fourier transformed dipolar spectrum after 3D homogeneous background correction (black trace), is well fitted by the dipolar spectrum corresponding to the distance distribution using Tikhonov regularization (red trace) **(Figure 4.10 A, B)**. Tikhonov regularization fit for K18311/322 on K19 seeds showed major component peak at 3.5nm with a width of 1.3 nm **(Figure 4.10 C)**. The L-curve is shown in **Figure 4.11 B** and the green marker in L-curve is at $\alpha = 100$. The distance distribution obtained for K8311/322 on K19 seeds was very similar to K19311/322 grown on K19 seeds and different from K18311/322 grown on K18 seeds. Narrowing of the distance distribution was seen when K18 was grown on K19 seeds. The distance distributions obtained when K18 was grown on K18 seeds, K19 on K19 seeds and K18 on K19 seeds showed that the mixture of filaments formed was heterogeneous.

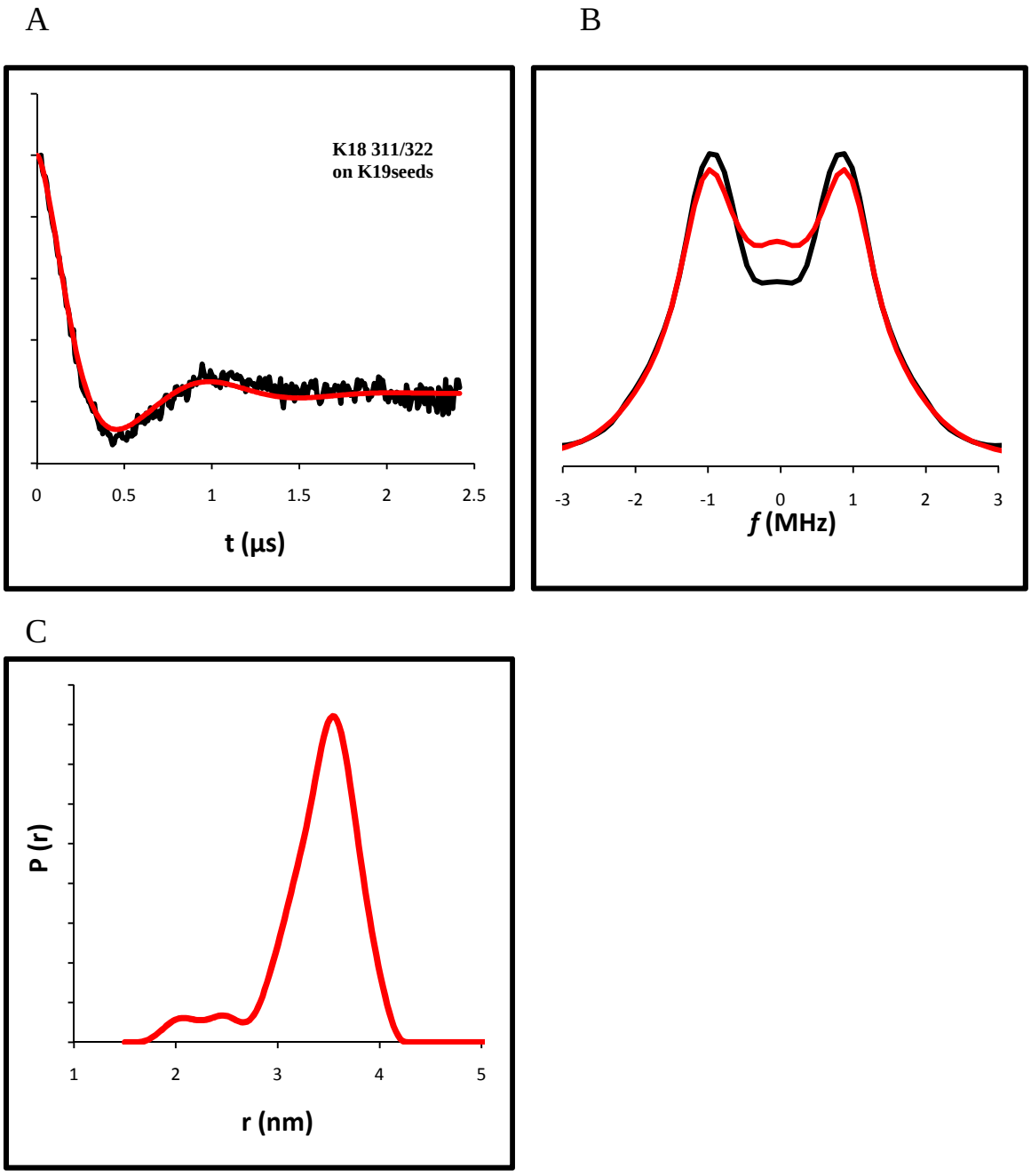

Figure 4.10: Tikhonov regularization fit for double mutant K18 311/322 templated on K19WT seeds. The seeds were formed after five cycles of seeded reaction. (A) Dipolar evolution curves in time and (B) frequency domains. (C) Resulting distance distribution with a major peak at 3.5 nm. Black traces are after background correction of the data while the red traces shows fits after Tikhonov regularization.

A. 3R on 3R

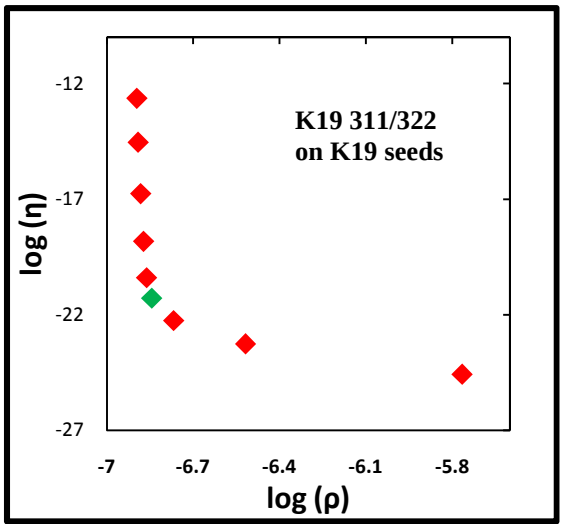

B. 4R on 3R seeds

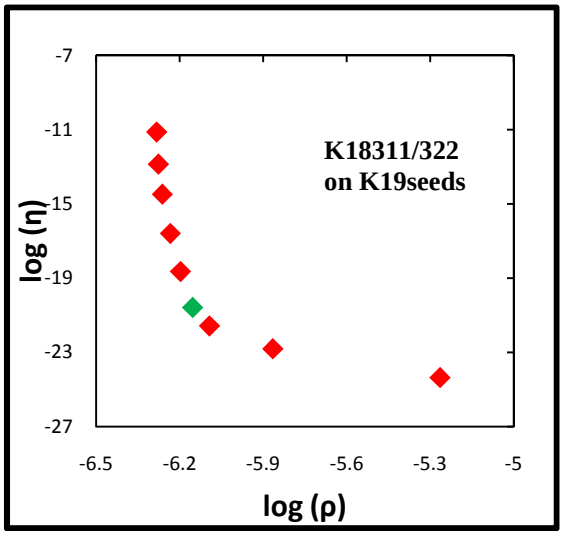

Figure 4.11: **Tikhonov L curves.** (A) K19 311/322 on K19 (3R) seeds (B) K18 311/322 templated on K19 (3R) seeds. The green data point corresponds to α = 100.

4.4 Discussion

Structural information on the PHF fibril has been obtained by different techniques, such as proteolysis, transmission electron microscopy (Goux, 2002; von Bergen et al., 2006), CD, FTIR spectroscopy (Barghorn & Mandelkow, 2002; Frost et al., 2009) and CW EPR (Margittai & Langen, 2004; Margittai & Langen, 2006a), but insight into the structural arrangement of tau PHFs on the residue-specific level is still scarce.

DEER measurements have been used in these studies as a 'spectroscopic ruler' to study conformational differences between various filaments (Jeschke et al., 2005). Studies in this chapter have for the first time showed molecular level structural differences in tau filaments using DEER measurements. For these experiments three different cysteine double mutants were created in K18 and K19 in the 3rd repeat region of the tau monomer. The 3rd repeat region is part of the core which forms the β parallel in-register structure in filaments. The intramolecular distances were defined by labeling the two cysteine residues in each double mutant by a nitroxide label and the distance measured was between two electrons localized in the N-O bond of the nitroxides (Schiemann, 2009). Variations in the intramolecular distances between filaments suggest differences in conformations (Fajer et al., 2007). For conformational studies by DEER, three different types of filaments growth were examined 1) growth of K18 monomers on K18 seeds 2) growth of K19 monomers on K19 seeds and 3) growth of K18 monomers on K19 seeds.

Comparison of the dipolar oscillation curves of K18 (4R) on 4R seeds, K19 (3R) on 3R seeds and K18 (4R) on 3R seeds of 311/322 double mutant showed that they were very similar. For the double mutant 311/326, the dipolar oscillation curve of K18 (4R) grown on K19 (3R) seeds was different from K18 (4R) grown on K18 (4R) seeds. The dipolar oscillation curve of 4R on 3R seeds was closer to 3R grown on 3R seeds **(Figure 4.6 B)**. This showed that in this region, the conformation of 4R grown on 3R seeds was similar to that of 3R on 3R seeds. The 3R seeds were able to conformationally template 4R of 311/326 double mutant. Similar results were obtained for 311/328 double mutant **(Figure 4.6 C)**. DEER measurements confirmed the conformational templating of 4R on 3R at the molecular level.

The dipolar evolution data were fit using Tikhonov regularization which is an unbiased way to fit data compared to other fitting programs available in DEER Analysis 2011(Jeschke et al., 2006). Homogeneous background correction to account for intermolecular interactions was done using d=3 dimensions. This spatial background correction was used for the double mutants because it showed better background correction with singly labeled mutants. The obtained distance distributions by Tikhonov regularization for the double mutants showed that the filaments formed were heterogeneous in nature. For the K18 on K18 seeds, double mutant 311/322 showed distance distribution from 2-5.3 nm with peaks at 3.4 and 3.9, 311/326 double mutant showed a distance distribution from 2.2 -5.3 nm with peak at 3.6 nm and for 311/328, 2-5.3 distance distribution was observed with peaks at 3.4, 3.9 and 4.8 nm. For the experiments, the seeds used for templating of the monomers were prepared by going

through multiple steps of seeded reactions as it had already been shown that samples with a homogeneous mixture of filaments could be prepared by repetitive seeded growth (Paravastu et al., 2008). Distance distributions of samples showed that the mixture of the double mutant formed were heterogeneous even after templating the double mutant onto the seeds from the 4th cycle of the multistep seeded reaction. Since the distance distributions observed were really broad, the actual distances may not be just because of the rotamer conformation of the spin label alone (Jeschke et al., 2005). During analysis of raw data using DEER Analysis 2011, smaller peaks at the base line could be seen which might denote noise artifacts (Jeschke et al., 2004). As observed in the distance distributions of double mutants, the smaller peaks in 311/322 and 311/326 double mutant may be ignored (Dockter et al., 2009) **(Figure 4.7 A, B)**. In the K18 311/328 double mutant distance distribution, observed peaks at 3.4 nm and 3.9 nm are almost one 3rd of the highest peak at 4.8 nm **(Figure 4.7 C)**. To check whether the smaller peaks were noise related, Tikhonov regularization fits were done at various scan numbers. The lower scan numbers with lower S/N showed the same heterogeneous distribution. These broad distributions may not be attributed to intermolecular interactions between nitroxide labels of different strands. To avoid intermolecular interactions between spin labels only 2% of the double mutant was labeled. As already mentioned, the interstrand distance between two β-strands is 4.8 Å, and hypothetically if the double mutant was incorporated after every 48th strand in the filament, the distance would be ~23nm which is much larger than the distances measured.

The distance distribution of K18 311/322 on K19 seeds was similar to K19 311/322 on K19 seeds than to K18 311/322 on K18 seeds. The distance distribution of K19 311/326 on K19 seeds could not be obtained. The dipolar oscillation curve of K19 311/326 on K19 seeds mutant is similar to the dipolar oscillation curve of the weighted sum of singly labeled 311 and 326. Hence, the distance between 311 and 326 in the K19 double mutant is more than 5.5 nm (Jeschke et al., 2006). When the Tikhonov regularization fit for distance distribution was done for K18 311/326 on K19 seeds, peaks were observed at 2.8 and 4 nm. When the dipolar oscillation curves were looked at in **Figure 4.6 B** for K18 311 326 on K19 seeds, the curve was closer to K19 311 326 on K19 seeds. This led to the conclusion that the maximum population of K18 311 326 on K19 seeds has a conformation which is similar to K19 311 /326 on K19 seeds. Therefore, the majority of conformers of K18 311/326 on K19 seeds have really long distances. For the double mutant 311/328 (K18, K19) on K19 seeds, Tikhonov regularization fits could not be done to obtain distance distribution. Here we may not exclude the presence of distances larger than 5 nm, which would be suppressed by the background correction for 2.5 µs evolution time. All of the above obtained distance distributions by DEER have shown that the filaments form heterogeneous mixture, K18 when grown on K19 looks more like K19 on K19 seeds rather than K18 on K18 seeds. The results have also shown that DEER could be a very good technique to study structural polymorphism in fibrils.

Solid state NMR was first used to study molecular level polymorphism in β-amyloid fibrils of AD (Petkova et al., 2005). Similar polymorphism now has been documented by solid-state NMR for α-synuclein fibrils (Heise et al., 2005), amylin (IAPP) fibrils (Madine et al., 2008) and other amyloid fibrils (Paravastu et al., 2006).

Previous studies on conformational templating differences between seeded reactions in tau filaments at the structural level have been shown based on circular dichroism spectroscopy (CD) and FTIR (Frost et al., 2009). These studies by CD and FTIR showed differences based on the secondary structures (β-sheet, random coil, α-helix and random coil) seen in tau filaments. Differences in the filament fragilities and morphologies based on the electron microscopy also helped in studying the structural differences. Though the mentioned studies have shown structural differences, the differences were not as dramatic as shown by our DEER studies at molecular level.

Studies of structural polymorphism in tau filaments due to conformational differences at the molecular level are important because it has been shown that in sporadic tauopathies, phenotypic diversities are seen due to conformational differences in wild type tau filaments (Frost et al., 2009; Legname et al., 2006; Tanaka et al., 2004b). Also structural polymorphism has been seen in multiple amyloid forming proteins due to formation of distinct conformers based on template conformation change (Petkova et al., 2005; Yamaguchi et al., 2005).

Evidence available in prion disease has suggested that there is a strong link between the conformation of a fibrillar protein and the resultant phenotype (Bessen & Marsh, 1994; Legname et al., 2006; Peretz et al., 2002). When prion monomers from one species were cross-seeded with preformed fibrils from another species, a new amyloid strain was produced which showed the secondary structure and morphology of the template fibrils. Conformational differences which were strain-specific because of cross-seeding were also found in yeast Sup35 prion amyloid fibrils by FTIR and EPR spectra (Tanaka et al., 2005). It has also been suggested that prion populations comprised of variety of conformers with the same sequence, constitutes 'quasi-species', from which the one replicating most efficiently in a particular environment is selected. The transfer of prions between cell types within the same species involves a selection of favored 'substrains', and propagation of prions in the presence of an inhibitory drug can result in the appearance of drug-resistant prion populations (Weissmann et al., 2011).

A very recent study in mice has shown that the transfer of tau filaments between synapses of neurons causes the spread of neurodegenerative disease (Liu et al., 2012). We have shown in our study that there are innumerable number of compositionally (Siddiqua & Margittai, 2010) and conformationally distinct filaments of tau (Dinkel et al., 2011). There might be some species of tau conformers which might be more infectious than the others as shown in prion populations and hence structural polymorphism could be a major contributor to the diversity of tauopathies.

Studies have also shown that in AD, the appearance of NFTs of tau correlates really well with the symptoms of the disease, while the same is not seen with β-amyloid plaques (Braak et al., 1994; Liu et al., 2012). Since most of the drugs which were targeted at β-amyloid have failed (Medina, 2011), this research work on basic understanding of tau filament structures is a stepping stone in coming up with better treatments targeted at molecular clearances of the filaments (Cohen & Kelly, 2003). The findings of our research in understanding structural polymorphism of tau filaments are highly significant in the ongoing research in neurodegenerative diseases and their treatments.

.

References

Adams, S. J., DeTure, M. A., McBride, M., Dickson, D. W., and Petrucelli, L. (2010) *PLoS One* 5, e10810

Alexandrescu, A. T. (2005). Amyloid accomplices and enforcers. *Protein Science, 14*(1), 1-12.

Altenbach, C., Marti, T., Khorana, H. G., & Hubbell, W. L. (1990). Transmembrane protein structure: Spin labeling of bacteriorhodopsin mutants. *Science, 248*(4959), 1088.

Altenbach, C., Oh, K. J., Trabanino, R. J., Hideg, K., & Hubbell, W. L. (2001). Estimation of inter-residue distances in spin labeled proteins at physiological temperatures: Experimental strategies and practical limitations. *Biochemistry, 40*(51), 15471-15482.

alz.org. (2011). http://www.alz.org/downloads/Fact_Figures_2011.pdf

Alzheimer's association. (2011). “Alzheimer’s disease in the U.S. population: prevalence estimates using the 2000 census.” archives of neurology 2003;60(8):1119–1122 and Alzheimer’s association. early-onset dementia: A national challenge, A future crisis. washington, D.C.: Alzheimer’s association; 2006; as published by the Alzheimer’s association, Alzheimer’s disease facts and figures, 2011.

Andronesi, O. C., Bergen, M., Biernat, J., Seidel, K., Griesinger, C., Mandelkow, E., & Baldus, M. (2008). Characterization of Alzheimer’s-like paired helical filaments from the core domain of tau protein using solid-state NMR spectroscopy. *Journal of the American Chemical Society, 130*(18), 5922-5928.

Anfinsen, C. (1973). Principles that govern the folding of protein chains. *Science, 181*(96), 223.

Aoyagi, H., Hasegawa, M., & Tamaoka, A. (2007). Fibrillogenic nuclei composed of P301L mutant tau induce elongation of P301L tau but not wild-type tau. *Journal of Biological Chemistry, 282*(28), 20309-20318.

Banham, J. E., Timmel, C. R., Abbott, R. J. M., Lea, S. M., & Jeschke, G. (2006). The characterization of weak protein–protein interactions: Evidence from DEER for the trimerization of a von willebrand factor A domain in solution. *Angewandte Chemie International Edition, 45*(7), 1058-1061.

Barghorn, S., & Mandelkow, E. (2002). Toward a unified scheme for the aggregation of tau into alzheimer paired helical filaments. *Biochemistry, 41*(50), 14885-14896.

Bedrood, S., Li Y, Isas, J., Hegde, G., Baxa, U., Haworth, I., & Langen, R. (2011). Fibril structure of human islet amyloid polypeptide. *Journal of Biological Chemistry,* (M11.327817)

Berliner, L. J. (2000). *Distance measurements in biological systems by EPR* Kluwer Academic Pub.

Berliner, L. J., Grunwald, J., Hankovszky, H. O., & Hideg, K. (1982). A novel reversible thiol-specific spin label: Papain active site labeling and inhibition* 1. *Analytical Biochemistry, 119*(2), 450-455.

Berriman, J., Serpell, L. C., Oberg, K. A., Fink, A. L., Goedert, M., & Crowther, R. A. (2003). Tau filaments from human brain and from *in vitro* assembly of recombinant protein show cross-β structure. *Proceedings of the National Academy of Sciences, 100*(15), 9034.

Bessen, R. A., & Marsh, R. F. (1994). Distinct PrP properties suggest the molecular basis of strain variation in transmissible mink encephalopathy. *Journal of Virology, 68*(12), 7859.

Braak, F., Braak, H., & Mandelkow, E. M. (1994). A sequence of cytoskeleton changes related to the formation of neurofibrillary tangles and neuropil threads. *Acta Neuropathologica, 87*(6), 554-567.

Braak, H., & Del Tredici, K. (2011). Alzheimer's pathogenesis: Is there neuron-to-neuron propagation? *Acta Neuropathologica,* , 1-7.

Bretteville, A., & Planel, E. (2008). Tau aggregates: Toxic, inert, or protective species? *Journal of Alzheimer's Disease, 14*(4), 431-436.

Brunden, K. R., Trojanowski, J. Q., & Lee, V. M. Y. (2008). Evidence that non-fibrillar tau causes pathology linked to neurodegeneration and behavioral impairments. *Journal of Alzheimer's Disease, 14*(4), 393-399.

Buée, L., & Delacourte, A. (1999). Comparative biochemistry of tau in progressive supranuclear palsy, corticobasal degeneration, FTDP-17 and pick's disease. *Brain Pathology, 9*(4), 681-693.

Butner, K. A., & Kirschner, M. W. (1991). Tau protein binds to microtubules through a flexible array of distributed weak sites. *The Journal of Cell Biology, 115*(3), 717.

Calamai, M., Kumita, J. R., Mifsud, J., Parrini, C., Ramazzotti, M., Ramponi, G., . . . Dobson, C. M. (2006). Nature and significance of the interactions between amyloid fibrils and biological polyelectrolytes. *Biochemistry, 45*(42), 12806-12815.

Cassimeris, L., & Spittle, C. (2001). Regulation of microtubule-associated proteins. *International Review of Cytology, 210*, 163-226.

Castilla, J., Morales, R., Saá, P., Barria, M., Gambetti, P., & Soto, C. (2008). Cell-free propagation of prion strains. *The EMBO Journal, 27*(19), 2557-2566.

Castilla, J., Saá, P., Hetz, C., & Soto, C. (2005). *In vitro* generation of infectious scrapie prions. *Cell, 121*(2), 195-206.

Chen, M., Margittai, M., Chen, J., & Langen, R. (2007). Investigation of α-synuclein fibril structure by site-directed spin labeling. *Journal of Biological Chemistry, 282*(34), 24970.

Chiang, D.W., Borbat, P.P., Freed, J.H. (2005).The determination of pair distance distributions by pulsed ESR using Tikhonov regularization. *Journal of Magnetic Resonance, 172(2), 279-295.*

Chiti, F., & Dobson, C. M. (2006). Protein misfolding, functional amyloid, and human disease. *Annu.Rev.Biochem., 75*, 333-366.

Clavaguera, F., Bolmont, T., Crowther, R. A., Abramowski, D., Frank, S., Probst, A., . . . Staufenbiel, M. (2009). Transmission and spreading of tauopathy in transgenic mouse brain. *Nature Cell Biology, 11*(7), 909-913.

Cleveland, D. W., Hwo, S. Y., & Kirschner, M. W. (1977). Physical and chemical properties of purified tau factor and the role of tau in microtubule assembly* 1. *Journal of Molecular Biology, 116*(2), 227-247.

Cleveland, D., Fischer, S. G., Kirschner, M. W., & Laemmli, U. K. (1977). Peptide mapping by limited proteolysis in sodium dodecyl sulfate and analysis by gel electrophoresis. *Journal of Biological Chemistry, 252*(3), 1102.

Cobb, N. J., Sönnichsen, F. D., Mchaourab, H., & Surewicz, W. K. (2007). Molecular architecture of human prion protein amyloid: A parallel, in-register β-structure. *Proceedings of the National Academy of Sciences, 104*(48), 18946.

Cohen, F. E., & Kelly, J. W. (2003). Therapeutic approaches to protein-misfolding diseases. *Nature, 426*(6968), 905-909.

Colby, D. W., Giles, K., Legname, G., Wille, H., Baskakov, I. V., DeArmond, S. J., & Prusiner, S. B. (2009). Design and construction of diverse mammalian prion strains. *Proceedings of the National Academy of Sciences, 106*(48), 20417.

Collinge, J. (2001). Prion diseases of humans and animals: Their causes and molecular basis. *Annual Review of Neuroscience, 24*(1), 519-550.

Collinge, J., Sidle, K. C. L., Meads, J., Ironside, J., & Hill, A. F. (1996). Molecular analysis of prion strain variation and the aetiology of'new variant'CJD.

Columbus, L., & Hubbell, W. L. (2002). A new spin on protein dynamics. *Trends in Biochemical Sciences, 27*(6), 288-295.

De Calignon, A., Fox, L. M., Pitstick, R., Carlson, G. A., Bacskai, B. J., Spires-Jones, T. L., & Hyman, B. T. (2010). Caspase activation precedes and leads to tangles. *Nature, 464*(7292), 1201-1204.

Dinkel, P. D., Siddiqua, A., Huynh, H., Shah, M., & Margittai, M. (2011). Variations in filament conformation dictate seeding barrier between three-and four-repeat tau. *Biochemistry*, 50, 4330-4336.

Dockter, C., Volkov, A., Bauer, C., Polyhach, Y., Joly-Lopez, Z., Jeschke, G., & Paulsen, H. (2009). Refolding of the integral membrane protein light-harvesting complex II monitored by pulse EPR. *Proceedings of the National Academy of Sciences, 106*(44), 18485-18490.

Drubin, D. G., & Kirschner, M. W. (1986). Tau protein function in living cells. *The Journal of Cell Biology, 103*(6), 2739-2746.

Dunker, A. K., Silman, I., Uversky, V. N., & Sussman, J. L. (2008). Function and structure of inherently disordered proteins. *Current Opinion in Structural Biology, 18*(6), 756-764.

Eaton, G. R., Eaton, S. S., Barr, D., & Weber, R. (2009). *Quantitative EPR* Springer Verlag Wien.

Endeward, B., Butterwick, J. A., MacKinnon, R., & Prisner, T. F. (2009). Pulsed electron− electron double-resonance determination of spin-label distances and orientations on the tetrameric potassium ion channel KcsA. *Journal of the American Chemical Society, 131*(42), 15246-15250.

Fajer, P. G., Brown, L., & Song, L. (2007). Practical pulsed dipolar ESR (DEER). *ESR Spectroscopy in Membrane Biophysics,* , 95-128.

Friedhoff, P., Von Bergen, M., Mandelkow, E. M., Davies, P., & Mandelkow, E. (1998). A nucleated assembly mechanism of alzheimer paired helical filaments. *Proceedings of the National Academy of Sciences, 95*(26), 15712.

Frost, B., Jacks, R. L., & Diamond, M. I. (2009). Propagation of tau misfolding from the outside to the inside of a cell. *Journal of Biological Chemistry, 284*(19), 12845.

Frost, B., Ollesch, J., Wille, H., & Diamond, M. I. (2009). Conformational diversity of wild-type tau fibrils specified by templated conformation change. *Journal of Biological Chemistry, 284*(6), 3546.

Gamblin, T., King M.E., Dawson, H., Vitek, M.P., Kuret, J., Berry, R.W., Binder, L.I.(2000). *In vitro* polymerization of tau protein monitored by laser light scattering: method and application to the study of FTDP-17 mutants. *Biochemistry, 39(20),6136-6144.*

Garcia, M. L., & Cleveland, D. W. (2001). Going new places using an old MAP: Tau, microtubules and human neurodegenerative disease. *Current Opinion in Cell Biology, 13*(1), 41-48.

Goedert, M., Clavaguera, F., & Tolnay, M. (2010). The propagation of prion-like protein inclusions in neurodegenerative diseases. *Trends in Neurosciences, 33*(7), 317-325.

Goedert, M., Jakes, R., Spillantini, M., Hasegawa, M., Smith, M., & Crowther, R. (1996). Assembly of microtubule-associated protein tau into alzheimer-like filaments induced by sulphated glycosaminoglycans. *Nature, 383*(6600), 550-553.

Goedert, M., Spillantini, M., Cairns, N., & Crowther, R. (1992a). Tau proteins of alzheimer paired helical filaments: Abnormal phosphorylation of all six brain isoforms. *Neuron, 8*(1), 159-168.

Goedert, M., Spillantini, M., Jakes, R., Rutherford, D., & Crowther, R. (1989a). Multiple isoforms of human microtubule-associated protein tau: Sequences and localization in neurofibrillary tangles of alzheimer's disease. *Neuron, 3*(4), 519-526.

Goedert, M., Spillantini, M., Potier, M., Ulrich, J., & Crowther, R. (1989). Cloning and sequencing of the cDNA encoding an isoform of microtubule-associated protein tau containing four tandem repeats: Differential expression of tau protein mRNAs in human brain. *The EMBO Journal, 8*(2), 393.

Goedert, M., Wischik, C., Crowther, R., Walker, J., & Klug, A. (1988). Cloning and sequencing of the cDNA encoding a core protein of the paired helical filament of alzheimer disease: Identification as the microtubule-associated protein tau. *Proceedings of the National Academy of Sciences, 85*(11), 4051.

Goedert, M., & Spillantini, M. G. (2006). A century of alzheimer's disease. *Science (New York, N.Y.), 314*(5800), 777-781. doi:10.1126/science.1132814

Goedert, M., & Spillantini, M. G. (2011). Pathogenesis of the tauopathies. *Journal of Molecular Neuroscience : MN*, doi:10.1007/s12031-011-9593-4

Goode, B. L., Chau, M., Denis, P. E., & Feinstein, S. C. (2000). Structural and functional differences between 3-repeat and 4-repeat tau isoforms. *Journal of Biological Chemistry, 275*(49), 38182.

Goode, B. L., & Feinstein, S. C. (1994). Identification of a novel microtubule binding and assembly domain in the developmentally regulated inter-repeat region of tau. *The Journal of Cell Biology, 124*(5), 769.

Goux, W. J. (2002). The conformations of filamentous and soluble tau associated with alzheimer paired helical filaments. *Biochemistry, 41*(46), 13798-13806.

Greenberg, S., Davies, P., Schein, J., & Binder, L. (1992). Hydrofluoric acid-treated tau PHF proteins display the same biochemical properties as normal tau. *Journal of Biological Chemistry, 267*(1), 564.

Gross, A., Columbus, L., Hideg, K., Altenbach, C., & Hubbell, W. L. (1999). Structure of the KcsA potassium channel from streptomyces lividans: A site-directed spin labeling study of the second transmembrane segment. *Biochemistry, 38*(32), 10324-10335.

Grundke-Iqbal, I., Iqbal, K., Tung, Y. C., Quinlan, M., Wisniewski, H. M., & Binder, L. I. (1986). Abnormal phosphorylation of the microtubule-associated protein tau (tau) in alzheimer cytoskeletal pathology. *Proceedings of the National Academy of Sciences, 83*(13), 4913.

Guo JL, & Lee VM. (2011). Seeding of normal tau by pathological tau conformers drives pathogenesis of alzheimer-like tangles. *Journal of Biological Chemistry, 286*, 15317-15331.

Hanson, P., Millhauser, G., Formaggio, F., Crisma, M., & Toniolo, C. (1996). ESR characterization of hexameric, helical peptides using double TOAC spin labeling. *Journal of the American Chemical Society, 118*(32), 7618-7625.

Hardy, J., & Selkoe, D. J. (2002). The amyloid hypothesis of alzheimer's disease: Progress and problems on the road to therapeutics. *Science, 297*(5580), 353.

Hardy, J. A., & Higgins, G. A. (1992). Alzheimer's disease: The amyloid cascade hypothesis. *Science*,

Heise, H., Hoyer, W., Becker, S., Andronesi, O. C., Riedel, D., & Baldus, M. (2005). Molecular-level secondary structure, polymorphism, and dynamics of full-length α-

synuclein fibrils studied by solid-state NMR. *Proceedings of the National Academy of Sciences of the United States of America, 102*(44), 15871.

Helmus, J. J., Nadaud, P. S., Höfer, N., & Jaroniec, C. P. (2008). Determination of methyl C–N dipolar couplings in peptides and proteins by three-dimensional and four-dimensional magic-angle spinning solid-state NMR spectroscopy. *The Journal of Chemical Physics, 128*, 052314.

Hibbs, R. E., Talley, T. T., & Taylor, P. (2004). Acrylodan-conjugated cysteine side chains reveal conformational state and ligand site locations of the acetylcholine-binding protein. *Journal of Biological Chemistry, 279*(27), 28483-28491.

Hilger, D., Jung, H., Padan, E., Wegener, C., Vogel, K. P., Steinhoff, H. J., & Jeschke, G. (2005). Assessing oligomerization of membrane proteins by four-pulse DEER: PH-dependent dimerization of NhaA na /H antiporter of E. coli. *Biophysical Journal, 89*(2), 1328-1338.

Hirokawa, N. (1982). Cross-linker system between neurofilaments, microtubules, and membranous organelles in frog axons revealed by the quick-freeze, deep-etching method. *The Journal of Cell Biology, ,* 129-142.

Hong, M., Zhukareva, V., Vogelsberg-Ragaglia, V., Wszolek, Z., Reed, L., Miller, B. I., . . . Goate, A. (1998). Mutation-specific functional impairments in distinct tau isoforms of hereditary FTDP-17. *Science, 282*(5395), 1914.

Hubbell, W. L., Gross, A., Langen, R., & Lietzow, M. A. (1998). Recent advances in site-directed spin labeling of proteins. *Current Opinion in Structural Biology, 8*(5), 649-656.

Hubbell, W. L., Cafiso, D. S., & Altenbach, C. (2000a). Identifying conformational changes with site-directed spin labeling. *Nature Structural Biology, 7*(9), 735-739. doi:10.1038/78956

Hubbell, W. L., Mchaourab, H. S., Altenbach, C., & Lietzow, M. A. (1996). Watching proteins move using site-directed spin labeling. *Structure (London, England : 1993), 4*(7), 779-783.

Huber, M., Lindgren, M., Hammarström, P., Mårtensson, L. G., Carlsson, U., Eaton, G., & Eaton, S. (2001). Phase memory relaxation times of spin labels in human carbonic anhydrase II: Pulsed EPR to determine spin label location. *Biophysical Chemistry, 94*(3), 245-256.

Ittner, L. M., & Götz, J. (2010). Amyloid-β and tau—a toxic pas de deux in alzheimer's disease. *Nature Reviews Neuroscience,*

Jayasinghe, S. A., & Langen, R. (2004). Identifying structural features of fibrillar islet amyloid polypeptide using site-directed spin labeling. *Journal of Biological Chemistry, 279*(46), 48420.

Jeganathan, S., von Bergen, M., Brutlach, H., Steinhoff, H. J., & Mandelkow, E. (2006). Global hairpin folding of tau in solution. *Biochemistry, 45*(7), 2283-2293.

Jeganathan, S., von Bergen, M., Mandelkow, E. M., & Mandelkow, E. (2008). The natively unfolded character of tau and its aggregation to alzheimer-like paired helical filaments†. *Biochemistry, 47*(40), 10526-10539.

Jeschke, G. (2002). Distance measurements in the nanometer range by pulse EPR. *ChemPhysChem, 3*(11), 927-932.

Jeschke, G., Bender, A., Paulsen, H., Zimmermann, H., & Godt, A. (2004). Sensitivity enhancement in pulse EPR distance measurements. *Journal of Magnetic Resonance, 169*(1), 1-12.

Jeschke, G., Bender, A., Schweikardt, T., Panek, G., Decker, H., & Paulsen, H. (2005). Localization of the N-terminal domain in light-harvesting chlorophyll a/b protein by EPR measurements. *Journal of Biological Chemistry, 280*(19), 18623.

Jeschke, G., Chechik, V., Ionita, P., Godt, A., Zimmermann, H., Banham, J., . . . Jung, H. (2006). DeerAnalysis2006—a comprehensive software package for analyzing pulsed ELDOR data. *Applied Magnetic Resonance, 30*(3), 473-498.

Jeschke, G., Panek, G., Godt, A., Bender, A., & Paulsen, H. (2004). Data analysis procedures for pulse ELDOR measurements of broad distance distributions. *Applied Magnetic Resonance, 26*(1), 223-244.

Jeschke, G., & Polyhach, Y. (2007). Distance measurements on spin-labelled biomacromolecules by pulsed electron paramagnetic resonance. *Phys.Chem.Chem.Phys., 9*(16), 1895-1910.

Jiménez, J. L., Nettleton, E. J., Bouchard, M., Robinson, C. V., Dobson, C. M., & Saibil, H. R. (2002). The protofilament structure of insulin amyloid fibrils. *Proceedings of the National Academy of Sciences, 99*(14), 9196.

Jones, E. M., & Surewicz, W. K. (2005). Fibril conformation as the basis of species-and strain-dependent seeding specificity of mammalian prion amyloids. *Cell, 121*(1), 63-72.

Karran, E., Mercken, M., & De Strooper, B. (2011). The amyloid cascade hypothesis for alzheimer's disease: An appraisal for the development of therapeutics. *Nature Reviews Drug Discovery, 10*(9), 698-712.

Karyagina, I., Becker, S., Giller, K., Riedel, D., Jovin, T. M., Griesinger, C., & Bennati, M. (2011). Electron paramagnetic resonance spectroscopy measures the distance between the external [beta]-strands of folded [alpha]-synuclein in amyloid fibrils. *Biophysical Journal, 101*(1), L1-L3.

Kayed, R., Head, E., Thompson, J. L., McIntire, T. M., Milton, S. C., Cotman, C. W., & Glabe, C. G. (2003). Common structure of soluble amyloid oligomers implies common mechanism of pathogenesis. *Science, 300*(5618), 486.

Khurana, R., Coleman, C., Ionescu-Zanetti, C., Carter, S. A., Krishna, V., Grover, R. K., . . . Singh, S. (2005). Mechanism of thioflavin T binding to amyloid fibrils. *Journal of Structural Biology, 151*(3), 229-238.

King, C. Y., & Diaz-Avalos, R. (2004). Protein-only transmission of three yeast prion strains. *Nature, 428*(6980), 319-323.

Kirkitadze, M. D., Bitan, G., & Teplow, D. B. (2002). Paradigm shifts in alzheimer's disease and other neurodegenerative disorders: The emerging role of oligomeric assemblies. *Journal of Neuroscience Research, 69*(5), 567-577.

Kodali, R., Williams, A. D., Chemuru, S., & Wetzel, R. (2010a). A [beta](1-40) forms five distinct amyloid structures whose [beta]-sheet contents and fibril stabilities are correlated. *Journal of Molecular Biology, 401*(3), 503-517.

Ladner, C. L., Chen, M., Smith, D. P., Platt, G. W., Radford, S. E., & Langen, R. (2010). Stacked sets of parallel, in-register β-strands of β2-microglobulin in amyloid fibrils revealed by site-directed spin labeling and chemical labeling. *Journal of Biological Chemistry, 285*(22), 17137.

Lakowicz, J. (2006). *Principles of fluorescence spectroscopy* (Third Edition ed.)

Lashuel, H. A., Hartley, D., Petre, B. M., Walz, T., & Lansbury, P. T. (2002). Neurodegenerative disease: Amyloid pores from pathogenic mutations. *Nature, 418*(6895), 291-291.

Lee, S. J., Desplats, P., Sigurdson, C., Tsigelny, I., & Masliah, E. (2010). Cell-to-cell transmission of non-prion protein aggregates. *Nature Reviews Neurology, 6*(12), 702-706.

Lee, V. M. Y., Goedert, M., & Trojanowski, J. Q. (2001). Neurodegenerative tauopathies. *Annual Review of Neuroscience, 24*(1), 1121-1159.

Legname, G., Baskakov, I. V., Nguyen, H. O. B., Riesner, D., Cohen, F. E., DeArmond, S. J., & Prusiner, S. B. (2004). Synthetic mammalian prions. *Science, 305*(5684), 673.

Legname, G., Nguyen, H. O. B., Peretz, D., Cohen, F. E., DeArmond, S. J., & Prusiner, S. B. (2006). Continuum of prion protein structures enciphers a multitude of prion isolate-specified phenotypes. *Proceedings of the National Academy of Sciences, 103*(50), 19105.

Levine III, H. (1993). Thioflavine T interaction with synthetic alzheimer's disease β-amyloid peptides: Detection of amyloid aggregation in solution. *Protein Science, 2*(3), 404-410.

Li, J., Browning, S., Mahal, S. P., Oelschlegel, A. M., & Weissmann, C. (2010). Darwinian evolution of prions in cell culture. *Science, 327*(5967), 869.

Li, L., von Bergen, M., Mandelkow, E. M., & Mandelkow, E. (2002). Structure, stability, and aggregation of paired helical filaments from tau protein and FTDP-17 mutants probed by tryptophan scanning mutagenesis. *Journal of Biological Chemistry, 277*(44), 41390.

Lietzow, M. A., & Hubbell, W. L. (2004). Motion of spin label side chains in cellular retinol-binding protein: Correlation with structure and nearest-neighbor interactions in an antiparallel β-sheet. *Biochemistry, 43*(11), 3137-3151.

Liu, L., Drouet, V., Wu, J. W., Witter, M. P., Small, S. A., Clelland, C., & Duff, K. (2012). Trans - synaptic spread of tau pathology in vivo . *PLoS One, 7(2)*(e31302) doi:10.1371/journal.pone.0031302

Los Angeles Times. (2011). http://articles.latimes.com/2011/dec/06/news/la-heb-derek-boogaard-brain-20111206

Madine, J., Jack, E., Stockley, P. G., Radford, S. E., Serpell, L. C., & Middleton, D. A. (2008). Structural insights into the polymorphism of amyloid-like fibrils formed by region 20− 29 of amylin revealed by solid-state NMR and X-ray fiber diffraction. *Journal of the American Chemical Society, 130*(45), 14990-15001.

Mahal, S. P., Baker, C. A., Demczyk, C. A., Smith, E. W., Julius, C., & Weissmann, C. (2007). Prion strain discrimination in cell culture: The cell panel assay. *Proceedings of the National Academy of Sciences, 104*(52), 20908.

Makrides, V., Massie, M. R., Feinstein, S. C., & Lew, J. (2004). Evidence for two distinct binding sites for tau on microtubules. *Proceedings of the National Academy of Sciences of the United States of America, 101*(17), 6746.

Margittai, M., Fasshauer, D., Pabst, S., Jahn, R., & Langen, R. (2001). Homo-and heterooligomeric SNARE complexes studied by site-directed spin labeling. *Journal of Biological Chemistry, 276*(16), 13169.

Margittai, M., & Langen, R. (2004). Template-assisted filament growth by parallel stacking of tau. *Proceedings of the National Academy of Sciences of the United States of America, 101*(28), 10278.

Margittai, M., & Langen, R. (2006a). Side chain-dependent stacking modulates tau filament structure. *Journal of Biological Chemistry, 281*(49), 37820.

Margittai, M., & Langen, R. (2006b). Spin labeling analysis of amyloids and other protein aggregates. *Methods in Enzymology, 413*, 122-139.

Margittai, M., & Langen, R. (2008). Fibrils with parallel in-register structure constitute a major class of amyloid fibrils: Molecular insights from electron paramagnetic resonance spectroscopy. *Quarterly Reviews of Biophysics, 41*(3-4), 265-297.

Maskevich, A. A., Stsiapura, V. I., Kuzmitsky, V. A., Kuznetsova, I. M., Povarova, O. I., Uversky, V. N., & Turoverov, K. K. (2007). Spectral properties of thioflavin T in solvents with different dielectric properties and in a fibril-incorporated form. *Journal of Proteome Research, 6*(4), 1392-1401.

Mchaourab, H. S., Lietzow, M. A., Hideg, K., & Hubbell, W. L. (1996). Motion of spin-labeled side chains in T4 lysozyme. correlation with protein structure and dynamics. *Biochemistry, 35*(24), 7692-7704.

McKee, A. C., Cantu, R. C., Nowinski, C. J., Hedley-Whyte, E. T., Gavett, B. E., Budson, A. E., . . . Stern, R. A. (2009). Chronic traumatic encephalopathy in athletes: Progressive tauopathy following repetitive head injury. *Journal of Neuropathology and Experimental Neurology, 68*(7), 709.

Medina, M. (2011). Recent developments in tau-based therapeutics for neurodegenerative diseases. *Recent Patents on CNS Drug Discovery, 6*(1), 20-30.

Miller, G. (2009). Could they all be prion diseases? *Science, 326*(5958), 1337.

Milov, A., Ponomarev, A., & Tsvetkov, Y. D. (1984). Electron-electron double resonance in electron spin echo: Model biradical systems and the sensitized photolysis of decalin. *Chemical Physics Letters, 110*(1), 67-72.

Milov, A., Salikohov, K., & Shchirov, M. (1981). Use of the double resonance in electron spin echo method for the study of paramagnetic center spatial distribution in solids. *Fizika Tverdogo Tela, 23*, 975-982.

Molin, I. U. N., Salikhov, K. M., & Zamaraev, K. I. (1980). *Spin exchange: Principles and applications in chemistry and biology* Springer.

Mukrasch, M. D., Bibow, S., Korukottu, J., Jeganathan, S., Biernat, J., Griesinger, C., . . . Zweckstetter, M. (2009). Structural polymorphism of 441-residue tau at single residue resolution. *PLoS Biology, 7*(2), e1000034.

Naiki, H., Higuchi, K., Hosokawa, M., & Takeda, T. (1989). Fluorometric determination of amyloid fibrils< i> *in vitro*</i> using the fluorescent dye, thioflavine T. *Analytical Biochemistry, 177*(2), 244-249.

Nonaka, T., Watanabe, S. T., Iwatsubo, T., & Hasegawa, M. (2010). Seeded aggregation and toxicity of α-synuclein and tau. *Journal of Biological Chemistry, 285*(45), 34885.

Novak, M., Kabat, J., & Wischik, C. (1993). Molecular characterization of the minimal protease resistant tau unit of the alzheimer's disease paired helical filament. *The EMBO Journal, 12*(1), 365.

Olmsted, J. B., & Borisy, G. G. (1973). Microtubules. *Annual Review of Biochemistry, 42*(1), 507-540.

Olmsted, J. (1986). Microtubule-associated proteins. *Annual Review of Cell Biology, 2*(1), 421-457.

Omalu, B., Bailes, J., Hamilton, R. L., Kamboh, M. I., Hammers, J., Case, M., & Fitzsimmons, R. J. D. (2011). Emerging histomorphologic phenotypes of chronic traumatic encephalopathy in american athletes. *Neurosurgery, 69*(1), 173.

Omalu, B., Hammers, J. L., Bailes, J., Hamilton, R. L., Kamboh, M. I., Webster, G., & Fitzsimmons, R. P. (2011). Chronic traumatic encephalopathy in an iraqi war veteran with posttraumatic stress disorder who committed suicide. *Neurosurgical Focus, 31*(5), 3.

Pannier, M., Veit, S., Godt, A., Jeschke, G., & Spiess, H. W. (2000). Dead-time free measurement of dipole-dipole interactions between electron spins. *Journal of Magnetic Resonance, 142*(2), 331-340.

Paravastu, A. K., Leapman, R. D., Yau, W. M., & Tycko, R. (2008). Molecular structural basis for polymorphism in alzheimer's β-amyloid fibrils. *Proceedings of the National Academy of Sciences, 105*(47), 18349.

Paravastu, A. K., Petkova, A. T., & Tycko, R. (2006). Polymorphic fibril formation by residues 10-40 of the alzheimer's [beta]-amyloid peptide. *Biophysical Journal, 90*(12), 4618-4629.

Paravastu, A. K., Qahwash, I., Leapman, R. D., Meredith, S. C., & Tycko, R. (2009). Seeded growth of β-amyloid fibrils from alzheimer's brain-derived fibrils produces a distinct fibril structure. *Proceedings of the National Academy of Sciences, 106*(18), 7443.

Peretz, D., Williamson, R. A., Legname, G., Matsunaga, Y., Vergara, J., Burton, D. R., . . . Scott, M. R. (2002). A change in the conformation of prions accompanies the emergence of a new prion strain. *Neuron, 34*(6), 921-932.

Petkova, A. T., Leapman, R. D., Guo, Z., Yau, W. M., Mattson, M. P., & Tycko, R. (2005). Self-propagating, molecular-level polymorphism in alzheimer's ß-amyloid fibrils. *Science, 307*(5707), 262.

Prusiner, S. B. (1998). Prions. *Proceedings of the National Academy of Sciences, 95*(23), 13363.

Schiemann, O. (2009). Mapping global folds of oligonucleotides by pulsed Electron–Electron double resonance. *Methods in Enzymology, 469*, 329-351.

Schiemann, O., & Prisner, T. F. (2007). Long-range distance determinations in biomacromolecules by EPR spectroscopy. *Quarterly Reviews of Biophysics, 40*(1), 1-54.

Schmitt, F. O. (1968). Fibrous proteins--neuronal organelles. *Proceedings of the National Academy of Sciences of the United States of America, 60*(4), 1092.

Schweers, O., Schönbrunn-Hanebeck, E., Marx, A., & Mandelkow, E. (1994). Structural studies of tau protein and alzheimer paired helical filaments show no evidence for beta-structure. *Journal of Biological Chemistry, 269*(39), 24290.

Serpell, L. C., Sunde, M., Benson, M. D., Tennent, G. A., Pepys, M. B., & Fraser, P. E. (2000). The protofilament substructure of amyloid fibrils1. *Journal of Molecular Biology, 300*(5), 1033-1039.

Sibille, N., Sillen, A., Leroy, A., Wieruszeski, J. M., Mulloy, B., Landrieu, I., & Lippens, G. (2006). Structural impact of heparin binding to full-length tau as studied by NMR spectroscopy. *Biochemistry, 45*(41), 12560-12572.

Siddiqua, A., & Margittai, M. (2010). Three- and four-repeat tau coassemble into heterogeneous filaments: An implication for alzheimer disease. *The Journal of Biological Chemistry, 285*(48), 37920-37926. doi:10.1074/jbc.M110.185728

Sigmaaldrich.com. http://www.sigmaaldrich.com/etc/medialib/docs/Sigma-Aldrich/Product_Information_Sheet/h9399pis.Par.0001.File.tmp/h9399pis.pdf

Silveira, J. R., Raymond, G. J., Hughson, A. G., Race, R. E., Sim, V. L., Hayes, S. F., & Caughey, B. (2005). The most infectious prion protein particles. *Nature, 437*(7056), 257-261.

Strohmeyer, R., Ramirez, M., Cole, G. J., Mueller, K., & Rogers, J. (2002). Association of factor H of the alternative pathway of complement with agrin and complement receptor 3 in the alzheimer's disease brain. *Journal of Neuroimmunology, 131*(1), 135-146.

Sunde, M., & Blake, C. (1997). The structure of amyloid fibrils by electron microscopy and X-ray diffraction. *Advances in Protein Chemistry, 50*, 123-124, C11-C12, 125-159.

Sunde, M., & Blake, C. C. F. (1998). From the globular to the fibrous state: Protein structure and structural conversion in amyloid formation. *Quarterly Reviews of Biophysics, 31*(01), 1-39.

Tanaka, M., Chien, P., Naber, N., Cooke, R., & Weissman, J. S. (2004a). Conformational variations in an infectious protein determine prion strain differences. *Nature, 428*(6980), 323-328.

Tanaka, M., Chien, P., Yonekura, K., & Weissman, J. S. (2005). Mechanism of cross-species prion transmission:: An infectious conformation compatible withTwo highly divergent yeast prion proteins. *Cell, 121*(1), 49-62.

Tanaka, M., Collins, S. R., Toyama, B. H., & Weissman, J. S. (2006). The physical basis of how prion conformations determine strain phenotypes. *Nature, 442*(7102), 585-589.

Telling, G. C., Parchi, P., DeArmond, S. J., Cortelli, P., Montagna, P., Gabizon, R., . . . Prusiner, S. B. (1996). Evidence for the conformation of the pathologic isoform of the prion protein enciphering and propagating prion diversity. *Science, 274*(5295), 2079.

The New York Times. (2011). http://www.nytimes.com/2011/05/03/sports/football/03duerson.html

Todd, A. P., Cong, J., Levinthal, F., Levinthal, C., & Hubell, W. L. (1989). Site-directed mutagenesis of colicin E1 provides specific attachment sites for spin labels whose spectra are sensitive to local conformation. *Proteins: Structure, Function, and Bioinformatics, 6*(3), 294-305.

Torok, M., Milton, S., Kayed, R., Wu, P., McIntire, T., Glabe, CG., Langen, R. (2002). Structural and dynamic features of Alzheimer's Aβ peptide in amyloid fibrils studied by site-directed spin labeling. *Journal of Biological Chemistry, 277(43), 40810-40815.*

Trojanowski, J. Q., & Lee, V. (1994). Paired helical filament tau in alzheimer's disease. the kinase connection. *The American Journal of Pathology, 144*(3), 449.

Tycko, R. (2011). Solid state NMR studies of amyloid fibril structure. *Annual Review of Physical Chemistry, 62,* 279.

von Bergen, M., Barghorn, S., Müller, S. A., Pickhardt, M., Biernat, J., Mandelkow, E. M., . . . Mandelkow, E. (2006). The core of tau-paired helical filaments studied by scanning transmission electron microscopy and limited proteolysis. *Biochemistry, 45*(20), 6446-6457.

Wang, Y., Biernat, J., Pickhardt, M., Mandelkow, E., & Mandelkow, E. M. (2007). Stepwise proteolysis liberates tau fragments that nucleate the alzheimer-like aggregation of full-length tau in a neuronal cell model. *Proceedings of the National Academy of Sciences, 104*(24), 10252.

Ward, R., Keeble, D. J., El-Mkami, H., & Norman, D. G. (2007). Distance determination in heterogeneous DNA model systems by pulsed EPR. *ChemBioChem, 8*(16), 1957-1964.

Wearsch, P. A., Voglino, L., & Nicchitta, C. V. (1998). Structural transitions accompanying the activation of peptide binding to the endoplasmic reticulum Hsp90 chaperone GRP94. *Biochemistry, 37*(16), 5709-5719.

Weingarten, M. D., Lockwood, A. H., Hwo, S. Y., & Kirschner, M. W. (1975). A protein factor essential for microtubule assembly. *Proceedings of the National Academy of Sciences, 72*(5), 1858.

Weissmann, C., Li, J., Mahal, P. S., & Browning, S. (2011). Prions on the move. *EMBO Reports, 12,* 1109 - 1117. doi:10.1038/embor.2011.192

Wickner, R. B., Dyda, F., & Tycko, R. (2008). Amyloid of Rnq1p, the basis of the [PIN] prion, has a parallel in-register β-sheet structure. *Proceedings of the National Academy of Sciences, 105*(7), 2403.

Wischik, C., Novak, M., Edwards, P., Klug, A., Tichelaar, W., & Crowther, R. (1988). Structural characterization of the core of the paired helical filament of alzheimer disease. *Proceedings of the National Academy of Sciences, 85*(13), 4884.

Wischik, C., Novak, M., Thøgersen, H., Edwards, P., Runswick, M., Jakes, R., . . . Klug, A. (1988). Isolation of a fragment of tau derived from the core of the paired helical filament of alzheimer disease. *Proceedings of the National Academy of Sciences, 85*(12), 4506.

Witman, G. B., Cleveland, D. W., Weingarten, M. D., & Kirschner, M. W. (1976). Tubulin requires tau for growth onto microtubule initiating sites. *Proceedings of the National Academy of Sciences, 73*(11), 4070.

Yamaguchi, K., Takahashi, S., Kawai, T., Naiki, H., & Goto, Y. (2005). Seeding-dependent propagation and maturation of amyloid fibril conformation. *Journal of Molecular Biology, 352*(4), 952-960.

Yan, Y., Marriott, G. (2003). Analysis of protein interactions using fluorescence technologies. *Current Opinion in Chemical biology*, 7(5), 635-640.

Zou, P., & Mchaourab, H. S. (2010). Increased sensitivity and extended range of distance measurements in spin-labeled membrane proteins: Q-band double electron-electron resonance and nanoscale bilayers. *Biophysical Journal, 98*(6), L18.

Appendix A

RECIPES

NZY media

NaCl	5 g
$MgSO_4*7H_2O$	2 g
Bacto-yeast extract	5 g
NZ amine (casein hydrolysate)	10 g
Total volume	1L
pH	7.5

NZY+ media

NZY media	
$MgCl_2$	12.5 mM
$MgSO_4$	12.5 mM
Glucose	20 mM

LB Media

LB Broth	25 g
Kanamycin	30 mg
Total volume	1.5L

Kanamycin-LB Agar plates

LB Broth	20 g
LB Agar	15 g
Kanamycin	50 mg
Total volume	1.0 L

Extraction buffer

NaCl	500 mM
PIPES (pH 6.5)	20 mM
EDTA (pH 8.0)	5 mM
Total volume	1L

PIPES buffer

PIPES	302.37 g	Conc. 1M
pH	6.5	
Total volume	1L	

Buffer A for ion exchange

NaCl	50 mM
PIPES (pH 6.5)	20 mM
EDTA	0.5 mM
DTT	2 mM

Buffer B for ion exchange

NaCl	1000 mM
PIPES (pH 6.5)	20 mM
EDTA	0.5 mM
DTT	2 mM

Gel Filtration buffer

NaCl	100 mM
Tris (pH 7.0)	20 mM
EDTA	1 mM
DTT	2 mM

SDS Running buffer

1X	
Glycine	28.8 g
Tris base	6.04 g
SDS	2 g
Total volume	2 L

SDS-PAGE 4x Sample Buffer

Reagent	Final Concentration	Volume	Mass
80% Glycerol	40%	5ml	
1M Tris-Cl, pH 6.8	240 mM	2.4ml	
SDS	8%		0.8 g
Bromophenol blue	0.1%		4 mg
H_2O		2.1ml	

SDS-PAGE Gel buffers

4X Lower gel buffer	1.5 M Tris-Cl (pH 8.8)
	0.4% SDS
4x Upper gel buffer	0.5 M Tris-Cl (pH 6.8)
	0.4% SDS

12% SDS PAGE Gel (For 2 Gels)

	Separation Gel (Lower)(12%)	Stacking (Upper)(4%)
Acryl-Bisacrylamide	4 ml	1.3
Tris-Cl (pH 6.8)		2.5
Tris-Cl (pH 8.8)	2.5 ml	
10 % SDS	0.1 ml	0.1
dH_2O	3.4 ml	6.1
10% APS	50 µl	50 µl
TEMED	5 µl	10 µl

15% SDS PAGE Gel (For 2 Gels)

	Separation Gel (Lower)(15%)	Stacking (Upper)(4%)
Acryl-Bisacrylamide	5 ml	1.3
Tris-Cl (pH 6.8)		2.5
Tris-Cl (pH 8.8)	2.5 ml	
10 % SDS	0.1 ml	0.1
dH_2O	2.4 ml	6.1
10% APS	50 µl	50 µl
TEMED	5 µl	10 µl

Coomassie blue stain solution

Coomassie blue	2.5 g
methanol	200 ml
Acetic acid	50 ml
dH_2O	250 ml

Destain solution

Glacial Acetic acid	125 ml
Methanol	50 ml
Total volume	1L

1X TBE buffer for Agarose Gel Electrophoresis

Tris base	1 M
Boric acid	1M
EDTA	20 mM

HEPES Buffer

HEPES	260.28	Conc. 1M
pH	7.4	
Total volume	1L	

Elution Buffer (EB)

NaCl	100 mM
HEPES (7.4 pH)	10 mM
NaN_3	0.1 mM
Total volume	1L

Appendix B

Genscript QuickClean 5M PCR Purification Kit protocol of PCR product purification purification

1. The PCR reaction sample was transferred to a 1.5 ml microcentrifuge tube and 400 µl of binding solution was added and thoroughly mixed.
2. The above mixture was transferred to a column and centrifuged at 12,000 rpm for one minute.
3. The flow –through was discarded and 500 µl of wash solution was added to column. The column was then centrifuged at 12,000 rpm for 30 seconds.
4. To remove the residual amount of wash solution, the column was centrifuged for an additional one minute.
5. The column was transferred to a clean 1.5 ml microcentrifuge tube. To the centre of the column membrane 30 µl of the elution buffer was added and incubated at room temperature for one minute. To collect the DNA the column was centrifuged again for one minute. The eluted DNA in the microcentrifuge tube was stored at -20°C.

Qiagen® Midiprep Plasmid Purification kit

1. For starter culture a single colony was picked for bacterial growth in LB medium with 30 mM kanamycin and kept in the shaking incubator at 37°C for 17 hrs.
2. Bacterial cells were harvested at 6000 x g for 15 minutes at 4°C.
3. The bacterial pellet was resuspended in 4 ml Buffer P1.
4. To the resuspended bacterial pellet, 4 ml of Buffer P2 was added, mixed thoroughly by vigorously inverting the sealed tube 4-6 times, and incubated at room temperature (15-25°C) for 5 minutes
5. To the above mixture, 4 ml of chilled Buffer 3 was added and immediately mixed by vigorously inverting 4-6 times. The sample was incubated on ice for 15 minutes.
6. After 15 minutes, the sample was centrifuged for 20,000 x g for 30 minutes at 4°C. The supernatant which has the plasmid DNA was removed immediately.
7. The supernatant was centrifuged again at 20,000 x g for 15 minutes at 4°C. The supernatant containing the plasmid was removed promptly.
8. QIAGEN-tip 100 was equilibrated by applying 4 ml of Buffer QBT and allowed the column to empty by gravity flow.
9. The supernatant from step 7 was applied to the QIAGEN-tip and allowed it to enter the resin by gravity flow.
10. The QIAGEN-tip was washed 2 times with 10 ml Buffer QC.
11. The DNA was eluted with 5 ml of Buffer QF.

12. The DNA was precipitated by adding 3.5 ml of isopropanol, mixed and centrifuged immediately at 15,000 x g for 30 minutes at 4°C. After centrifugation the supernatant was carefully decanted.
13. The DNA pellet was washed with 1.8 ml of room temperature 70% ethanol and centrifuged at 15,000 x g for 10 minutes. The supernatant was carefully decanted without disturbing the pellet.
14. The pellet was air dried and redissolved in TE buffer of pH 8.0.

GenScript Quickclean 5M Miniprep kit protocol for plasmid purification

1. For overnight culture a single colony was picked and put into a polypropylene tube with 5 ml LB medium and 30 mM kanamycin and kept in the shaking incubator at 37°C for 17 hrs for bacterial growth.
2. From the overnight culture, 1.5 ml was transferred to 1.5 ml microcentrifuge tube and centrifuged at 12,000 rpm for 30 seconds. The supernatant was discarded. This was continued until all the bacteria were pelleted from the overnight culture.
3. To the pellet 100 µl of solution I was added and the cells were resuspended. The cells were resuspended by running the narrow end of the microcentrifuge tube along an empty microcentrifuge storage rack.
4. To the mixture 200 µl of solution II was added. The solution was mixed gently by inverting the tube 4-6 times.
5. After this 300 µl of solution III was added and mixed gently by inverting the tube 4-6 times.

6. The sample was centrifuged at 12,000 rpm for five minutes and the supernatant was transferred to the column. The column was centrifuged for 30 seconds at 12,000 rpm.
7. The flow through was discarded and 500 µl of the wash solution was added and centrifuged for 30 seconds.
8. The flow through was discarded and the column was centrifuged for additional 60 seconds to remove the residual wash solution
9. The column was transferred to a clean 1.5 ml microcentrifuge tube. To the centre of the column 30 µl of the elution buffer was added and allowed the column to stand at room temperature for one minute. After one minute the column was centrifuged at 12,000 rpm for one minute. The eluted sample which has the plasmid DNA was stored at -20°C until further use.

Appendix C

Protein concentration determination was done using the Lambert Beer's law:

A Full length tau protein concentration determination was done at 280 nm:

$A=\varepsilon cl$

Molar extinction coefficient of full length tau: 7395 $mol^{-1}Lcm^{-1}$, path length of the cuvette = 1cm.

Appendix D

Cation exchange method parameters

Mono S 10 GL 100 method on Unicorn 5.11 was used to purify proteins by ion exchange

	Flow rate (ml/min)	3
	Column Pressure limit (mPa)	3
	Averaging time for UV	2.60
	Fraction size (ml)	3
Gradient segment 1	Target conc (%B)	15
	Length of gradient (CV)	3
	Fraction size (ml)	3
Gradient segment 2	Target conc (%B)	60
	Length of gradient (CV)	8
	Fraction size	3
Gradient segment 3	Target conc (%B)	100
Gradient delay (ml)		5
Clean after elution (CV)		5

Gel filtration parameters

Manual run was used in Unicorn 5.11.

Flow rate (ml/min)	5
Fraction size (ml)	5
Column Pressure limit (MPa)	0.8

Appendix E

Protein concentration measurement by Pierce® BCA Protein Assay kit

1. Bovine serum albumin (BSA) standards were prepared from 2000 µg/ml to 62.5 µg/ml
2. Working reagent of BCA was prepared by mixing 50ml Reagent A with 1ml of Reagent B
3. Test-tube Procedure in the protocol was used to find the concentration of the unknown protein
4. 85 µl of each standard and unknown sample were pipetted in appropriately labeled test tube
5. 1.7 ml of the working reagent was added to each tube and mixed well
6. The Standard Protocol was followed. The tubes were incubated for 30 minutes at 37°C.
7. All the tubes were cooled to room temperature
8. The absorbance of the samples was measured at 562 nm with water as the blank.
9. Standard curve was plotted and the protein concentration of the unknown was determined.

Appendix F

Publications

1. Ayisha Siddiqua, Martin Margittai
Three- and Four-repeat Tau Coassemble into Heterogeneous Filaments: AN IMPLICATION FOR ALZHEIMER DISEASE (2010). *Journal of Biological Chemistry,* 286(45), 37920-37930.

2. Paul Dinkel[‡], Ayisha Siddiqua[‡], Huy Huynh, Monil Shah,and Martin Margittai
Variations in Filament Conformation Dictate Seeding Barrier between Three-and Four-Repeat Tau (2011). *Biochemistry*, 50, 4330-4336.

[‡]Equal contribution